Deploying an unmanned aerial vehicle (UAV) equipped with a multispectral sensor for detecting between differing levels of barley (*H vulgare* L.) fungal diseases in Northern Ontario.

by

Alexander James Graham

NRMT

Thesis Advisor: Dr. Ulf Runesson

FACULTY OF NATURAL RESOURCES MANAGEMENT
LAKEHEAD UNIVERSITY
THUNDER BAY, ONTARIO

January 20th, 2017

Deploying an unmanned aerial vehicle (UAV) equipped with a multispectral sensor for detecting between differing levels of barley (*H vulgare* L.) fungal diseases in Northern Ontario.

by

Alex Graham

A Master's Thesis Submitted in
Partial Fulfillment of the Requirements for the
Master of Science in Forestry Degree.

Faculty of Natural Resources Management

Lakehead University

January 20th 2017

X_____

Major Advisor

LIBRARY RIGHTS STATEMENT

In presenting this thesis in partial fulfillment of the requirements for the HBEM degree at Lakehead University in Thunder Bay, I agree that the University will make it freely available for inspection.

Signature: _____

Date: _____

A CAUTION TO THE READER

This MScF thesis has been through a semi-formal process of review and comment by at least two faculty members. It is made available for loan by the Faculty of Natural Resource Management for the purpose of advancing the practice of professional and scientific forestry.

The reader should be aware that opinions and conclusions expressed in this document are those of the student and do not necessarily reflect the opinions of either the thesis supervisor, the faculty or Lakehead University.

ABSTRACT

Graham, A.J. Deploying an unmanned aerial vehicle (UAV) equipped with a multispectral sensor for detecting between differing levels of barley (*H vulgare* L.) fungal diseases in Northern Ontario. 137 pp.

Keywords: barley, disease detection, farm, multispectral, precision agriculture, remote sensing, UAV.

To date, no studies exist exploring the multispectral detection of fungal diseases in barley (*H Vulgare* L.) with UAV imagery. The purpose of this work was to determine if the spectral response (VI) of barley fungicide treatment levels (Control, Stratego, Stratego + Prosaro) could be distinguished between two farmers' fields and four growth stages (Feekes 8 to Feekes 11.4), when evaluating UAV multispectral imagery (Blue- 475 nm +/- 20 nm, Green- 560 nm +/- 20 nm, Red- 668 nm +/- 10 nm, Red Edge- 717 nm +/- 10 nm, Near Infrared- 840 nm +/- 40 nm) of 6.7 cm/pixel spatial resolution. Radiometrically and geometrically corrected orthomosaics were generated and intrusive features such as weeds and crop damage were classified and extracted before the analyses of canopy level barley. Each photo was registered with RTK accuracy to ensure the analysis of identical pixelated areas between dates. A randomized complete block design was performed for 5 separate VIs: NDVI, RE-NDVI, RDVI, RE-RDVI, and TGI. 3-way interactions (Field x Growth Stage x Treatment) were found to be non-significant for NDVI (p=0.415), RE-NDVI (p=0.383) and TGI (p=0.780), with RDVI (p=0.003) and RE-RDVI (p=0.005) being significant. Despite some differences, a consistent trend in the spectral separability of fungal intensity by treatment type was observed regardless of field, from Feekes 10.51 onwards. With ground truthing, the mapping of fungicide intensity is possible with potential towards savings and environmental benefits from reduced fungicide use.

TABLE OF CONTENTS

ABSTRACT ..... **IV**

TABLE OF CONTENTS ..... **V**

LIST OF FIGURES ..... **VII**

LIST OF TABLES ..... **IX**

ACKNOWLEDGEMENTS ..... **X**

LITERATURE REVIEW **1**

BRIEF HISTORY: REMOTE SENSING APPLICATIONS IN AGRICULTURE **1**

REMOTE SENSING OF VEGETATION WITH INDICES **4**

FUNGAL DISEASE DETECTION WITH SPECTROSCOPIC AND REMOTELY SENSED DATA **8**

UAV REMOTE SENSING IN PRECISION AGRICULTURE **11**

BRIEF HISTORY 11

RADIOMETRIC CORRECTIONS 13

EFFECTS OF SOIL MANAGEMENT TYPE ON CROP HEALTH 20

UAV AGRICULTURAL RESEARCH 22

INTRODUCTION **25**

MULTISPECTRAL FUNGAL DETECTION OF CEREALS **30**

EXPERIMENT **31**

HYPOTHESIS AND RESEARCH QUESTIONS 32

MATERIALS AND METHODS **34**

SITES AND CONDITIONS **34**

TREATMENT EFFECTS AND PLOTS **37**

EQUIPMENT AND FLIGHTS **41**

RADIOMETRIC CORRECTIONS **42**
SURFACE REFLECTANCE 42
THE MINIMUM NOISE FRACTION (MNF) TRANSFORM 43

GEOMETRIC CORRECTIONS **47**

HISTOGRAM MATCHING **48**

WEED PIXEL CLASSIFICATION AND EXTRACTION **51**

CROP BLOWDOWN PIXEL EXTRACTION **53**

VEGETATION INDICES AND CLIPPED AOI **57**
CLIPPED AOI 57
VEGETATION INDICES 59

GRAIN HARVEST EXPERIMENT **62**

STATISTICAL ANALYSES **64**
REGRESSION 64
TWO-WAY ANOVA 65
RANDOMIZED COMPLETE BLOCK DESIGN (RCBD) 65

RESULTS **67**

CORRECTED IMAGERY **67**

VISUAL ASSESSMENT ACCURACY VERIFICATION **68**

RCBD STATISTICAL RESULTS **71**
MAIN EFFECTS, INTERACTIONS AND POST-HOC FINDINGS 71

GRAIN YIELD RESULTS **82**

DISCUSSION **83**

VISUAL ASSESSMENT ACCURACIES **83**
EARLY DISEASE DETECTION 83
SOURCES OF ERROR 85
ACCURACY RESULTS 89

RCBD RESULTS **91**
THE IMPACT OF DIFFERENT CROP MANAGEMENT REGIMES ON REMOTELY SENSED DATA 91
DISTINGUISHING FUNGAL DISEASE SEVERITY 95

FUNGICIDE TIMING AND IMPACT ON YIELD AND SENESCENCE 98
SEPARATING FUNGAL DISEASE FROM OTHER STRESSES 100
ROBUSTNESS OF RCBD MODEL USED IN THIS RESEARCH 102

CONCLUSION 103

LITERATURE CITED 105

APPENDICES 132

APPENDIX I: ADDITIONAL INDEX FIGURES 133

LIST OF FIGURES

Figure 1. Hanna Farm treatment rows delineated in black (left), Trumar Farm treatment rows delineated in black (right). Visual assessment plots are outlined by the thick asterisks, GCPs are indicated by the thin asterisks (not all GCPs are visible). C=Control; S=Stratego; SP= Stratego + Prosaro. Not to scale. 37
Figure 2. Standardized area diagram for barley and wheat leaves, modified from Bock (2010). 40
Figure 3. Observer-6 (OB-6) hexacopter (0.5 m frame) equipped with the 5-channel multispectral sensor (Micasense). Hanna Farms, SW Corner, July 22nd, 2015. 42
Figure 4. Maximum Noise Fraction (MNF) Transform for July 22nd, 2015. Band 1 (left) is shown with the lowest signal-to-noise ratio, and Band 5 is shown (right) with the highest signal-to-noise ratio. 46
Figure 5. Eigenvalues (Y-axis) and Eigenvalue Numbers/Bands (X-axis), for July 22nd, 2015 scene. The eigenvalue approaches 1 at the 5th band, showing a high degree of noise presence. 46
Figure 6. Image correction process, including initial radiometric corrections to surface reflectance, noise removal, inter-scene and between-date histogram matching and pixel data extraction from AOI clips. 47

Figure 7. Histogram match of Trumar Farm scene from July 28th, 2015. The targeted side (master) and cloud-covered side (slave). A histogram match was then performed (right side) matching the slave to the master. 50
Figure 8. Clover infestation visible as bright green (upper) and classification as a yellow thematic layer (lower). 53
Figure 9. Section of Trumar Farm on GS3 showing blown-down barley in brightened areas. A: Unclassified. B: Classified. 56
Figure 10. All orthomosaics highlighting classified sections of crop with clover infestation for Hanna Farm, and barley blow down damage for Trumar Farm. Not to scale. 57
Figure 11. A) Strip plot shapefiles outlining the clipped AOI for Hanna Farm; B) 4 of 18 Visual Assessment (VA) plot shapefiles outlining the clipped AOI for Hanna Farm. Plot 7N is the uppermost yellow polygon, which was the only VA plot to fall within the clover infestation. 58
Figure 12. A: Hanging barley grain at TBARS. B: Threshing machine at TBARS. C: Barley grain after threshing. D: Process of cleaning the barley grains before dry weighing. 63
Figure 13. A: Control treatment row in Trumar Farm. B: Stratego + Prosaro treatment row in Trumar Farm. C: Comparison of grain from Control treatment (left head) and Stratego + Prosaro treatment (right head). August 14th, 2015 (GS3). 64
Figure 14. RE-NDVI imagery before inter-scene histogram matching and clipping. Not to scale. 68
Figure 15. Linear regressions for fields at Trumar and Hanna Farms, each with combined data from Growth Stages 2 and 3 (36 observations per regression). 70
Figure 16. Main effect of treatments on spectral response from all measured vegetation indices. Error bars represent one standard deviation. 72
Figure 17. Main effect of growth stage on spectral response from all measured vegetation indices. Error bars represent one standard deviation. 74
Figure 18. Plots for the interaction effect of Field and Treatments on spectral vegetation indices. Error bars show one standard deviation. 76

Figure 19. Plots for the interaction effect of Growth Stage and Field on spectral vegetation indices. 77
Figure 20. Interaction plots for the interaction effect of Growth Stage and Treatments on spectral vegetation indices. 79
Figure 21. Non-significant 3-way interaction effects between Treatment x Growth Stage x Field. Error bars show one standard deviation. 80
Figure 22. Significant 3-way interaction effects between Treatment x Growth Stage x Field. Error bars show one standard deviation. 81
Figure 23. Mean grain yield values for each respective treatment type. Error bars show one standard deviation. 83
Figure 24. Spectral profile from equalized random point sampling regime. 100 points were collected and averaged within each respective treatment AOI. Feekes 11.2 (GS3), Trumar Farm. 90

LIST OF TABLES

Table 1. Weather data recorded at the Thunder Bay Agricultural Research Station (TBARS) for 2015. 36
Table 2. Data acquisition dates and relative barley growth stages for respective fields, during spring-summer 2015. 39
Table 3. Vegetation indices used for regression between visual assessments and spectral averages, and for randomized complete block design of spectral strip averages. 61

ACKNOWLEDGEMENTS

This has been a long journey and there are countless people to whom I would like to express my utmost gratitude. First, my wife Shoko, for supporting and believing in me, and for making healthy meals which prevented me from eating too much cup ramen. Also thanks to my family for supporting and believing in me to pursue even more years of education. Thanks to Dr. Ulf Runesson for securing NSERC IPS for me and providing support for my Master's Thesis. Ulf has been a very motivational supervisor and I will always keep him as a mentor. Thanks to Sumac Geomatics Inc.: Todd Domney, Jarin Stewart, Adam Boczek, for being patient with my research and providing the necessary support and equipment used for this study. A huge thanks to local farmers John Hanna and Mark Bolt: two of the nicest human beings you will ever meet. They provided the fields for this study and took a risk in altering from their regular management regimes for the sake of this study (at the risk of trampling their crops!). Thanks to the Thunder Bay Agricultural Research Station (TBARS), including Dr. Tarlok Singh Sahota and Blaine Tomeck for providing equipment and advice when needed. Dr. Sahota helped secure me local presentations and bring local awareness to my study. He also gave guidance in treatment selection and helped establish a connection with both Mark Bolt and John Hanna. Thanks to the Thunder Bay District Soil and Crop Improvement Association for providing two venues where I gave some wonderful talks. Thanks to the students and professors from the Faculty of Natural Resources Management for always remaining openly available for much needed support. Lastly, a big thanks to LU-CARIS and all my office-mates, including Ben Ong, Alex Bilyk and Kevin Shorthouse for providing occasional feedback and advice on my incredibly complex thesis methodology.

LITERATURE REVIEW

BRIEF HISTORY: REMOTE SENSING APPLICATIONS IN AGRICULTURE

Long before coining the term ‘remote sensing’ in 1958, by Evelyn Pruitt of the U.S. Office of Naval Research, aerial photography had been used by scientists to spatially survey for soil and crop variability in the United States, and other parts of the world (Goodman 1959). The eventual progression of infrared photography during World War II encouraged the development of multiple new techniques for assessing the general health status of crops. Robert Colwell was a pioneer in the field of remote sensing who gained attention to his innovative methods in multispectral crop analysis at the University of California in the 1950s. He was among the first to demonstrate the ability of VNIR (Visible to Near-Infrared) multispectral data to detect between diseased and healthy plants (Colwell, 1956). Subsequent investigations during this period included the examination of different sensor types for developing livestock inventories (Huddleston et al., 1968), VNIR reflectance in relation to plant physiological stress at the leaf and canopy level (Knipling, 1970; Myers & Allen, 1968), the effects of organic matter on the multispectral properties of soils (Baumgardner et al. 1970), and the relationship of remote sensing aerial photography to crop yields (Von Steen, 1969), among others. To summarize, the early age of remote sensing research in agriculture explored mainly proximal (leaf-level

spectroscopy) and aerial (canopy level) based soil and crop detection with analog sensors. The year 1972 saw the launch of the first Landsat space-based sensor, which instantly made possible the notion of regional and global-scale crop assessments. Such research was implemented through the Large Area Crop Inventory Experiment (LACIE), which was the first U.S. government program aimed towards gathering and assessing satellite data for estimating wheat production, over large geographic areas (Nellis et al., 2009). It is from 1972 onward that a huge growth in remote sensing research is seen, exploring both space-based and aerial sensor technology for the purpose of understanding observed light response for quantifying field and crop parameters. Ultimately, regarding the practical application of such research, the overarching goal of scientists is to improve the management of crops relating to the scale of the remotely sensed imagery. Up until the 1980s, performing spatial input management regimes was a difficult task, namely at the field/canopy scale. Along with the advent of GPS (Global Positioning System) technology in the 1980s, the early concept of precision agriculture was formed, and such GPS technology was soon adopted into commercial practice in the early 1990s (Mulla, 2013).

Precision agriculture (PA), or site specific crop management (SSCM) is a farming concept based on a combination of observing, monitoring and responding to variability in crop growth. It is a practice of input stewardship: adapting input materials (e.g. fertilizers, herbicides, irrigation, etc.) to the needs of the crop plants or identified management zone. Additionally, as stated by

Sparovek & Schnug (2001) “The basic concepts of PA can also be applied to agronomic inputs other than materials such as labour and time which influence efficiency” (p.48). Since being realized in the mid-1980s, PA has been continuously developing alongside advances in technology. Traditionally, inputs such as herbicides have been uniformly dispersed throughout an entire field. Adapting to the needs of the plant by selective input application can offer the prospect of an improved crop yield, farm profitability and environmental quality (Hedley, 2014; Mulla, 2013). Some additional benefits associated with precision agriculture can be seen through selective hybrid utilization, intensive soil sampling and management, selective fertilizers/fungicides/herbicides and variable rate application, reduced chemical bills and fuel costs, and reduced soil compaction (Bongiovanni & Lowenberg-Deboer, 2004; Mulla, 2013). In general, the practice of precision agriculture includes spatio-temporal data collection and analysis, the integration of computing systems and processing, remote sensing technology, GPS systems for field positioning, and yield monitoring systems (Mulla, 2013). As precision agriculture technology improves, it is expected that more advanced systems such as GPS RTK (Real Time Kinetic) auto-steer guidance, variable rate irrigation and fertilizer spray controllers will become interconnected with real-time remote sensing data (Urbahs & Jonaite, 2013).

From the 1990s onward, remote sensing research has demonstrated many applications towards small-scale precision agricultural practices; however, a well-known limitation is the cost, and spatio-temporal resolution associated with manned and space-based imaging platforms. Recently, unmanned aerial

vehicles (UAVs) have shown promise to be an effective remote sensing tool for agriculture (Link et al. 2013; Zhang et al. 2012), with great potential towards increasing farm profitability through spatial mapping. Till the crop season of 2015, much research regarding UAVs in agriculture had been done with do-it-yourself (DIY) hobbyist platforms and consumer-grade sensors. There is currently, as of the year 2016, a transition being seen towards commercial UAV platforms and specialized sensors for the purpose of crop health detection. More on specific scientific research exploring the application of unmanned aerial vehicles will be discussed later in this literature review.

REMOTE SENSING OF VEGETATION WITH INDICES

Naturally, there exists electromagnetic waves of all frequencies and wavelengths, the full extent of which is known as the electromagnetic spectrum. The electromagnetic spectrum is divided into distinguishable bandwidth regions, such as for x-rays (0.01 to 10 nm) and radio waves (>1mm). The visible region (VIS: 390-700nm) of the electromagnetic spectrum describes light to which the human eye is sensitive. A similar range (400 to 700nm) overlapping the visible region is known as the photo-synthetically active region (PAR), which in general describes the amount of light available for photosynthesis (Jones & Vaughan, 2010). Chlorophylls A and B are essential pigments for the conversion of light energy to stored chemical energy. The amount of photosynthetic pigment in a leaf is well known to be directly related to the amount of absorbed solar radiation (Gitelson et al. 2003; Ingenhousz, 1779); thus, the presence or absence of such pigments represents the photosynthetic potential of a plant

(Filella et al. 1995; Jones & Vaughan, 2010). Numerous studies depict an indirect relationship with chlorophyll and leaf/plant nutrient status, as leaf nitrogen is incorporated in chlorophyll (Bojović & Marković, 2009; Daughtry et al. 2000). Furthermore, studies such as by Schlemmer et al. (2013) also have shown that a strong relationship exists between chlorophyll and nitrogen (plant nutrition) at both the leaf and canopy level. Vegetation Indices (VI) are widely adopted and explored in remote sensing research, in particular for their ability to measure vegetation cover. The nature of plant material to absorb, reflect and transmit radiation at known wavelengths allows for reflectance data to be incorporated into ratio-based indices. Thus, VIs are usually dimensionless measures of particular surface properties based on the ratio of reflected light between two or more wavelengths (Jones & Vaughan, 2010). Most VIs exploit the phenomenon of vegetation reflectance and absorption. Blue (430nm) and red (660nm) wavelengths are absorbed strongly by the presence of chlorophyll A in plant pigment, as well as blue (450nm) and red (650nm) for chlorophyll B (Mulla, 2013). The transition from the red region (620-700nm) to the near-infrared region (700-1300nm) sees a drastic increase in reflectance, which has formed the premise for many VIs over the years (Hunt et al., 2013). First described by Collins (1978), it is known that plants with high chlorophyll absorb light strongly in the red region, and reflect strongly in the near-infrared, which characterizes the slope known as the red-edge (RE: 650-720nm). The red-edge can shift depending on vegetation vigour, phenology, or species and can also be characterized by its maximum slope known as the red-edge position (REP)

(Baranoski & Rokne, 2005; Horler et al., 1983). It is also known that the red-edge can be observed at both leaf and canopy scale (Baranoski & Rokne, 2005; Baret et al., 1987), which has translated to many vegetation indices being relevant for both aerial and space-based remote sensing platforms. VIs in general are most often used to observe vegetation at either global, regional or canopy-level scales, associated with either space-based or aerial platforms.

One of the earliest and most popular VIs is known as the Normalized Difference Vegetation Index (NDVI). This equation was originally created by Rouse et al. (1974) for assessing the amount of vegetation on the earth, using Landsat data at 80m resolution. An early study by Tucker (1979) examined multiple different combinations of the Landsat Multispectral Scanner System (MSS) bands, and discovered NDVI was among a few combinations that could accurately estimate photosynthetically active biomass. The continuing popularity of NDVI, among many other VIs, is attributed to their positive relationships with canopy density or vigour, and their ability to adjust for soil and atmospheric interference. Leaf-area index (LAI), which is the ratio of one-sided green leaf area to ground area, is known to have a non-linear relationship with NDVI and exhibits variation amongst cover types. However, for both cereal and broad-leaf crops, NDVI is sensitive to LAI when LAI is less than 2 (Gitelson et al., 2003). Canopy nitrogen (N) status has also shown to be detectable utilizing VIs. The Chlorophyll Index developed by Gitelson & Merzlyak (1996) is reportedly more sensitive to canopy N status than NDVI. Soil effects can also be corrected for with certain VIs when there is low canopy density. The Soil-Adjusted Vegetation

Index (SAVI) developed by Huete (1988) corrects for varying soil reflectance, and has seen subsequent modifications in the form of the Transformed SAVI (TSAVI) (Baret et al.1989), and the Modified SAVI (MSAVI) (Qi et al., 1994). There are also indices which work specifically well for dense or sparse vegetation cover, such as the Renormalized Difference Vegetation Index (RDVI). The RDVI was first proposed by Roujean & Breon (1995) as a means to combine the advantages of NDVI (estimating healthy vegetation based on chlorophyll absorption) with the advantages of the Difference Vegetation Index (DVI) (an index which distinguishes well between soil and vegetation at low LAI). This index is reported to work well under dense or sparse canopy coverage and is insensitive to the effects of sun and soil viewing geometry.

Other indices have been proposed which exploit only the RGB bands of a sensor. The Triangular Greenness Index was first proposed by (Hunt et al., 2010) specifically for the detection of leaf chlorophyll content at the canopy scale. Subsequently, this index has been tested successfully on many occasions. Notably, a study by Hunt et al. (2014) evaluated simulated UAV imagery tested at differing spatial resolutions. A high correlation between TGI ($r = -0.72$) and sampled green pixels (0.5 mm/pixel) was seen; however, when computing plot spectral averages which included shadow and soil pixels, the relationship between chlorophyll meter readings was much lower.

FUNGAL DISEASE DETECTION WITH SPECTROSCOPIC AND REMOTELY SENSED DATA

Of particular interest in precision agriculture is spatio-temporal stress detection and classification using remotely sensed data. Stress can take many forms in field crops: nutrient deficiency, moisture deficiency or over-saturation of soil, environmental stressors (temperature, insect or pest damage, storm event damage), fungal disease, etc. (Mulla, 2013). For years scientists have examined proximal and spectroscopic data at the leaf-scale, attempting to understand the natural spectral response of stress types with respect to vegetation type. Fungal disease in particular has been extensively examined in spectroscopic studies and its negative impact on the health and yield of major cash crops in Canada is undeniable. In general, fungal pathogens which form as necrotic or chlorotic lesions on plant tissues tend to cause a reduction in plant chlorophyll, impacting reflectance in the visible (VIS: 400-650nm) and red-edge region (RE: 650-720nm) of the electromagnetic spectrum (Blazquez & Edwards, 1986). As disease progresses, an increase in dryness is observed in infected brown patches on leaf tissue (Ashourloo et al., 2014), generally increasing reflectance in the red region, and decreasing reflectance in the NIR region.

It is also known that severe disease infections can impact the overall rate of photosynthesis, restricting yield production in certain crops and affecting harvest time due to early senescence (Mulla, 2014; Robert et al., 2004; Roermund & Spitters, 1990; Spitters et al., 1990). The spectral response of diseased vs. healthy plant leaves are well documented in spectroscopic

research. Blazquez & Edwards (1986) examined the spectral reflectance of diseased and healthy watermelon leaves using a spectrophotometer. Significant differences were found in reflectance values, particularly in the VIS and NIR region when comparing disease severity levels. Zhang et al. (2012) examined the ability of hyperspectral imagery to detect yellow rust disease from nutrient stress in a crop. They were able to accurately detect the response of yellow rust at 4 out of 5 observed growth stages. Ashourloo et al. (2014) collected spectroscopic data from wheat leaf rust for the purpose of optimizing spectral vegetation indices. They found that the various symptoms of leaf rust (*Puccinia recondite*) each have a distinct spectral signature. Early symptoms in the form of yellow chlorotic lesions were noted to have low spectral seperability, while later symptoms in the form of necrotic patches and dried tissue were found classifiable with a high correlation to disease severity (R^2=0.94).

It has also been documented that there is little global effect on the photosynthetic capability of a given leaf, when fungal-infected lesions are present. This has been demonstrated in many studies examining wheat (*Triticum aestivum* cv. Soissons) leaf reflectance. Photosynthetic activity on a specific leaf was found to be negatively impacted only in areas where fungal lesions are present (Ashourloo et al., 2014; Kuckenberg, 2009; Robert et al., 2005). This however does not mean that the overall, or global health of a plant is insensitive to fungal disease. Rather, the rate of leaf senescence and subsequent discoloration can increase, affecting harvest timing and yield,

particularly for wheat (Robert et al., 2004; Roermund & Spitters, 1990; Spitters et al., 1990).

Canopy-scale data have traditionally been remotely detected with sensors mounted on space-based or manned aerial platforms. Such data are increasingly more complicated for analysis due to many uncontrollable factors covered later in this review. With multispectral sensors, there are more limitations in the detection of early fungal disease due to less data dimensionality, when compared with spectrometers or hyperspectral sensors. However, since hyperspectral sensors are not currently economically feasible to most users due to high cost, the multispectral approach appears to be gaining more attention.

There is current interest to explore fungal disease detection using high-resolution multispectral sensors. Qin & Zhang (2005) used multispectral imagery to detect rice sheath blight. They examined potential correlations between measured field and aerial image data, and concluded the potential for specific VIs to detect rice sheath blight. There were however limitations in detecting between light-infected and healthy plants due to spectral similarities. They found higher levels of ground truth accuracy when disease reached medium to severe levels. Franke & Menz (2007) examined the potential of multispectral imagery for spatio-temporal detection of powdery mildew (*Blumeria graminis*) and leaf rust (*Puccinia recondite*) pathogens in wheat. They determined that classification accuracies were low early in the season, and high late in the season. Accuracy only seemed to improve towards the end of the season,

showing that early disease detection was difficult with their equipment and methodologies. Zhang et al. (2014) explored multispectral imagery for the purpose of detecting powdery mildew in winter wheat using multi-temporal satellite imagery. All explored vegetation indices (VIs) were capable of generating disease maps; however, there was a variable degree of error when correlating with ground survey data. The drawback from many such studies utilizing space-based or aerial data is the lack of spatial resolution. Large pixels can contain mixes of various surface features, such as bare soil, shadows, and crop residue, which add reflectance error to the target. Conversely, too high of a spatial resolution can also become tedious for spectral analysis. Smaller pixels will cover less surface features but inherently have greater pixel-to-pixel variability (Hunt et al., 2014). It is the general consensus of the above authors that higher spatial resolution datasets have potential in detecting fungal disease with a higher degree of spatio-temporal accuracy (Franke & Menz, 2007; Qin & Zhang, 2005; Zhang et al., 2014). In this light, there is novelty in understanding to what extent UAV-based multispectral datasets can detect disease presence within crops.

UAV REMOTE SENSING IN PRECISION AGRICULTURE

BRIEF HISTORY

Although aerial photography has long been a part of remote sensing-based agricultural research, there is still great novelty with respect to UAV image acquisition. Very few papers exist in the 90s which explicitly evaluate UAVs for precision agriculture, as both sensor and UAV technology were still

premature. Schnug et al. (1998) published a paper which highlighted necessary developments for soil sampling and nutrient mapping moving into the future. A constraint in remote sensing methodologies at the time was the lack of sensor resolution, and the dependency on satellite imagery which had poor revisit times and periodic cloud interference. UAVs were recommended as a possible alternative to improve the spatial mapping of farm crops, allowing for less intensive soil sampling regimes, and better ability to delineate management zones in crops. In the early 2000s, remote-control (RC), hobby-grade UAVs equipped with digital cameras were evaluated for application in precision agriculture (Simpson et al., 2003). At the time, much promise was shown in the ability to acquire timely imagery at high spatial resolutions; however, electronic sensor technology in general was still new and limited due to high unit weight and costs, low digital pixel quality and intensive radiometric and geometric correction requirements. Nonetheless, studies persisted in this period. Hunt et al. (2005) evaluated digital photography from RC model aircraft purposed for the detection of crop nitrogen and biomass. The authors noted difficulties in radiometric corrections due to the digital camera's exposure settings skewing the digital number (DN) pixel values. They had satisfactory results; however, they noted that the technology still had limitations, and that imagery from the current digital sensors were more suitable for visual interpretation.

In recent years, more varieties of precision agriculture research utilizing UAVs and related imagery now exist, due to the rise in commercial and industrial popularity of drones and related sensors. The advancements of UAV

technology have now reached a level where more emphasis can now be focused towards sensor quality, processing methods and image analysis.

Before going more in depth with UAV-specific crop research, it is important to explore existing methodologies regarding pre and post processing of UAV imagery.

RADIOMETRIC CORRECTIONS

As discussed in the work by Jones & Vaughan (2010), the dynamics of canopy-level remote sensing of vegetation can be very complicated. Often, necessary radiometric corrections are required to account for various illumination effects at the canopy-level: bare soil noise, sun angle and viewing geometry, atmospheric effects, bidirectional scattering of light from angular leaves, among others. These corrections are well documented in scientific literature with emphasis on space-based sensors; however, very little literature exists which explicitly explores radiometric corrections of UAV data. Corrections involving UAV data can also be complicated, particularly due to the large number of images required, variations in image quality because of changing illumination conditions, and limits over the control of acquisition parameters (Laliberte et al., 2011). Some discussion on the general concepts of radiometric correction will be discussed in this section, with emphasis on relevant techniques that have been applied towards UAV data sets.

SENSOR NOISE

A source of error independent of collected sensor radiance is that of background noise. Raw pixel data picked up in the sensor as intensity values will carry some component of noise interference. In general there are two types of noise: random and systematic (Al-amri et al., 2010). Systematic noise describes statistical fluctuations of error due to precision limitations of the sensor type (such as ISO parameters). Conversely, the random portion describes the unpredictable and unrepeatable element of noise which appears as errors in imagery. Thus, there is a need for a correction methodology to be applied to most raw UAV data; the sensor type will dictate to what degree noise has impacted pixel values. It is important to note that the unpredictable nature of random noise limits the effectiveness of many removal techniques (Al-amri et al., 2010; Kelcey & Lucieer, 2012). Dark Offset Subtraction is a technique where raw image data are created absent of radiance, so that only noise is present (Kelcey & Lucieer, 2012; Mansouri et al. 2005; Mullikin et al., 1994). An individual dark offset image represents a sample of per-pixel noise, where multiple images of this kind can be put into a database to obtain more accurate per-pixel noise characteristics. Through repetition, mean per-pixel values pertaining to noise presence can be determined and used to eliminate most noise present. Following subtraction, the per-pixel standard deviation of dark offset imagery gives an estimation of the average noise remaining, thus allowing one to quantify any potential remaining error for their image analyses (Mullikin et al., 1994). Kelcey & Lucieer (2012) used a mini multispectral camera

(manufactured by Tetracam Inc.) for their research and performed, among other calibrations, noise correction using the Dark Offset Subtraction method. To ensure that no radiance would be present in the imagery, captures were taken in a dark room, and they enveloped the sensor in a Gore-Tex hood. All six channels had 125 captures taken which were later averaged. When the per-pixel means and standard deviations were calculated the Dark Offset Subtraction was performed and utilized for the correction of UAV imagery.

Another effective technique, known as the Minimum Noise Fraction (MNF) Transform (sometimes referred to as the *Maximum* Noise Fraction Transform), performs two principal component analyses (PCA) and re-orders the bands of an image with respect to subsequently decreasing signal quality (Qi et al., 1994). As pointed out by Green et al. (1988), a general PCA will re-order bands based on subsequently decreasing variance; this is not always reliable for exclusively reducing noise in a multispectral dataset. Thus, the MNF transform presents a more reliable method for consistently improving signal quality by subsetting out noise from the image space.

Bare soils reflect a certain amount of radiation which is dependent on soil moisture and organic matter content (Thomasson et al., 2001; Viscarra Rossel et al., 2006). It is often unavoidable that bare soil appears in images containing crop canopies, causing spectral contamination of the true signature values of a target. There are however known techniques regarding the isolation or improvement vegetation spectral signals, such as spectral unmixing algorithms (Asner & Heidebrecht, 2002), derivative spectra (Demetriades-Shah et al.,

1990), VIs that adjust for the effects of soil (Qi et al., 1994), and signal/noise ratio transformations such as the MNF Transform (Pereira & Carreiras, 2005). A few studies involving UAV data have used techniques to subset soil noise from imagery. Gevaert et al. (2014) used spectral unmixing successfully to improve correlation values between the Weighted Difference Vegetation Index (WDVI) and measured potato field crop parameters. Object-based image segmentation has also been used to classify between bare soil, sparse vegetation on bright soils, and sparse vegetation on dark soils using assigned thresholds from the blue band of a multispectral UAV data set (Laliberte et al., 2011). In situations where there is complete canopy closure, the effects of soil noise are negligible on incoming sensor irradiance (Heege, 2013). However, as highlighted by Heege (2013), soil noise may sometimes be a factor as the sensor may have an oblique viewing angle towards the canopy. Additionally, in small canopy openings, soil unimpeded by shade can reflect strongly in the green channel which can mimic vegetation spectral values (Huete et al., 1985).

LENS AND GEOMETRIC DISTORTION

Lens distortion is typically characterised by two effects: radial distortion and tangential distortion (Wang, Qiu, & Shao, 2009). Radial distortion can be explained as the slight radial shift in magnification towards or away from the centre of the lens, which results in an inward or outward shift of image points from their natural perspective. Decentering is a type of tangential distortion where the actual at-nadir point is shifted in the image data. In academic literature, the Brown-Conrady Model is widely used, and provides a medium to

correct for both radial and tangential distortion. This is an even-order polynomial model that can calculate the amount of distortion at a given image point. In order to do this manually, you first need to calculate the radial and tangential distortion coefficients, highlighted by Kelcey & Lucieer (2012) and Wang et al. (2009). One should first image a planar surface with known geometric properties, and differentiate between any image frame discrepancies. These differences allow for a coefficient to be derived which is used for correction of distortion.

Bouguet's calibration toolbox (Bouguet, 2001) is a method utilizing Matlab software to perform a geometric correction of imagery, by acquiring the intrinsic sensor parameters when they are not known (focal distance, principal point coordinates, lens radial distortion). There is a tutorial outlined on the web: http://www.vision.caltech.edu/bouguetj/calib_doc/. Berni et al. (2009) used this method for the calibration of thermal and multispectral UAV imagery in their study. They placed a black and white checkered panel in a fixed location and acquired images from different distances and orientations. Extracting the grid-corner coordinates from the imagery allowed for the intrinsic parameters to be calculated for the multispectral sensor. For the thermal sensor, a panel was created using resistive wires in specific patterns to allow the heat signatures to correlate with panel-specific areas.

VIGNETTING CORRECTION OF UAV IMAGERY

Vignetting has been described as a reduction of an image's brightness or saturation towards the periphery of an image, typically caused by the geometry

of a sensor's optics (Goldman, 2010; Kelcey & Lucieer, 2012). A radial shadowing effect is a typical documented phenomenon that occurs with the use of wide-angle lenses, where differences in magnification exist in the optical glass. In other words, occlusion of light is increased through wide-angle lenses leading to a reduction of light around the peripheral of photos. Kelcey & Lucieer (2012) describe how there are two broad approaches for the correction of vignetting: modelling the optical pathway or image-based techniques. Modelling techniques are typically applied when sensor-specific parameters are known, which allow for corrections in illumination reductions from vignetting. Image-based approaches utilize the per-pixel correction factor look-up table (LUT). Image-based approaches using LUT have been documented as being simpler to calculate, and more accurate (Kelcey & Lucieer, 2012; Yu, 2004). The LUT is generated into something known as a 'flat field' from a Lambertian surface assumed to be spectrally homogeneous and uniform. A correction factor is generated by comparing sensor imagery to the Lambertian surface, where differences in image pixel intensity between the two highlight vignetting effects. Kelcey & Lucieer (2012) used a white artist canvas to act as a Lambertian surface. They evenly illuminated the canvas in the dark room where they took 125 flat field photos, later to be averaged for each channel. The averaging compensates for the random noise component of the flat field imagery, helping for a more accurate generation of the LUT. This method of flat field correction can also be verified as effective in a few other studies (Hakala, Suomalainen, & Peltoniemi, 2010; Herrero-Huerta, Hernandez-Lopez, Rodriguez-Gonzalvez et

al., 2014; Kelcey & Lucieer, 2012), as they were also able to eliminate peripheral illumination deficiencies with high effectiveness.

CALIBRATING TO SURFACE REFLECTANCE

Many methods exist regarding the calibration of raw sensor data to surface reflectance values. The Empirical Line Method (ELM) uses in-situ targets of ground-measured reflectance for calibration to surface reflectance. It does this by extracting the DN (Digital pixel number values: expressed as intensity) values of the targets in the imagery and correlating them to the spectrometer-measured data of the targets. From this, a linear equation is calculated for each waveband, which can predict and convert DN pixel values to expressed reflectance absent of illumination and atmospheric effects (Vaudour et al., 2008). While this method has been widely used for the purposes of aerial and satellite imagery calibration (Moran et al., 2001; Vaudour et al., 2008), Berni et al. (2009), have used it for the calibration of higher resolution UAV-imagery. They placed 2 x 2 m leveled dark and white targets in the field, where measurements were taken with a field spectrometer in the spectral range of 350-1050nm (this covered the range of the multispectral sensor). They first calibrated the spectrometer with the Spectralon white panel: this panel make is commonly used in many studies for field spectrometer calibration. After this, the field was aerially imaged, and a linear equation was derived using the target pixel DN vs. target spectrometer values. Calibration coefficients can be derived from this and in turn be used to correct for the rest of the image, which was demonstrated in this study. The downside to this technique, much like the

method of Hakala et al. (2010), is that reflectance panels need to be present in each image. For large areas this presents a problem, as either an unfeasible amount of targets need to be placed or flights need to be conducted at higher altitudes. However, as shown by Smith & Milton, (1999), if other flat surfaces are present, they may be used as calibration targets where correction coefficients can be derived. A combination of concrete, asphalt and grass targets were collected for their in-situ spectral signatures and the ELM was used successfully (Smith & Milton, 1999). In summary, flat surfaces/targets are required so that bidirectional reflectance remains consistent throughout and between flights.

EFFECTS OF SOIL MANAGEMENT TYPE ON CROP HEALTH

The effects of fractional vegetation cover on vegetative indices can change depending on tilling practice (Huete, 1988; Huete et al., 1985). When full canopy coverage is achieved, variations in crop health may be observed due to inherent conditions within the field affecting crop health, such as differences in soil moisture (Huete et al., 1985). Since almost all remote sensing research exploring the detection of tillage practice focuses on soil and crop residue-based imagery, this section will explore the effects of tillage practice on crop health in general.

In general, soil tillage is considered an important factor in field crop management which affects soil properties and crop yield (Alam et al., 2014). Tillage is often performed for the purposes of controlling weeds and obtaining good tilth for seeding crops. Conversely, no-tillage practices also have benefits in the form of reduced time, labor, and increased fuel savings (Derpsch et al.,

2010). All crops under the no-tillage system can in fact be produced adequately and there has yet to be found a crop that would not grow under this regime (Derpsch et al., 2010). A modification of the no-tillage methodology is that of conservation tillage (no-tillage combined with crop residue from previous rotation). Much literature has shown that conservation tillage is one method which can significantly increase water content and water use efficiency in soil (Arshad et al., 1995; Lafond et al., 1992; Willis & Bond, 1971). Zero tillage with crop residue can increase water penetration due to reduced runoff and evaporation, thus conserving soil moisture for longer periods (Acharya et al., 1998; Baumhardt & Jones, 2002). A study by Ma et al. (2008) compared three different tillage systems (zero tillage, minimum tillage, conventional tillage), residue cover (with and without cover) and crop rotation (continuous cropping and rotation). For all three tillage treatments, soil water content was significantly higher with residue cover. Additionally, it was found that either no-tillage or minimum tillage combined with crop residue cover were the most viable options for farming practice. In Northwestern Ontario, the Thunder Bay Agricultural Research Station (TBARS) performed tillage experiments on a barley-soybean rotation from 2004 to 2007 (Sahota, 2008). These experiments evaluated 11 different tillage systems, stemming from the conventional, zero, and alternative tillage regimes. Two experimental plots were used which had previously been rotated with oats and clover, respectively; however, there were no significant effects on barley tillage regimes influenced from previous crops. The general findings reported were that conventional tillage regimes produced higher barley

and soybean grain yield than zero tillage. Alternative tillage (fall or spring disking, and spring cultivation) methods were however recommended over conventional tillage due to reduced labour and fuel consumption (Sahota, 2008).

UAV AGRICULTURAL RESEARCH

Lelong et al. (2008) were among the first to evaluate UAV multispectral imagery (blue: 420-510 nm, green: 490-580 nm, red: 570-650 nm, and near infrared: 720-850 nm) for the analysis of wheat crops. Sample plots were ground-truthed and measured for nitrogen and LAI, and spectral averages of plots were calculated. Lelong et al. (2008) were able to produce nitrogen uptake maps (highlighting nitrogen deficit and underdeveloped crops) for the whole field of wheat surveyed, with high precision. Higher accuracies were observed from mid-season to flowering stage, showing the difficulties in detecting nitrogen uptake heterogeneity in earlier growth stages. Berni et al. (2009) explored both thermal (40 cm resolution) and narrowband multispectral imagery (400-800 nm range, 20 cm resolution) acquired by a UAV over multiple different crop types. Results showed that biophysical parameters (biomass, chlorophyll, LAI) were able to be quantified with reasonable accuracy using multiple narrowband vegetation indices: NDVI, Transformed Chlorophyll Absorption In Reflection Index/Optimized Soil-Adjusted Vegetation Index (TCARI/OSAVI), and Photochemical Reflectance Index (PRI). Thermal data were also able to spatially identify areas of water stress with reasonable accuracy. Water stress was a topic of focus for Bellvert et al. (2014), who evaluated thermal UAV imagery of a “Pinot-noir” vineyard. Thermal UAV imagery were compared to

leaf-level thermal measurements. It was found that UAV-based thermal sensors with a resolution of 0.3 m were highly effective in estimating the spatial variability of water stress across the field. This was however a species-specific study, and nothing was explored towards the separation of water-stress with other stress-inducers.

In the area of fungal disease detection, very few studies exist exploring the utility of UAV imagery. A study by Calderón et al. (2014) examined high spatial resolution (20 cm/pixel) thermal and multispectral imagery to detect Downy Mildew (DM) infection. This research was conducted on two artificially infected opium poppy fields, where airborne thermal and multispectral imagery were acquired over three dates in 2009. The authors were able to relate canopy temperature and the green/red ratio to physiological stress. Additionally, they were able to use visible, red-edge and near-infrared spectral ranges for the classification of asymptomatic leaves. Red Edge-based NDVI was particularly useful in identifying between asymptomatic and symptomatic plants. Thermal was effective at monitoring for areas with water stress, which is a result of DM's impact of heightened transpiration rates in canopy leaves. For UAV hyperspectral imagery, a study by López-López et al. (2016) evaluated the early detection and quantification of almond red leaf blotch (*Prunus amigdalus*). They were particularly interested in the early detection of this foliar fungal pathogen, and therefore evaluated canopy-level imagery and related vegetation indices. They demonstrated a successful methodology for the early detection of almond red leaf blotch using UAV hyperspectral data. The utilization of hyperspectral

UAV data currently require complex methodologies (Gevaert et al., 2014); however, generally hyperspectral data are preferred due to the higher spectral resolution which allows for detailed spectral profile analyses and customized vegetation indices (Ashourloo et al., 2014; Mahlein et al., 2013).

INTRODUCTION

Fungicide effectiveness can be better understood if there is accurate knowledge regarding the spatio-temporal occurrence of in-situ stress. Traditionally, visual assessments have been conducted for the purpose of verifying the type of crop stress in a field. The weakness with this method is the infeasibility to spatially assess an entire field by foot. Larger fields inherently have more chance for assessment error—either by failing to recognize all varieties of in-situ stressors (e.g. fungal diseases), or for not locating secluded problem areas subject to stress/lack of productivity.

Remote sensing has long been identified as an effective way to spatially evaluate any heterogeneity in crop health, whether brought on from crop nutrient deficiency (Hedley, 2014), site-specific conditions related to soil (Anderson & Croft, 2009; Aubert et al., 2013; Buttafuoco et al., 2010; Klemas et al., 2014), crop disease and pest presence (Bauriegel, 2011; Yue et al., 2012), and recently weed presence (Armstrong, 2007; Eddy et al., 2014; Lopez Granados 2011; Rasmussen et al., 2013). Additionally, detected crop vigor constraints can potentially lead to decisions regarding fertilizer or herbicide application (Velandia et al. 2008), and fungicide application (Larsolle & Muhammed, 2007; Mahlein et al., 2012; Shaw & Kelley, 2005), which can be

generalized as management zone delineation (Chenghai Yang et al., 2013; Dewitte et al., 2012).

Fungal diseases are a well-known yield restrictor for cereal crops in Northwestern Ontario. Foliar fungal disease presence will often restrain the overall rate of plant development, impacting harvest time, total yield, and even grain quality (Mulla, 2014; Robert et al., 2004; Roermund & Spitters, 1990; Spitters et al., 1990). It is known that fungal diseases in general tend to occur in patches hard to spatially delineate without the aid of remote sensing techniques (Oerke, 1999; Oerke et al., 2005). Fungal infections are often unpredictable, and influenced by the arrival of airborne spores which reside in soil, from crop residue of previous rotations, and from weather conditions. Early treatment is required to prevent their spread which can be amplified by specific weather conditions such as from temperature (Murray et al., 1994; Park et al., 1992) and precipitation (Broscious, 1985; Hansen et al., 1994). As an example, leaf rust infections are correlated with temperature, which can be higher in areas of sparse vegetation cover (Dammer & Ehlert, 2006; Murray et al., 1994; Park et al., 1992). Also, raindrops are known to be capable of transmitting soil-born spores to cereal plant leaves, with some authors reporting a higher occurrence in areas of low LAI due to increased rain splash (Broscious, 1985; Dammer & Ehlert, 2006). The multiple factors which dictate the early development and spread of fungal diseases make them hard to spatially predict, and incidentally have influenced the wide use of broad spectrum preventative fungicides applied uniformly across fields. Unfortunately, fungicides in Northwestern Ontario are

costly and could have negative environmental effects (West et al., 2003). As such, the notion of site-specific treatment has garnered much interest amongst local farmers. Typically, fungicides are sprayed at specific timings related to a crop's phenological development. Disease control in cereals often focus on fungicide application to the upper three leaves, as these are the main contributors to yield production (West et al., 2003). Switching to fungicides that are spatially applied to infected crop areas require accurate detection of in-situ disease in its early stages of development.

In remote sensing literature, much is already known regarding the spectral response of foliar fungal disease. In general, pathogens reduce chlorophyll content in what are described as necrotic or chlorotic lesions, affecting spectral reflectance in the Visible (VIS: 400-650 nm), Red-Edge (RE: 650-720 nm) and Near Infrared (NIR:720-900 nm) regions of the electromagnetic spectrum (Blazquez & Edwards, 1986). This reduction in chlorophyll is caused by early senescence of infected lesions which often appear as browned or darkened spots for rust (leaf rust, crown rust or stripe rust), and blotch (spot blotch, net blotch, septoria) disease varieties (Franke & Menz, 2007). A canopy's spectral properties are known to also change with increased fungal disease presence. Much like spectral observations at the leaf level, canopy reflectance will change in certain portions of the VNIR (visible to near-infrared) spectrum when under stress (Gitelson et al., 2005). The difficulty in detecting chlorophyll at the canopy level, while indirectly detecting for stress presence, is that canopy reflectance is strongly affected by other factors, such

as canopy architecture, soil background, and LAI (Gitelson et al., 2005). Several past studies have managed to establish relationships with the biophysical properties of crops, when evaluating canopy-level remote sensing imagery. In-situ parameters such as chlorophyll (Gitelson et al., 2005), grain yield (Cao et al., 2015), nitrogen uptake (Fitzgerald, 2010; Schlemmer et al., 2013), and even biomass (Moges et al., 2004) have been verified as quantifiable with reasonable accuracy at the canopy level. Since a reduction in chlorophyll is linked to phenomenon such as nitrogen uptake, changing leaf area index (LAI) and biomass (Bojović & Marković, 2009; Daughtry et al., 2000; Gitelson et al., 2005), indirect linkages may be drawn between such observed phenomenon as fungal disease presence at the canopy scale. The unavoidable issue with this is the necessity of ground-truthing to verify the source of in-situ stress. However, for intensive field crop management regimes where soil moisture is controlled with drainage tiles, and fertilizer is spatially applied, this method for spatial fungal detection may be applicable.

A critical review of the literature revealed that most past remote sensing methodologies utilize workflows adapted for space-based sensors and course resolution datasets. An exciting and seldom explored topic in current scientific research will explore the utilization of high spatial resolution unmanned aerial vehicle (UAV) data sets to assess fungal disease at the canopy level. Since not much is known on the subject, it is desired to evaluate how such data sets may improve upon previously reported spatio-temporal accuracies for fungal disease detection. The limitations in space-based platforms and manned aircraft are well

known. Particularly, they are hindered by course spatial resolution, high costs of image acquisition and poor revisit times. UAVs propose an alternative platform with high potential towards precision agriculture applications. Primarily, such aerial platforms offer temporal flexibility towards preferred operational flight times, are unhindered by cloud interference, can be flown at low altitudes allowing for high spatial resolution data sets, and accommodate the use of GCPs which allow final orthomosaic products to be registered with high geometric accuracy. Such high geometric accuracy allows for accurate spatial mapping products which may be adapted for ground-based precision spraying equipment. UAV technology has progressed considerably over the past few years, and now such platforms are highly reliable, user-friendly and affordable. Sensor technology has also progressed with regards to UAVs, and now we are seeing advanced sensors designed specifically for precision agriculture. The majority of lightweight, affordable sensors in 2016 have VNIR (Visible to Near-Infrared) multispectral parameters. The application of such sensors in operational farm fields for precision agriculture has seldom been explored. Thus, multispectral UAV data are currently a topic of scientific interest in both academia, and industry. Hyperspectral sensors are generally considered to be more accurate and effective than multispectral counterparts due to the increased spectral resolution and contiguous bands (Ashourloo et al., 2014; Mahlein et al., 2013). However, the technology is still expensive and the data from such sensors are currently infeasible for conventional image processing solutions. Since there is currently very few publications on UAV multispectral

imagery, specifically for the detection of fungal disease, there is novelty and great interest in this specific topic.

MULTISPECTRAL FUNGAL DETECTION OF CEREALS

In general, multiple remote sensing publications have noted the difficulties in detecting between symptomatic and asymptomatic fungal-infected leaves during early growth stages (Ashourloo et al., 2014; Devadas et al., 2015; Devadas et al., 2008; Franke & Menz, 2007; Qin & Zhang, 2005). In particular for cereal crops, very few studies exist which explore the use of high resolution multispectral data sets for the detection of fungal diseases. To date, sub-millimeter UAV multispectral data have been examined for the successful detection of canopy chlorophyll levels in cereal rye (Hunt, 2014). Since a reduction in chlorophyll has been documented from pathogens such as leaf rust (Robert et al., 2005), the study by Hunt (2014) shows promise towards indirect fungal disease detection measures. Lelong et al. (2008) explored UAV multispectral imagery (Blue:420-510 nm, Green:490-580 nm, Red:570-650 nm, NIR:720-850 nm, 10 cm/pixel) for the quantitative monitoring of wheat biophysical parameters in plots. While the authors did not specifically explore the detection of fungal disease, they were able to establish a relationship between nitrogen uptake and the green normalized difference vegetation index (gNDVI). Since nitrogen uptake is known to have an indirect relationship with chlorophyll content at the canopy scale (Schlemmer et al., 2013), this study shows some potential in detecting chlorophyll response to fungal presence with UAV multispectral imagery. Quickbird-2 multispectral imagery (Blue:450-520

nm, Green:520-600 nm, Red:630-690 nm, NIR:760-900 nm, 2.4 m/pixel) have been used for the detection of early leaf rust and powdery mildew (*Blumeria graminis*) development in wheat, related to different fungicide application intensities (Franke & Menz, 2007). In this particular study the authors noted difficulties in the early detection and spectral separation of symptomatic and asymptomatic plots. However they were increasingly successful in detecting between fungicide application intensities as the season progressed.

EXPERIMENT

An in-depth review of the literature has indicated that more needs to be understood regarding how effectively fungal disease can be spatio-temporally delineated with UAV multispectral imagery. Notably, no known studies have evaluated the spectral response of barley with UAV multispectral imagery. As indicated in the literature review and briefly in the introduction, a handful of studies have evaluated wheat field crops with UAV multispectral imagery. Positive results have been seen with regards to the separation of fungal disease intensity in wheat with multispectral satellite imagery (2.4 m/pixel with broad bands in the VNIR) as early as Feekes 10.4 (Franke & Menz, 2007). However, a recent study in Northeastern Ontario has shown that a difference in spectral reflectance exists between barley and wheat, allowing them to be effectively separated throughout multiple stages of their phenology (Wilson et al., 2014).

Local farmers in the Thunder Bay region have expressed interest in the spatial detection of fungal diseases in barley, which is one of the important forage, feed and malt crops. Amongst major field crops in Thunder Bay, Barley

contributes the highest towards the provincial total, at 3.53% (Statistics Canada, 2011). Two farms provided operational barley field crops for this experiment, detailed in the methodology section (Pg. 33). Each field was managed differently (till vs. no-till), and was treated with 3 different levels of fungicide intensity. The spectral response of barley was then monitored over four growth stages with UAV multispectral imagery.

HYPOTHESIS AND RESEARCH QUESTIONS

Further detailed in the methodology, multiple UAV flights were performed over each field covering four general growth stages for barley: GS1 (Feekes 8-9), GS2 (Feekes 10.51), GS3 (Feekes 11.2), GS4 (Feekes 11.4). The Feekes Growth Scale for cereals, first introduced by Large (1954), was used to describe the phenological development of barley. Three treatments were applied: No-Fungicide/Control (C), Stratego (S), Stratego + Prosaro (SP).

In this experiment, the dependent variable (DV) tested is spectral response, represented as five vegetation indices (VI): Normalized Difference Vegetation Index (NDVI), Red Edge Normalized Difference Vegetation Index (RE-NDVI), Renormalized Difference Vegetation Index (RDVI), Red-Edge Renormalized Difference Vegetation Index (RE-RDVI), and Triangular Greenness Index (TGI). The effectiveness of these indices will not be tested against each other, rather, the ability to distinguish fungal disease severity with be considered regardless of VI type. The independent variables (IV) are represented as Field, Growth Stage, and Treatment. The models for this

experiment may be viewed in the Methodology section (Pg. 63-64). The null hypothesis (H_0) and alternate hypothesis (H_a) are as follows:

H_0=The Spectral response (VI) of barley fungicide treatments (Control, Stratego, Stratego + Prosaro) cannot be distinguished between fields and growth stages (GS2, GS3, GS4), when evaluating UAV multispectral imagery (Blue- 475 nm +/- 20 nm, Green- 560 nm +/- 20 nm, Red- 668 nm +/- 10 nm, Red Edge- 717 nm +/- 10 nm, Near Infrared- 840 nm +/-40 nm; 64-bit depth tiff format) of 6.7 cm/pixel spatial resolution.

H_a= The Spectral response (VI) of barley fungicide treatment levels (Control, Stratego, Stratego + Prosaro) can be distinguished between fields and growth stages (GS2, GS3, GS4), when evaluating UAV multispectral imagery (Blue- 475 nm +/- 20 nm, Green- 560 nm +/- 20 nm, Red- 668 nm +/- 10 nm, Red Edge- 717 nm +/- 10 nm, Near Infrared- 840 nm +/-40 nm; 64-bit depth tiff format) of 6.7 cm/pixel spatial resolution.

To accompany and expand discussion from the main hypothesis, multiple research questions were formed:

How early can fungal infection severity be distinguished during the growth season for barley?

If alternative stress sources appear during the season in ground-truthing plots, can the multispectral sensor distinguish between types of stress in those respective plots?

Did soil management regimes affect the 3 way interaction of Growth Stage and Treatment between different Fields?

MATERIALS AND METHODS

SITES AND CONDITIONS

A single experiment was conducted in Thunder Bay, ON, Canada, from July 7th to August 31st 2015. Two locations, Trumar Farm (UTM Zone 16U, 318033E, 5352745N), and Hanna Farm (UTM Zone 16U, 318002E, 5355909N) provided operational barley fields for this experiment. Trumar Farm (20.64 Hectares) is a dairy farming operation, with manure application to fields during the fall. Hanna Farm (10.12 Hectares) is a cash cropping operation, without any manure availability or application. Trumar Farm's field is intensively managed, which is tilled (Alternative Tillage: fall disking, spring cultivation), measured and annually treated for variable soil nutrient deficiency levels by a local crop consultant. Soil optimum levels are maintained based on Cation Exchange Capacity (CEC) and are monitored for available Phosphorus (P), Potassium (K), Calcium (C), Magnesium (Mg), among a suite of other nutrients. Additionally, drainage tiles are present throughout the whole field, giving relatively homogeneous levels of moisture. Hanna Farm's field is less-intensively managed. No tilling takes place, and there are no variable rate control measures taken for soil nutrients on this site. There are also drainage tiles present in Hanna Farm, which allow for a consistent moisture level throughout the field. Both fields

have similar soil types, being a silty clay loam composition. In Hanna Farm, at the northern-most extent of Figure 1 (left image) the field was blocked off to avoid drastic changes in elevation and moisture. Thus, the extent of observations taken from this field maintain a fairly consistent elevation. Based on local research from the Thunder Bay Agricultural Research Station (TBARS), each field was seeded mid-May 2015 with the Spring Barley (*H vulgare* L.) cultivar 'Synasolis' due to its positive growth response in the Thunder Bay district. Seed row-spacings were 7.5 inches at Trumar Farm, and 7 inches at Hanna Farm. Full canopy closure was expected for both crops. Also, both fields have experienced regular rotation of crops season-to-season. Trumar Farm was previously rotated with Soy (*Glycine max* L.), and Hanna Farm was rotated with wheat *(Triticum* L.). The weather for 2015 was average for the region of southern Thunder Bay, detailed below in Table 1. August 2015 had the highest amount of precipitation during the growth season of barley both at Hanna and Trumar Farms.

Table 1. Weather data recorded at the Thunder Bay Agricultural Research Station (TBARS) for 2015.

Weather 2015					
Month	Precipitation (mm)	Max Temp (°C)	Min Temp (°C)	Growing Degree Days (GDD)	Corn Heat Units (CHU)
May	104.4	25.0	-7.0	78	188
June	104.4	27.6	-2.0	219	384
July	90.8	29.0	3.0	327	552
August	121.8	29.0	2.0	309	510
Total/Mean	421.4	27.7	-1.0	933	1634

*Fields are approximately 2.5 km apart from one another. Trumar Farm is 4.9 km from TBARS; Hanna Farm is 5.6 km from TBARS.
TBARS Annual Report (2015).

Figure 1. Hanna Farm treatment rows delineated in black (left), Trumar Farm treatment rows delineated in black (right). Visual assessment plots are outlined by the thick asterisks, GCPs are indicated by the thin asterisks (not all GCPs are visible). C=Control; S=Stratego; SP= Stratego + Prosaro. Not to scale.

TREATMENT EFFECTS AND PLOTS

The purpose of this experiment was to determine if multispectral observations of barley from two different crop management regimes, at changing growth stages, could be used to differentiate between fungicide

treatment types and visual disease assessments. To introduce heterogeneity into the two fields, 1 treatment with 3 levels was applied:

1) No Fungicide (control), 2) Stratego, 3) Stratego + Prosaro. In brief, both Stratego (Propiconazole and Trifloxystrobin) and Prosaro (Prothioconazole and Tebuconazole) are broad spectrum fungicides aimed at controlling foliar and head fungal diseases of wheat and barley. In applying different treatments, different health levels were expected between rows, along with differing levels of fungal disease and crop stress susceptibility. Each treatment type was applied 3 times, in each field (9 rows per field). The width of rows was dictated by the sprayer boom width. At Trumar Farm, rows were 90 feet; Hanna Farm rows were 75 feet. All rows were sprayed in the evening when there was minimal wind in attempt to mitigate potential cross-contamination between treatment strips. Herbicide was initially blanket sprayed across both fields when there was evident weed emergence, on June 26, 2015 (Feekes 4), after tiller formation. Subsequently, at Feekes 8-9, Stratego was randomly sprayed on six of nine rows for each field (see Table 1 for specific dates). Stratego is recommended to be applied at the four-leaf stage in barley (Feekes 4); however, due to rainfall events the application was delayed until Feekes 8-9 for this study. Shortly after, Prosaro was randomly sprayed along three of six rows previously treated with Stratego, at Feekes 10.51 for each field (Table 2).

Table 2. Data acquisition dates and relative barley growth stages for respective fields, during spring-summer 2015.

Flight	Date	Farm Field	Growth Stage
N/A	July 7, 2015	Hanna & Trumar	Feekes 6-7
F1*	July 15, 2015	Trumar	GS1: Feekes 8-9
F1*	July 22, 2015	Hanna	GS1: Feekes 8-9
F2 **	July 28, 2015	Trumar	GS2: Feekes 10.51
F2 **	Aug 5, 2015	Hanna	GS2: Feekes 10.51
F3	Aug 14, 2015	Trumar	GS3: Feekes 11.2
F3	Aug 21, 2015	Hanna	GS3: Feekes 11.2
F4	Aug 27, 2015	Trumar	GS4: Feekes 11.4
F4	Aug 31, 2015	Hanna	GS4: Feekes 11.4

** Stratego application date. Note that herbicide (control) was already sprayed previously.*
*** Prosaro application date.*

To visually verify evidence of ground-level barley disease, 3x3 m plots (2 per treatment row, 18 per field) were randomly assigned, and marked with flags at each corner. These flags were placed close to the middle of each row to avoid any potential spray drift effects during treatments. Each flag's respective coordinates were recorded using an RTK GPS (Real Time Kinematic Global Positioning System) unit, with a horizontal accuracy of +/- 2 cm. Disease was rated using a Standardized Area Diagram (SAD), as it has been reported in previous research to reduce rater bias for disease scoring (Bock, 2010; Nutter, 1990). Since there was more than one rater for this experiment, SADs were chosen to reduce bias. Diseases were rated in a percentage score based on surface area of infected flag leaf tissue (Figure 2), and recorded in the field with an electronic tablet. When there wasn't a flag leaf present the uppermost leaf

was rated (GS1: Feekes 8-9). Twenty scores per corner were recorded from eighty randomly chosen plants within each enclosed square plot (80 total/plot). All spectral observations from UAV imagery were later clipped and extracted using the RTK GPS coordinates for the respective treatment plots, and later compared to the disease assessment scores.

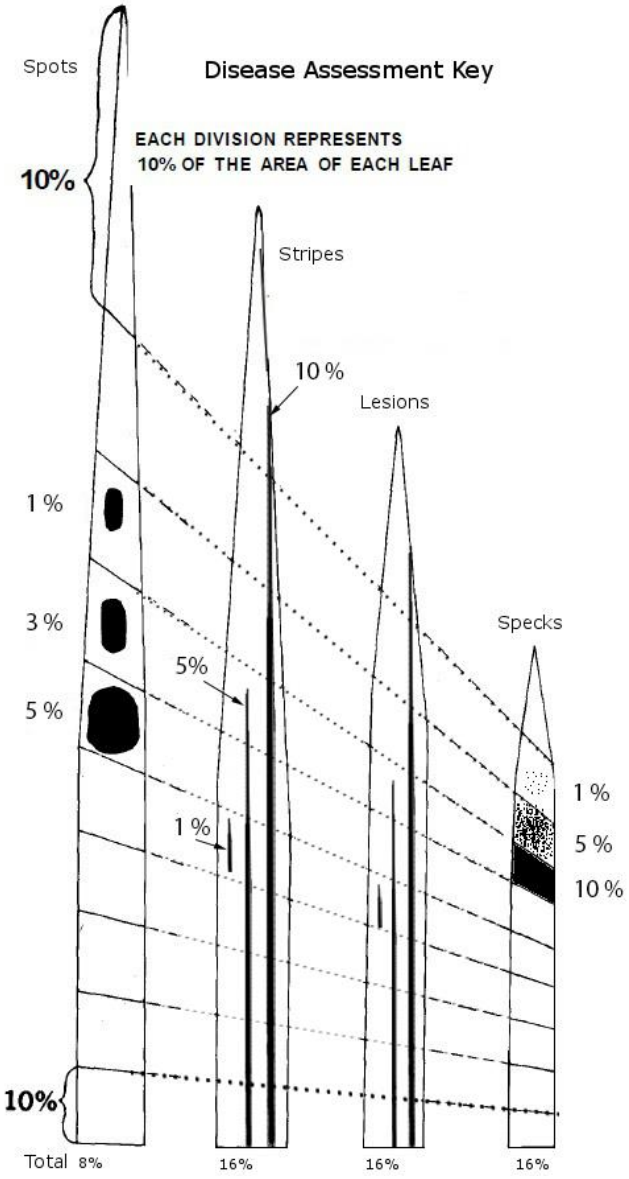

Figure 2. Standardized area diagram for barley and wheat leaves, modified from Bock (2010).

EQUIPMENT AND FLIGHTS

Four flights per field were conducted between July 15th (Feekes 8-9) and August 31st, 2015 (Feekes 11.4). These were divided into four general growth stages: GS1: Feekes 8-9, GS2: Feekes 10.51, GS3: Feekes 11.2, GS4: Feekes 11.4 (Table 2). It was infeasible to consistently monitor all growth stages and perform flights at exactly the same phenology due to the remote location of the farms, different seeding times and management regimes. Since Trumar Farm seeded their field one week ahead of Hanna Farm, most flights were conducted on alternating dates for respective fields. This allowed for observations of similar Feekes growth stages between fields. The Observer-6 Hexacopter (OB-6) was deployed (Figure 3), fitted with the Micasense 5-channel multispectral sensor (Blue- 475 nm +/- 20 nm, Green- 560 nm +/- 20 nm, Red- 668 nm +/- 10 nm, Red Edge-717 nm +/- 10 nm, Near Infrared- 840 nm +/-40 nm; 64-bit depth tiff format). The OB-6 is capable of performing preprogrammed flight paths, and based on sensor field of view, flew with 85 % overlap along the entirety of each field. Flight altitude was maintained at 100 metres, which allowed for a spatial resolution of 6.7 cm/pixel. The sensor was affixed to a gimbal and pointed at nadir for each flight.

Figure 3. Observer-6 (OB-6) hexacopter (0.5 m frame) equipped with the 5-channel multispectral sensor (Micasense). Hanna Farms, SW Corner, July 22nd, 2015.

RADIOMETRIC CORRECTIONS

SURFACE REFLECTANCE

Corrections for both vignetting and surface reflectance were done using proprietary algorithms and software provided by Micasense Inc. The extent to which these corrections can be detailed is limited due to intellectual property rights. To radiometrically correct pixel data to surface reflectance, a black and white reflectance calibration tile (Lambertian surface) was imaged with the Micasense before and after each flight. The Empirical Line Method is well suited for radiometric calibration of remotely sensed imagery (Berni et al., 2009; Vaudour et al., 2008). This method was used in proprietary software where in-

situ tile reflectance values were compared to lab-measured spectrometer values. With these data, a linear equation was derived to predict pixel intensity values as surface reflectance across the orthomosaics.

The limitation to the Micasense methodology for radiometric correction is that it necessitates consistent illumination before and after imaging Lambertian surface reflectance tiles. This caused some issues in the data, which forced further radiometric corrections to be applied (see Histogram Matching section). Final orthomosaics were generated in the Atlas cloud server by stitching all single-frame geotagged images (5-band composites) together and averaging any overlapping pixel values. Vignetting and radiometric surface reflectance calibration algorithms were performed just before stitching to achieve a balanced scene. Further methods for noise correction, geometric correction, and histogram matching are detailed in the proceeding subsections. The effects of atmosphere were not corrector for. A study by Herrero-Huerta et al. (2014) showed that atmospheric effects on aerial multispectral imagery captured at two different altitudes (145 m and 245 m) were insignificant. Thus, for this study, no corrections were made for atmospheric effects.

THE MINIMUM NOISE FRACTION (MNF) TRANSFORM

It is well known that multispectral imagery carry similarities among pixel data between adjacent narrow bands (Avena et al., 1999). Statistical data compression tools such as principal component analysis (PCA) are effective for decorrelating such information and redistributing image data content. Additionally, PCAs are good for reducing the amount of redundant information,

which could otherwise impact image classification accuracy. Typically a PCA will be conducted to linearly produce a new set of bands where information content is secluded, and no correlation exists among components/bands. In a multispectral or hyperspectral dataset, the number of principal components are equal to the total number of bands. These are arranged in such a way that the first component accounts for the maximum proportion of the variance in the original dataset, and subsequent orthogonal components account for the maximum remaining variance reducing until the final component is computed (Demšar et al., 2013). The higher/final principal components in multispectral imagery are typically representative of soil background or sensor noise (Piwowar & Millward, 2002); however, this is not always reliable, and it would be more-so desired to produce components that subsequently and reliably reduce in image signal quality (Green et al., 1988).

The Minimum Noise Fraction (MNF) transform is a technique first introduced by Green et al. (1988), which maximizes the signal-to-noise ratio with increasing components. It consists of two consecutive principal component transforms: the first to identify noise content and the second is to remove it, while reducing the dimensionality of the original dataset. The resulting MNF transform image will typically have the same number of bands as the input image, unless there was a sub set performed. The first few components often have higher eigenvalues associated with high signal quality and low noise, and the last components approach an eigenvalue of 1, representing high noise/low signal quality. The original development of the MNF transform technique by

Green et al. (1988) was purposed for improving the PCA noise reduction capability in multispectral data sets. However, most literature featuring the MNF transform uses hyperspectral data sets due to the high proportion of noise presence amongst bands. Yang & Everitt (2010) evaluated hyperspectral and multispectral imagery for the classification of broom snakeweed (*Gutierrezia sarothrae*). They performed the MNF using ENVI software (ITT Visual Information Solutions, Boulder, CO) to reduce the high spectral dimensionality and inherent noise in the hyperspectral dataset. They were able to eliminate redundant bands dominated by noise in order to improve the classification accuracy (Yang & Everitt, 2010). Mitchell et al. (2012) used the MNF transform for similar purposes, improving the classification accuracy of UAV hyperspectral imagery for dryland vegetation monitoring.

For this study, both MNF transform and Inverse MNF transform were performed for all final orthomosaics (Figure 6). After a MNF transformation is performed, it is often desirable to reconstruct the data back to its original space without the isolated noise channels. This process is called an Inverse MNF transform. Before performing the Inverse MNF transform, either smoothing (low-pass filter technique) or band elimination (subsetting) must be conducted on the noise-dominated components from the MNF transform output (Figure 4). For this study, most noise was able to be secluded to the 5^{th} component for all flights (Figure 5). A subset was created with the first four components from each scene, and further transformed back into its original five-band space as an Inverse MNF transformed image.

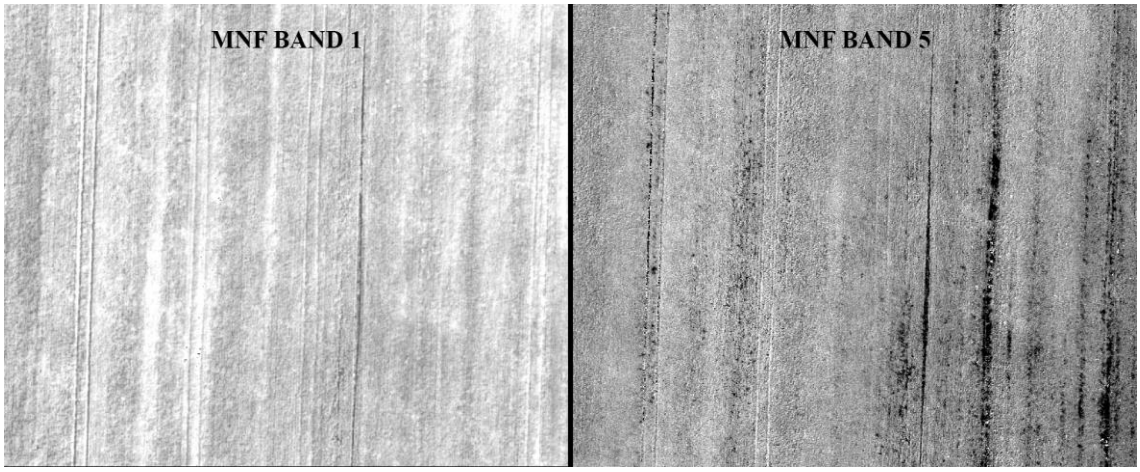

Figure 4. Maximum Noise Fraction (MNF) Transform for July 22nd, 2015. Band 1 (left) is shown with the lowest signal-to-noise ratio, and Band 5 is shown (right) with the highest signal-to-noise ratio.

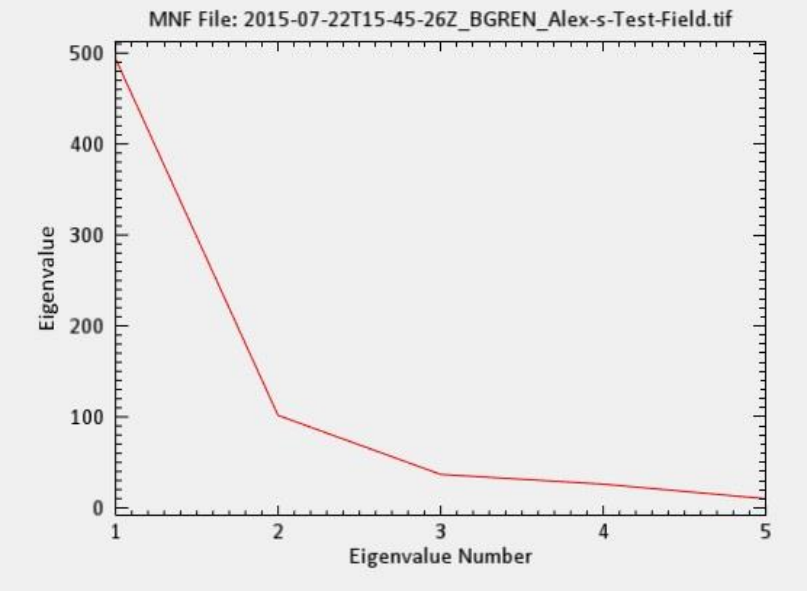

Figure 5. Eigenvalues (Y-axis) and Eigenvalue Numbers/Bands (X-axis), for July 22nd, 2015 scene. The eigenvalue approaches 1 at the 5th band, showing a high degree of noise presence.

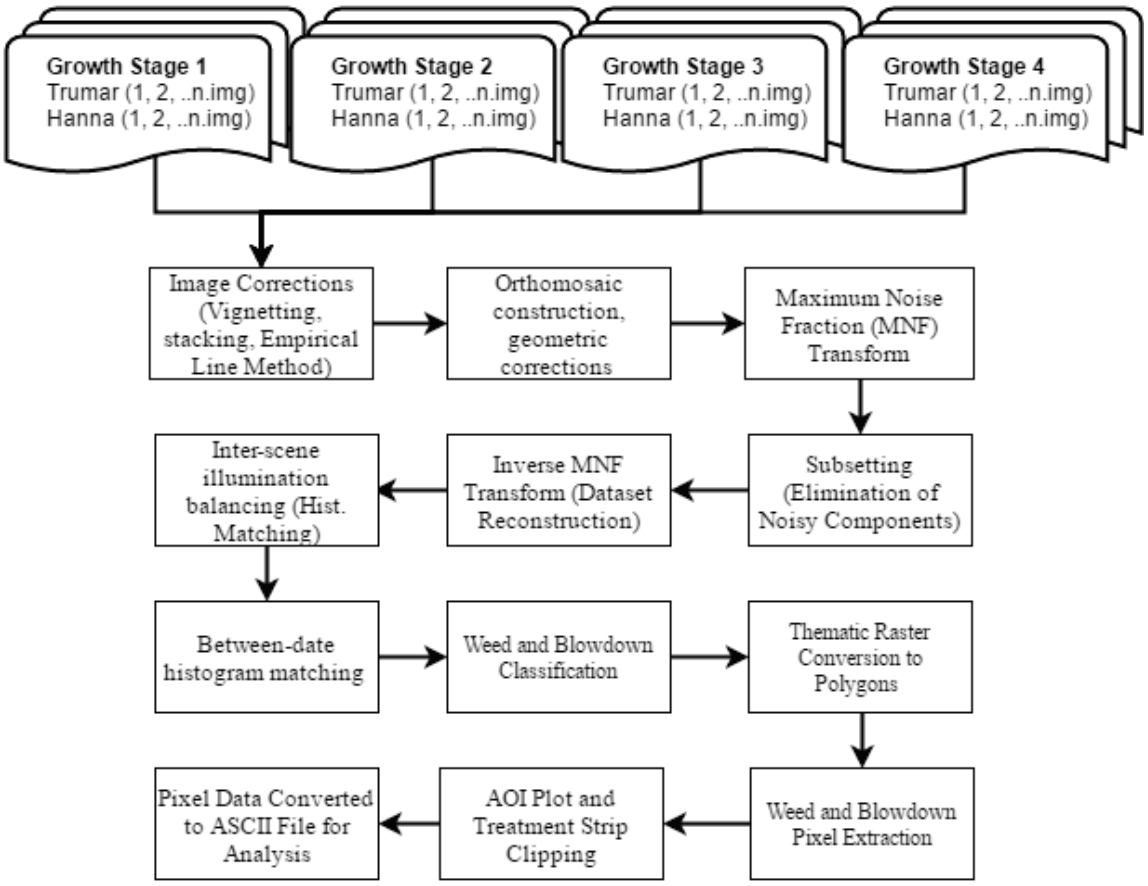

Figure 6. Image correction process, including initial radiometric corrections to surface reflectance, noise removal, inter-scene and between-date histogram matching and pixel data extraction from AOI clips.

GEOMETRIC CORRECTIONS

While the raw imagery were geotagged by the GPS unit built into the OB-6, the accuracy of +/- 5 m was unacceptable for performing precise image clipping. Additionally, since the visual assessment plot flags were assigned RTK GPS coordinates, it was necessary to register each orthomosaic to the same accuracy. Due to canopy coverage, the flags could not be visually located in the imagery which necessitated the use of ground control points (GCPs). The GCPs took the form of concrete tiles (18 x 18 inches), painted with a checkered black and white matte paint design. Multiple GCPs were placed along the perimeter of

each field, and measured in the centre with the same RTK GPS unit. The same geodetic survey benchmarks were used to record points for both the GCPs and plot flags.

HISTOGRAM MATCHING

This step in radiometric scene balancing employs the relative radiometric normalization approach. The method is preferred because input parameters requiring sun angle positioning, cloud cover or acquisition time are not required (Hong & Zhang, 2008). A popular technique within the relative radiometric normalization methodology is that of histogram matching. Histogram matching is a radiometric enhancement technique which uses a reference image (radiometric master) to modify the histogram of a slave image. This process makes the slave image's histogram distribution similar to that of the reference image. Thus, the normalized slave image will appear to have been captured under similar atmospheric and illumination conditions to the master (Hall et al., 1991). Chavez & Mackinnon evaluated the ability to automatically detect temporal vegetation changes in remotely sensed satellite imagery. Importantly, they noted that when comparing between-date histogram match results between static targets (i.e. pavement) and changing vegetation (crop rotations and phenology change), there were little differences. Although vegetation reflectance can change between dates, the overall dynamic range and distribution of reflectance remained stable. DN values changed very little between scenes and AOIs, allowing for comparisons of temporal vegetation change expressed by NDVI (Chavez & Mackinnon, 1994).

While all final orthomosaics were initially corrected to surface reflectance, there were a few scenes that experienced minor illumination imbalances, mainly due to unexpected cloud cover during flights. In order to ensure all images retained similar spectral characteristics, further radiometric correction was necessary. First, inter-scene histogram matching was performed to ensure consistent illumination over each scene. Scenes from July 15th & 28th, August 5th & 21st were acquired over the unfavourable conditions of partial cloud cover. The Micasense Atlas software had issues in processing that necessitated further inter-scene corrections. Within an individual scene, targets were selected for histogram matching. Target selections were based on sun illuminated areas from fungicide treatment AOI (masters) and cloud-covered areas of the same treatment type (slaves) (Figure 7). After inter-scene histogram matching was performed, only between-scene histogram matching was performed for the July 15th orthophoto (Trumar Farm). Before matching the scene, band alignment had to be performed. Since the Trumar Farm GS1 scene was the only scene manually processed, extra steps were required to create a georegistered orthomosaic with composite bands. The 5-band orthomosaic was generated using Agisoft Photoscan. The bands were slightly misaligned; thus, manual alignment was conducted in Adobe Photoshop. This utilized the differential filter and warp transform functions to perfectly align the bands before stacking. Finally, the Trumar Farm GS1 image was matched to the Trumar Farm GS2 scene (Master) to equalize the lighting conditions for this date.

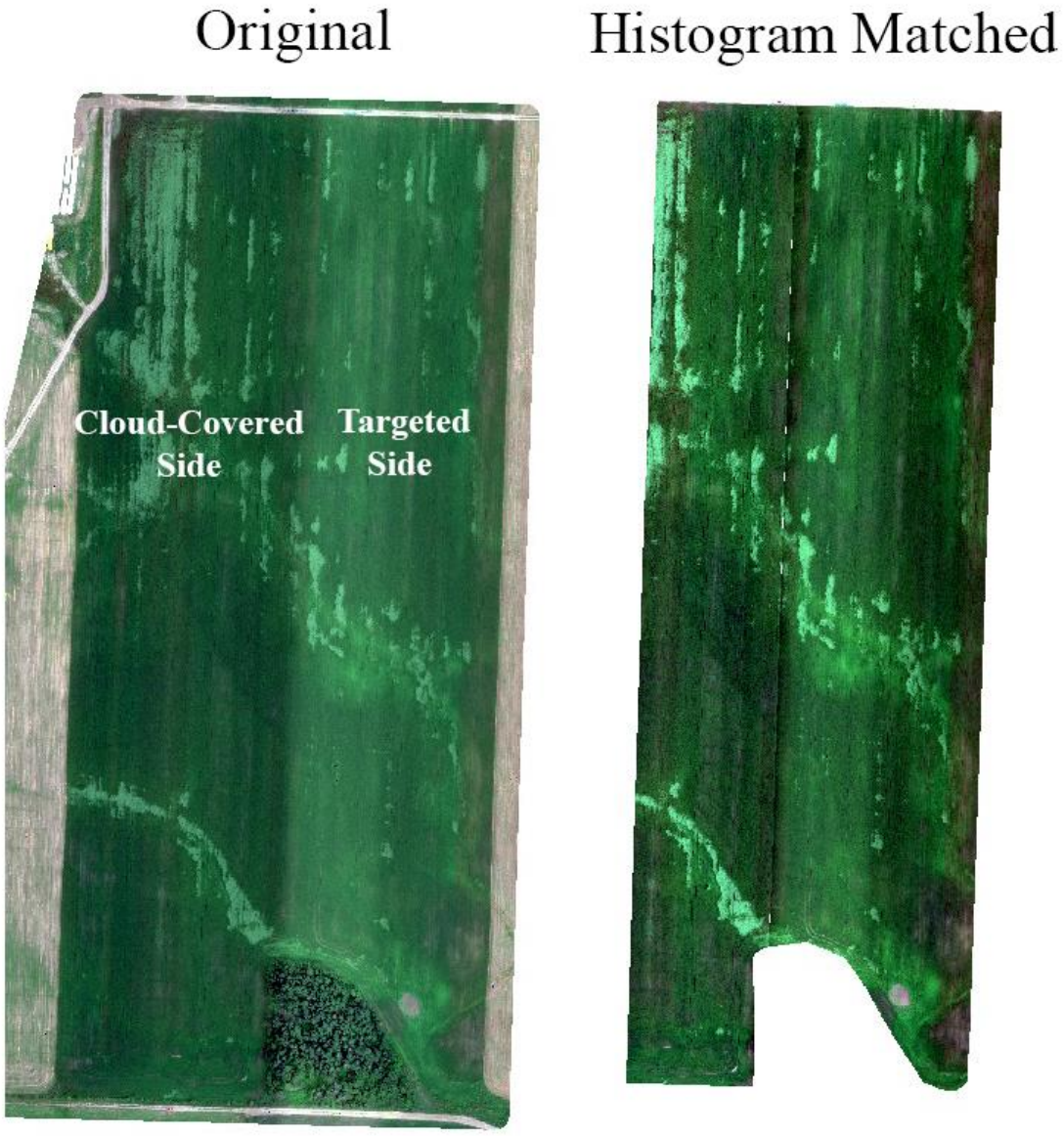

Figure 7. Histogram match of Trumar Farm scene from July 28th, 2015. The targeted side (master) and cloud-covered side (slave). A histogram match was then performed (right side) matching the slave to the master.

WEED PIXEL CLASSIFICATION AND EXTRACTION

Presented here is a new methodology regarding the classification, isolation and extraction of weed pixels from a barley crop scene. Recall that herbicide (Control Treatment) was blanket sprayed over each field in order to prevent the dominance of multiple weed species throughout the season. For Trumar Farm, minimal to no weed presence was documented in VA plots throughout the entire season. This was attributed to both the effectiveness of the herbicide, to the slim row spacings, complete canopy closure, and also to the implementation of alternate tillage methods. Despite the same control treatment being applied at Hanna, weeds still emerged in patches throughout the field. Multiple weed species were documented, with the most dominant being clover infestations in the north portion of the field (Figure 8 & 11). The clover infestation was first spotted on July 7th, 2015 (Feekes 6). Subsequently, as the season progressed, the onset of senescence in barley was observed on August 5th, 2015, in the north portion of the field. The barley in this section had been almost completely killed by August 22nd, 2015. Fortunately, only one VA plot appeared in the clover-infested area of Hanna Farm. Most other VA plots were unaffected by weeds, and documented as having minimal to no weed presence. Other sections of the field, primarily tram lines, were affected with clover outbreak, which made necessary the spectral extraction of infestation areas.

Some authors have used object-based segmentation procedures to extract weeds based on the orientation of crop rows (Peña et al., 2013).

However, since weeds occurred in patches, and in cases entire sections of Hanna Farm, this method was inapplicable. In general, weeds and crops display similar spectral reflectance characteristics in the early growth stages (Lopez Granados & López Granados, 2011; Peña et al., 2013; Torres Sanchez et al., 2013). This has posed a huge problem for multiple researchers attempting to isolate weeds for site specific weed management practices. An alternative method proposed here works well for weeds with distinguished contrast in color when compared to field crops. A PCA band subtraction method was developed in order to distinguish vegetation types at the canopy level. In brief, the components from PCA analysis were able to effectively separate vegetation types more robustly than conventional supervised classification methods. The components of the PCA were analyzed and subtracted (PCA1-PCA2) to obtain an output where darker areas were associated with clover outbreak. From this, Erdas Imagine Knowledge Engineer was used to perform a decision tree classification for pixels of low intensity. The resulting thematic layers (Figure 8) worked well for isolating clover from barley.

A simple accuracy assessment was performed for each image date by clipping AOI containing only barley and clover pixels. One hundred equalized random points were generated (50 per class) for two classes: barley and clover. The orthomosaic images were used as reference data to determine classification accuracy of the thematic data. From GS1 to GS4, the overall classification accuracy was > 84 % for all data. Before conducting spectral analysis of both treatment strips and plots, the classified clover data were used

to clip out pixels from the original raster data to avoid spectral contamination. Figure 10 shows the final orthomosaics containing clipped out features of classified clover, and Figure 8 shows a close-up of the classification.

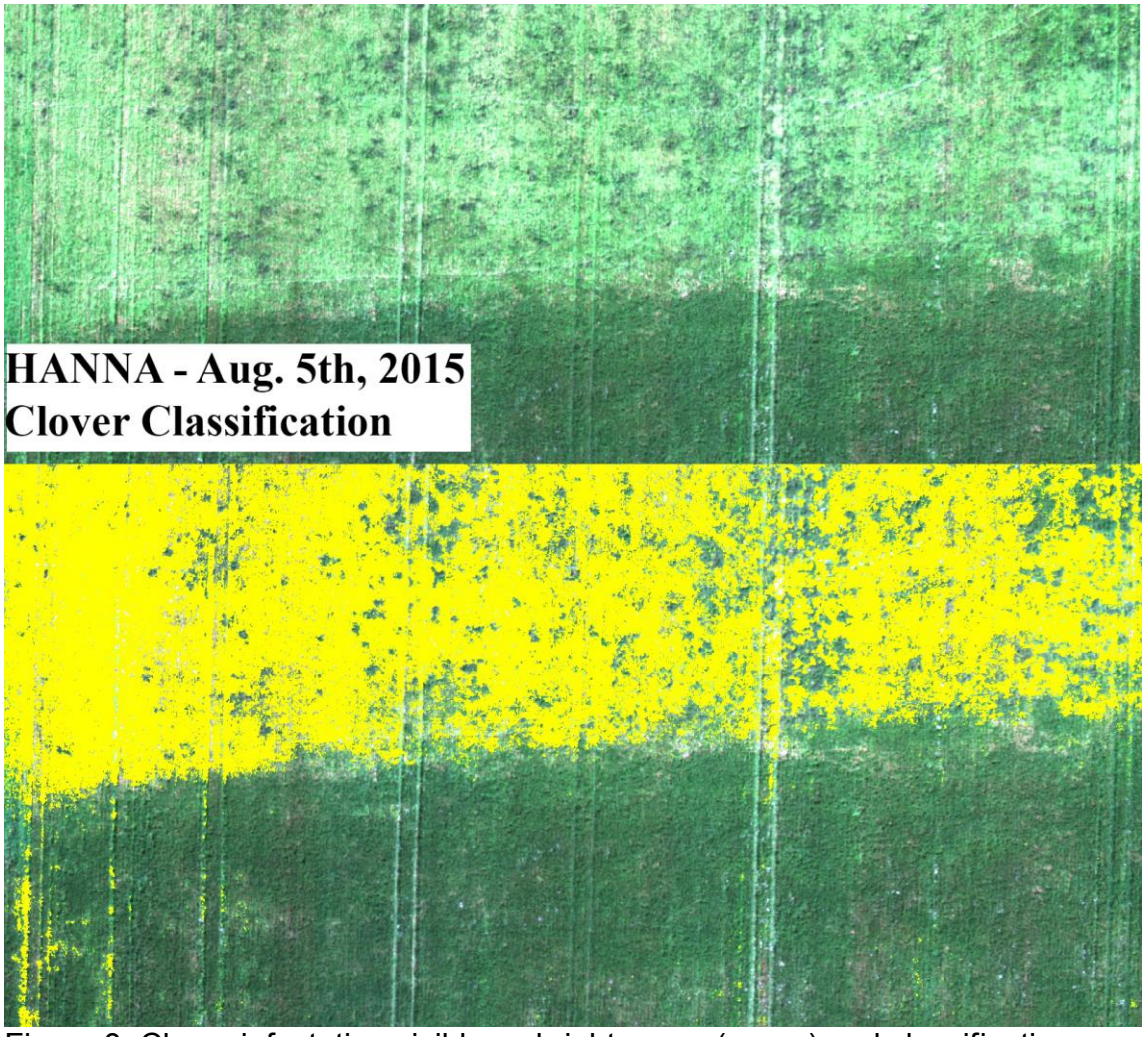

Figure 8. Clover infestation visible as bright green (upper) and classification as a yellow thematic layer (lower).

CROP BLOWDOWN PIXEL EXTRACTION

A severe wind event occurred on July 24th and 25th, 2015 which caused crop damage to Trumar Farm with winds up to 30 km/h. The damage was first initiated as small isolated patches of blown-down barley, and eventually spread

as the season progressed. When visual assessment (VA) plots were affected by blowdown, new plots were set up by measuring precise distances from the old plots which had assigned RTK points. The main issue with the blown-down sections of barley is that a profile view of the plants existed from the canopy. This affected pixel intensity values and created contrast from standing barley in the field. Since the purpose of this study was to evaluate canopy level foliage of standing barley, the extraction of blown-down barley pixels was necessary.

In order to classify areas of blowdown, an object-based image segmentation was employed. Object-based classification schemes have been used successfully by a variety of researchers and continue to increase in popularity for datasets acquired from UAVs. Peña-Barragán et al. (2011) successfully verified the Object-Based Image Analysis (OBIA) approach for identifying between crop types, phenology, and vigor using decision tree rule sets and multiple vegetation indices. Hall & Wilson (2013) had also had success with the OBIA approach to predictively map wine grape yield, quality and ripeness with high spatial resolution multispectral imagery. The approach taken for this study proposes a simple hue-saturation-intensity (HSI) transformation, using the intensity band, which is applied after multiresolution segmentation. To achieve multiresolution segmentation, a homogeneity criterion must be set which will group pixels and relative neighbours into objects based on: shape compactness and smoothness, standard deviation from reflectance/colour values, and a scale factor. The refined orthomosaics from all fields and dates were loaded into Trimble Ecognition software (Trimble GeoSpatial, Munich,

Germany) individually for multiresolution segmentation. Values used were 500, 0.1, and 0.5 for scale, shape and compactness, respectively. Additionally, band weights were applied at 1, 1, 10, 1, and 100 for the blue, green, red, NIR, and RE bands, respectively. More emphasis was put in the red-edge and red bands based on average spectral profile analysis for all photos, which showed the difference between RE and red bands to be the most pronounced (Figure 24). To perform classification, a threshold-based rule set was created which assigns classes to objects if they fall within a specific defined intensity range. Ranges were as follows for Trumar Farm: GS2(Intensity >= 0.05, <= 0.45), GS3(Intensity >=0.35, <=0.60), GS4(Intensity >=0.08, <=0.36). Results of the classification can be seen in Figure 9, and Figure 10. The final thematic classification files were converted to polygon shapefiles, which were used for masking pixels out of the final orthomosaics for Trumar Farm. Masked out areas appeared as ‘no-data’ values in the pixel numeric data, which were excluded from the spectral plot and strip averages.

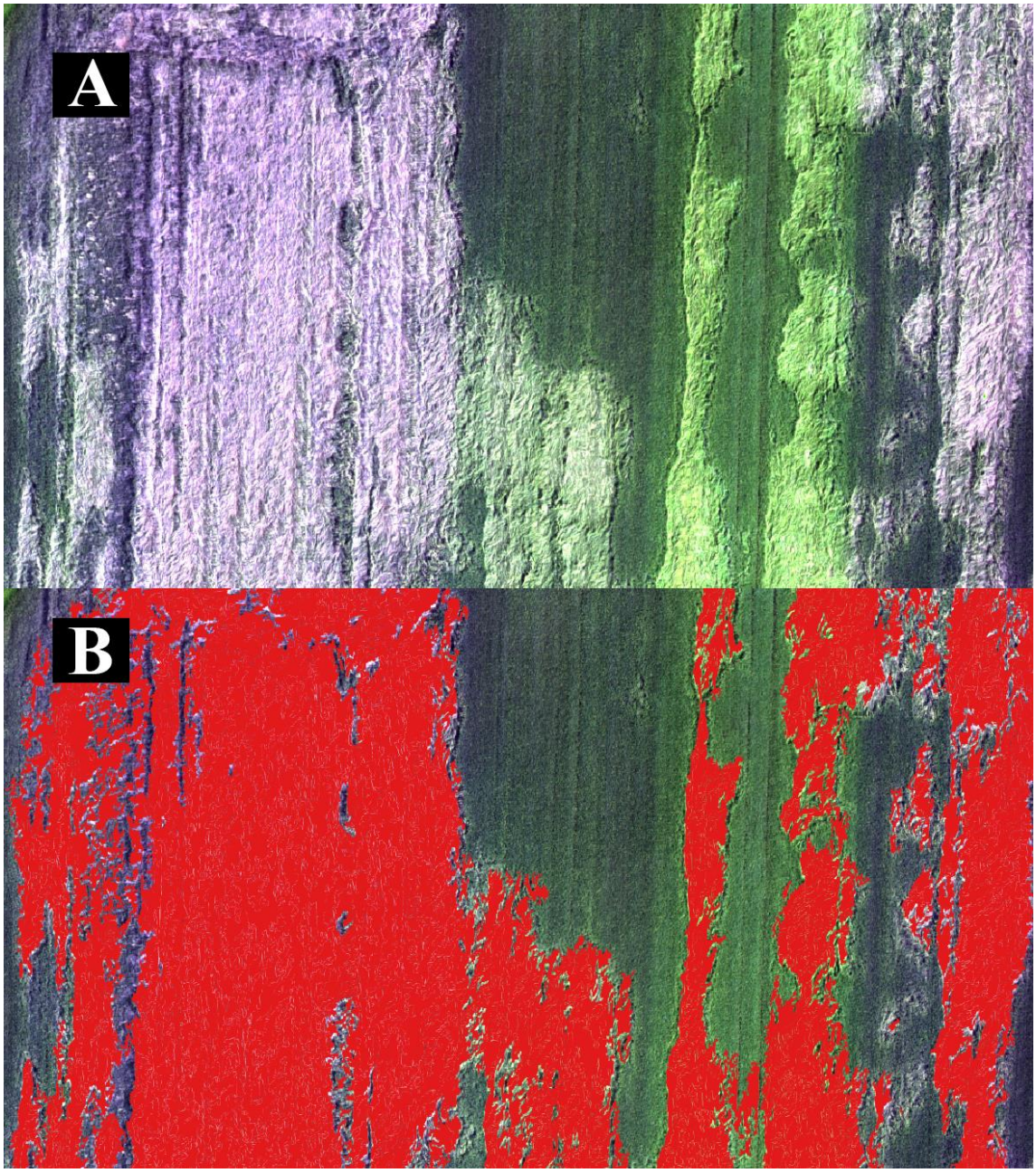

Figure 9. Section of Trumar Farm on GS3 showing blown-down barley in brightened areas. A: Unclassified. B: Classified.

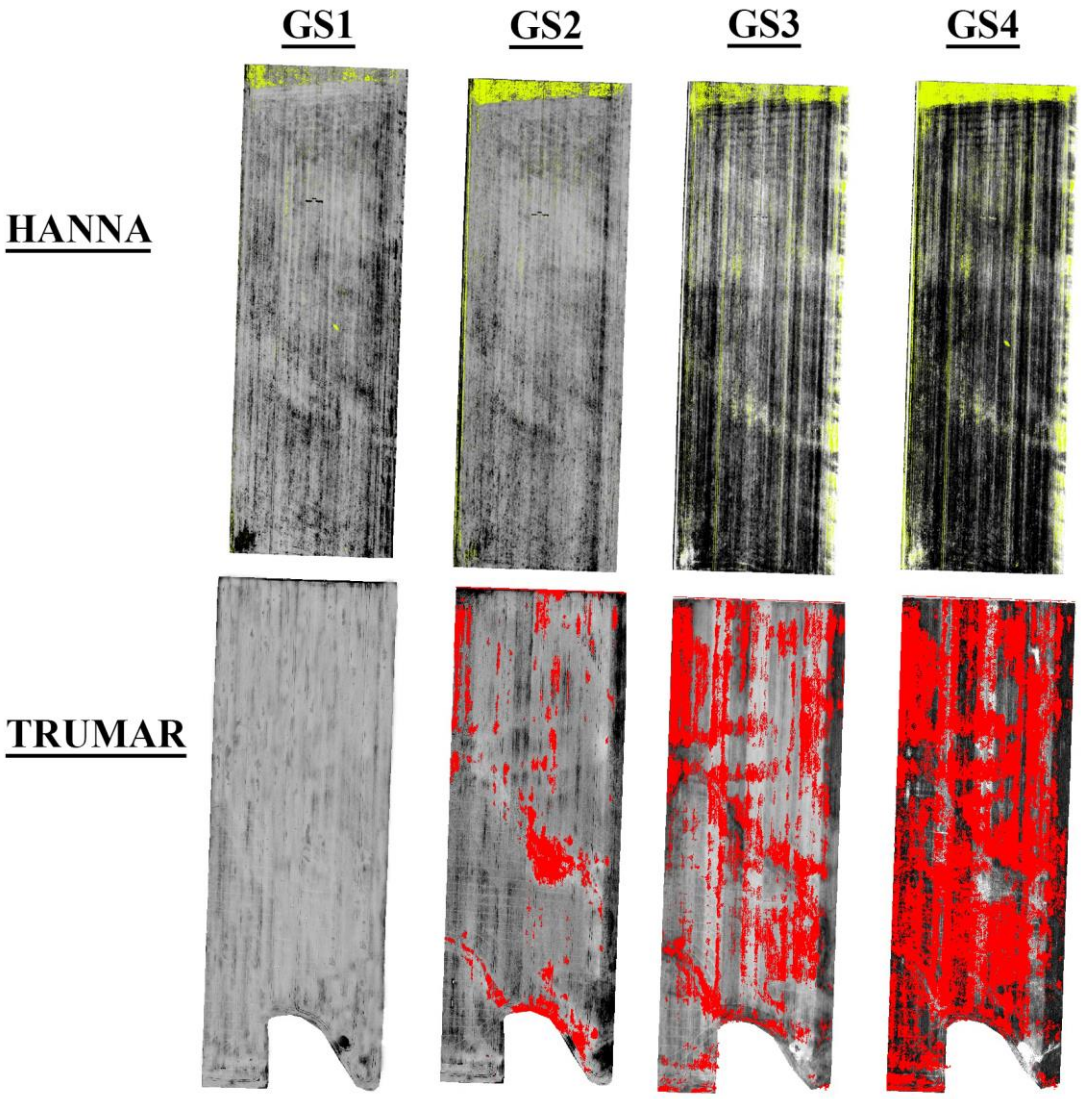

Figure 10. All orthomosaics highlighting classified sections of crop with clover infestation for Hanna Farm, and barley blow down damage for Trumar Farm. Not to scale.

VEGETATION INDICES AND CLIPPED AOI

CLIPPED AOI

Two types of AOI were clipped in all imagery (Figure 11). 18 VA Plots (3 x 3 m) were clipped out of each image for the purpose of performing regression analysis (detailed in next section). Eighteen strip plots were also clipped,

representing the north and south portion of a treatment strip within a respective field.

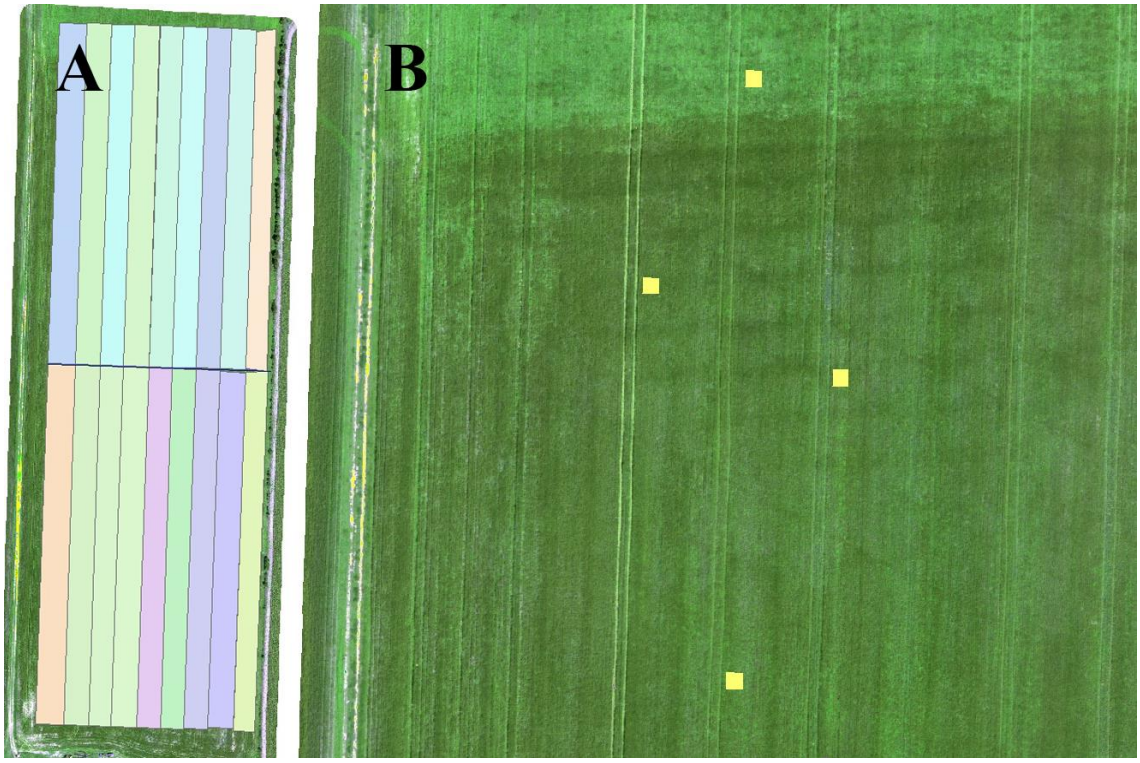

Figure 11. A) Strip plot shapefiles outlining the clipped AOI for Hanna Farm; B) 4 of 18 Visual Assessment (VA) plot shapefiles outlining the clipped AOI for Hanna Farm. Plot 7N is the uppermost yellow polygon, which was the only VA plot to fall within the clover infestation.

To measure spectral response of the clipped plots, digital pixel intensity values were summed and averaged using the following formula:

$$Spectral\ Response = \frac{\Sigma Pixel\ Value}{\#\ of\ Pixels/Plot} \quad (1)$$

All AOI plots were clipped as 5-band rasters maintaining the same bit depth (64-bit) and format (.tiff) as the original data. The clipped raster data were then converted into a tabular format which made for easy analyses of multiple vegetation indices.

VEGETATION INDICES

Multiple vegetation indices were modified from their original formulation to accommodate both the specific bandwidths of the Micasense multispectral sensor, and specifically the red-edge band. Five indices were chosen based on previous publications which indicated potential suitability for this study, and may be viewed in Table 3.

The normalized difference vegetation index (NDVI) (Rouse et al. 1974) is well known to be capable of detecting photosynthetically active biomass (Tucker, 1979), and has recently been used in multiple studies involving UAVs. Berni et al. (2009) evaluated a suite of narrowband (10 nm) vegetation indices—including NDVI—for quantifying field crop biophysical parameters (biomass, chlorophyll, water stress, LAI) with UAV multispectral imagery. In particular, the relationship between chlorophyll flux and NDVI was strong, indicating the capability to detect stress with high spatial resolution imagery at the canopy scale. The downside with the NDVI is that it is susceptible to over-saturation from dense vegetative canopies. The RE-NDVI (Table 3) was modified from Rouse et al. (1974) to replace the NIR band with the RE Band (RE-NDVI).

The renormalized difference vegetation index (RDVI) was also evaluated, as it is reported to work well in eliminating over-saturation from dense canopy vegetation cover, and is insensitive to the effects of sun and soil viewing geometry (Roujean & Breon, 1995). It was important to include this index to compensate for possible over-saturation of imagery subject to NDVI analyses.

This index was also modified from Roujean & Breon (1995) to replace the NIR band with the RE band (RE-RDVI).

The Triangular Greenness Index (TGI) was first proposed by Hunt et al. (2010) specifically for the detection of chlorophyll in agricultural crops at the canopy scale. The TGI assumes the area of a triangle with three points: (λR, ρR), (λG, ρG), (λB, ρB), where λ and ρ are the centre wavelength and reflectance, respectively. In the initial study in 2010, TGI was correlated with chlorophyll content at both the leaf and canopy scale. Subsequent studies exploring this index have evaluated UAV imagery, furthering the promise for this index to effectively quantify areas of chlorophyll deficiency at the canopy scale (Hunt et al., 2013; Hunt et al. 2014). It was important to include this index to evaluate how effectively the RGB bands could detect fungal disease severity.

Table 3. Vegetation indices used for regression between visual assessments and spectral averages, and for randomized complete block design of spectral strip averages.

Name	Formula	Publication
Normalized Difference Vegetation Index (NDVI)	$\frac{NIR_{840} - R_{668}}{NIR_{840} + R_{668}}$	Rouse et al., 1974
Red-Edge Normalized Difference Vegetation Index (RE-NDVI)	$\frac{RE_{717} - R_{668}}{RE_{717} + R_{668}}$	Modified from Rouse et al., 1974
Renormalized Difference Vegetation Index (RDVI)	$\frac{NIR_{840} - R_{668}}{\sqrt{NIR_{840} + R_{668}}}$	Roujean & Breon, 1995
Red-Edge Renormalized Difference Vegetation Index (RE-RDVI)	$\frac{RE_{717} - R_{668}}{\sqrt{RE_{717} + R_{668}}}$	Modified from Roujean & Breon, 1995
Triangular Greenness Index (TGI)	$-0.5[(\lambda R - \lambda B)(\rho R - \rho G) - (\lambda R - \lambda G)(\rho R - \rho B)]$	Hunt et al., 2010

***Note**: All indices are unique in that they feature specific bandwidths to the Micasense Multispectral Sensor.*

λ = centre wavelength of a particular band

ρ = *reflectance of a band (digital pixel value)*

GRAIN HARVEST EXPERIMENT

An additional small experiment within this study explored the relationship between yield and fungicide treatment intensity. It is already known that a relationship exists between grain yield and fungal severity (Gooding et al., 2000; Pepler et al., 2005). Thus, no research question was formed to address this issue. However, for the specific fields in this study, it was desired to ensure that some effect on yield occurred from treatments. This helps verify the effect of fungicide on general crop vigour. To perform this experiment, hand harvesting was required on multiple ground plots within each field. Eighteen plots total were harvested (9 plots per field), with 3 replications per treatment, on August 31st, 2015. A 1 x 1 m portion was measured out from the same plots originally used for visual assessments. Fresh produce was first weighed in the field immediately after hand harvest. Afterwards, samples were taken to the Thunder Bay Agricultural Research Station for further analysis. Data collection procedures followed the same standards as TBARS, where samples were dried, threshed, and loose grains were cleaned before weighing (Figure 12).

Figure 12. A: Hanging barley grain at TBARS. B: Threshing machine at TBARS. C: Barley grain after threshing. D: Process of cleaning the barley grains before dry weighing.

Figure 13. A: Control treatment row in Trumar Farm. B: Stratego + Prosaro treatment row in Trumar Farm. C: Comparison of grain from Control treatment (left head) and Stratego + Prosaro treatment (right head). August 14th, 2015 (GS3).

STATISTICAL ANALYSES

There are three types of results in this work: the first results reflect the relationship between visual disease assessment ratings and vegetation indices observed from plots; the second results reflect the ability of vegetation indices to predict treatment type by growth stage, and the third look at the impact of fungicide treatment type on grain yield.

REGRESSION

A simple linear regression was performed for each growth stage and field, to measure the relationship between assessed disease and spectral

response of plots, regardless of treatment type. Multiple vegetation indices were measured against visual assessment disease ratings recorded over multiple growth stages: NDVI, RE-NDVI, RDVI, RE-RDVI. TGI was not evaluated for this analysis, as the assumptions for a regression model could not be met for such data.

TWO-WAY ANOVA

The dry grain yields (grams/plot) were considered a response variable in a 2-way fixed factor ANOVA to determine if there was a significant effect of treatment (3 levels) and field (two levels) on grain yield. Spectral response could not be measured due to the wind blow down which impacted harvest plots in Trumar on GS4.

$$Y = \mu + T_i + F_j + TF_{ij}\, \varepsilon_{(ij)} \qquad (2)$$

Where Y = Dry Grain Yield (g)

T = treatment effect (fixed)

F = field effect (fixed)

RANDOMIZED COMPLETE BLOCK DESIGN (RCBD)

This experiment was laid out as a 3-way fixed factor randomized complete block design (RCBD), performed in R-Studio (RStudio Team 2015). The linear model is illustrated in equation 3:

$$Y = \mu + B_i + \delta_{(i)} + T_j + BT_{ij} + G_k + BG_{ik} + TG_{jk} + BTG_{ijk} + \varepsilon_{(ijk)l} \qquad (3)$$

Where Y = Spectral Average of treatment strips

B = block effect (field, fixed effect)

T = treatment effect (fixed)

G = growth stage (fixed)

δ = random effect of randomization of fungicide treatments i^{th} block

The spectral average for all five VIs were calculated by clipping 18 AOI per field and growth stage (GS1-GS4), represented as 6 replications of fungicide treatment intensity (Figure 11). The strips were later averaged by dividing the sum of all pixel values by the number of pixels per strip (Equation 1). The strips were divided into two regions per treatment swath to double the observations in each field (Figure 11). This totaled 144 observations made over all growth stages for each field (18 Observations/Flight × 8 Flights = 144 Observations). The treatment levels were: Control (C), Stratego (S), Stratego + Prosaro (SP). There is no measurement on the significance of block main effect, due to the effect of restriction on randomization in the RCBD model.

RESULTS

CORRECTED IMAGERY

The following images were produced from the Micasense Atlas server, asides from Trumar Farm GS1 which was processed in Agisoft Photoscan. Some illumination inconsistencies may appear. These images were not used in the analysis and are for display purposes only. These images all underwent further radiometric corrections: MNF Transform, and Histogram Matching. Also, recall that areas of crop blowdown and clover infestation were extracted before spectral analysis. The other indices may be viewed in Appendix I.

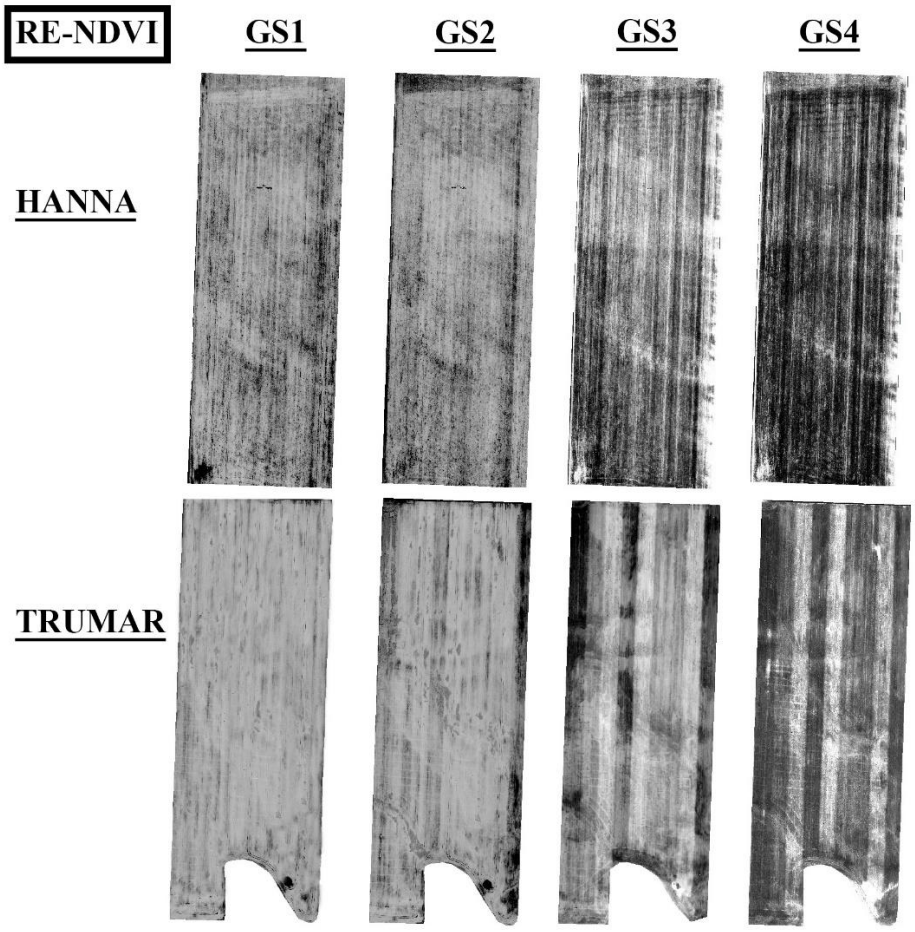

Figure 14. RE-NDVI imagery before inter-scene histogram matching and clipping. Not to scale.

VISUAL ASSESSMENT ACCURACY VERIFICATION

Regressions were performed separate for each respective field and vegetation index. It was determined that during the first growth stage (GS1) for both Trumar and Hanna Farms (Feekes 8 to 9), it was difficult to establish a solid relationship between observed disease and spectral response. Percentage of infected leaf areas were too low to detect by the sensor. Thus, GS1 data were omitted from regressions; the data for GS1 will however be elaborated upon in the discussion section. During GS4, disease assessment ratings were not recorded in the field due to leaf senescence. At this stage, it was not

possible to distinguish fungal disease from senesced leaf area when conducting visual assessments; thus, GS4 data were also omitted from the regression analyses. GS2 and GS3 VA data were pooled together (36 observations) and modelled against the multiple VIs (Figure 15). Results showed for NDVI an adjusted R^2 of 0.681 and 0.683, for Trumar and Hanna Farms, respectively. RE-NDVI had an adjusted R^2 of 0.737 and 0.703, for Trumar and Hanna Farms, respectively. RDVI had an adjusted R^2 of 0.789 and 0.698, for Trumar and Hanna Farms, respectively. Lastly, RE.RDVI had an adjusted R^2 of 0.734 and 0.633, for Trumar and Hanna Farms, respectively.

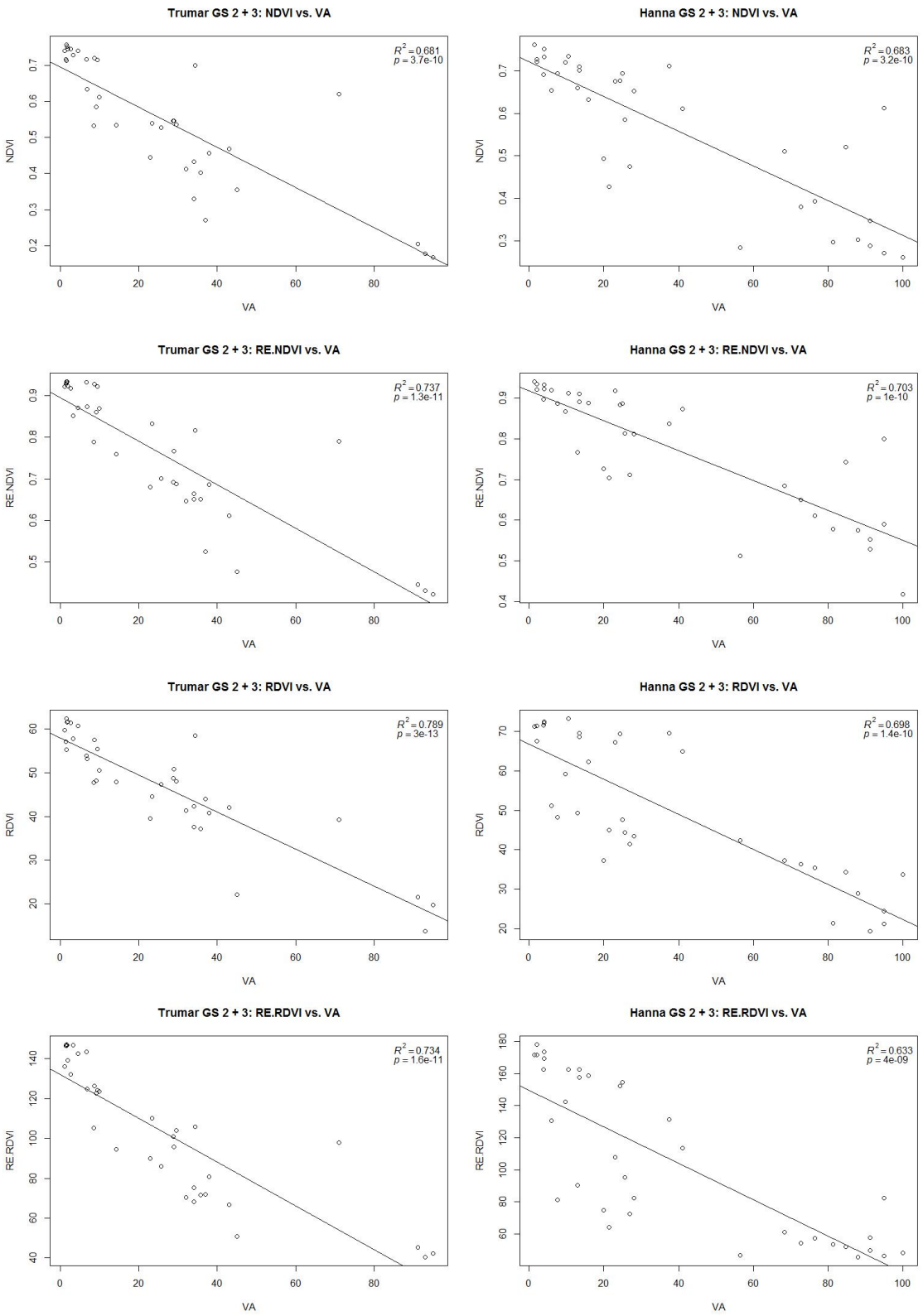

Figure 15. Linear regressions for fields at Trumar and Hanna Farms, each with combined data from Growth Stages 2 and 3 (36 observations per regression).

RCBD STATISTICAL RESULTS

F-Tests for the RCBD statistical results may be viewed in Appendix II, Table A.

MAIN EFFECTS, INTERACTIONS AND POST-HOC FINDINGS

While the majority of measured effects on spectral response from VIs were found to be significant in the RCBD test, the more important information is yielded from the post-hoc tests. A Tukey HSD post-hoc was performed for select main effects and interactions. Some of these will be elaborated upon in this section.

MAIN EFFECTS ON VEGETATION INDICES

The main effect of treatment had a significant impact on spectral response for all measured indices. Additionally, The Tukey HSD post hoc test showed the spectral response of VIs from the Treatment effect (pooling both fields) being significantly different between all treatment levels for measured VIs. The plot in Figure 16 shows the main effect of treatment on VIs, pooling both fields together. These data demonstrate how the spectral VI means iteratively increase with increasing fungicide application intensity. This indicates a general positive effect of fungicide on crop health when combining both fields. While it was certain that these data sets could robustly delineate disease severity, more will be explored regarding the differentiation of effects with

respect to field and growth stage, and their interactions

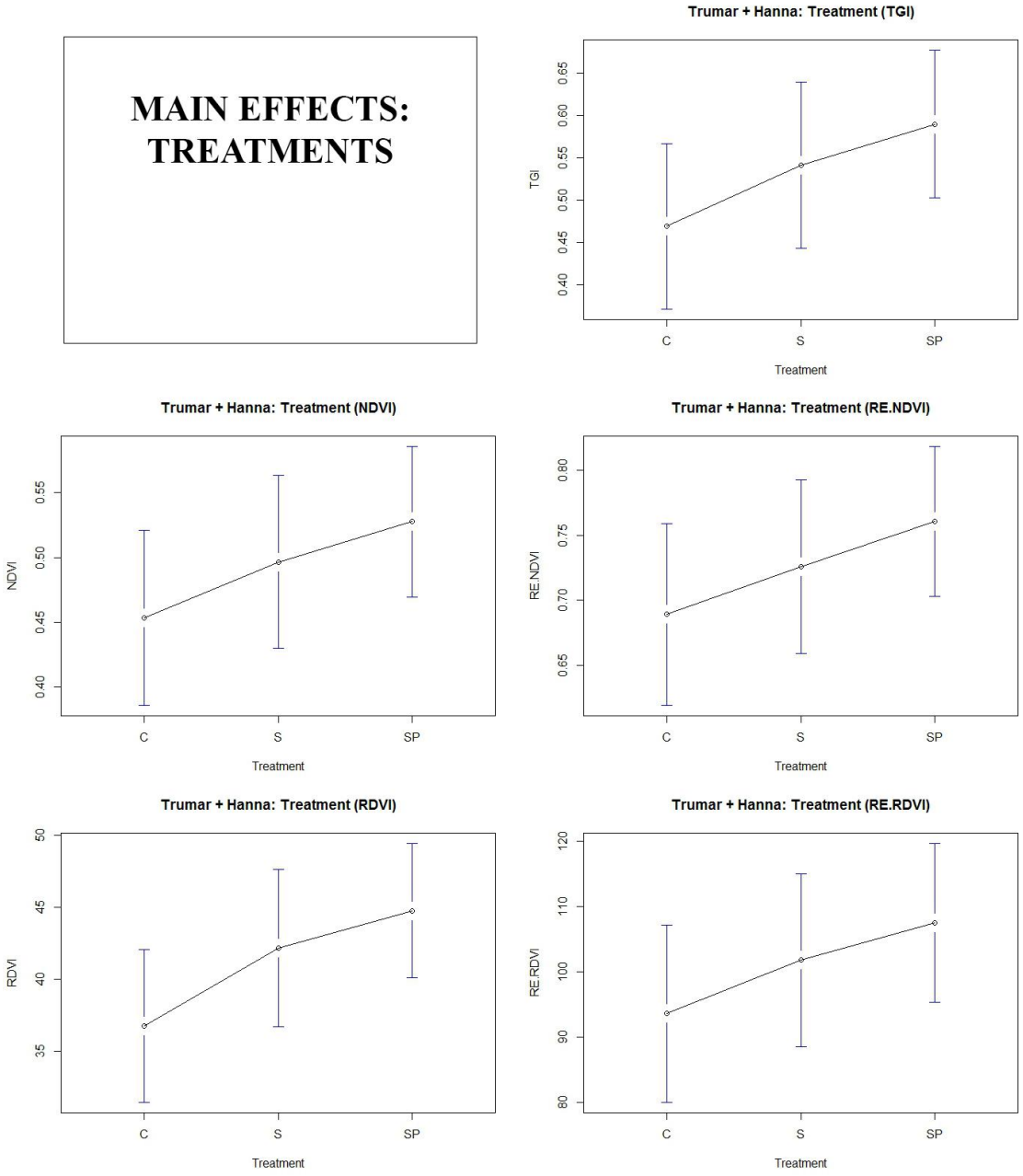

Figure 16. Main effect of treatments on spectral response from all measured vegetation indices. Error bars represent one standard deviation.

There was also a significant main effect of growth stage on spectral response, for all measured VIs. These results were expected due to the

changing health conditions of the crops throughout the season. The Tukey HSD showed the least difference exists between GS1 and GS2 (p=0.326) for RE-NDVI, while the rest of the growth stages showed a significant difference between the means (Figure 17). In general the largest observed range of VI values occurred during GS3. This agrees with the visual assessment data, which also saw the largest contrast in health between treatment plots during GS3, Trumar Farm (M_{GS3}=40.931, SD_{GS3}=24.885) and Hanna Farm (M_{GS3}=58.227, SD_{GS3}=31.991). Little observed difference in rated disease occurred during GS1 for Trumar Farm (M_{GS1}=1.643, SD_{GS1}=0.625) and Hanna Farm (M_{GS1}=1.753, SD_{GS1}=1.400), which agrees with the range of spectral VI data for GS1.

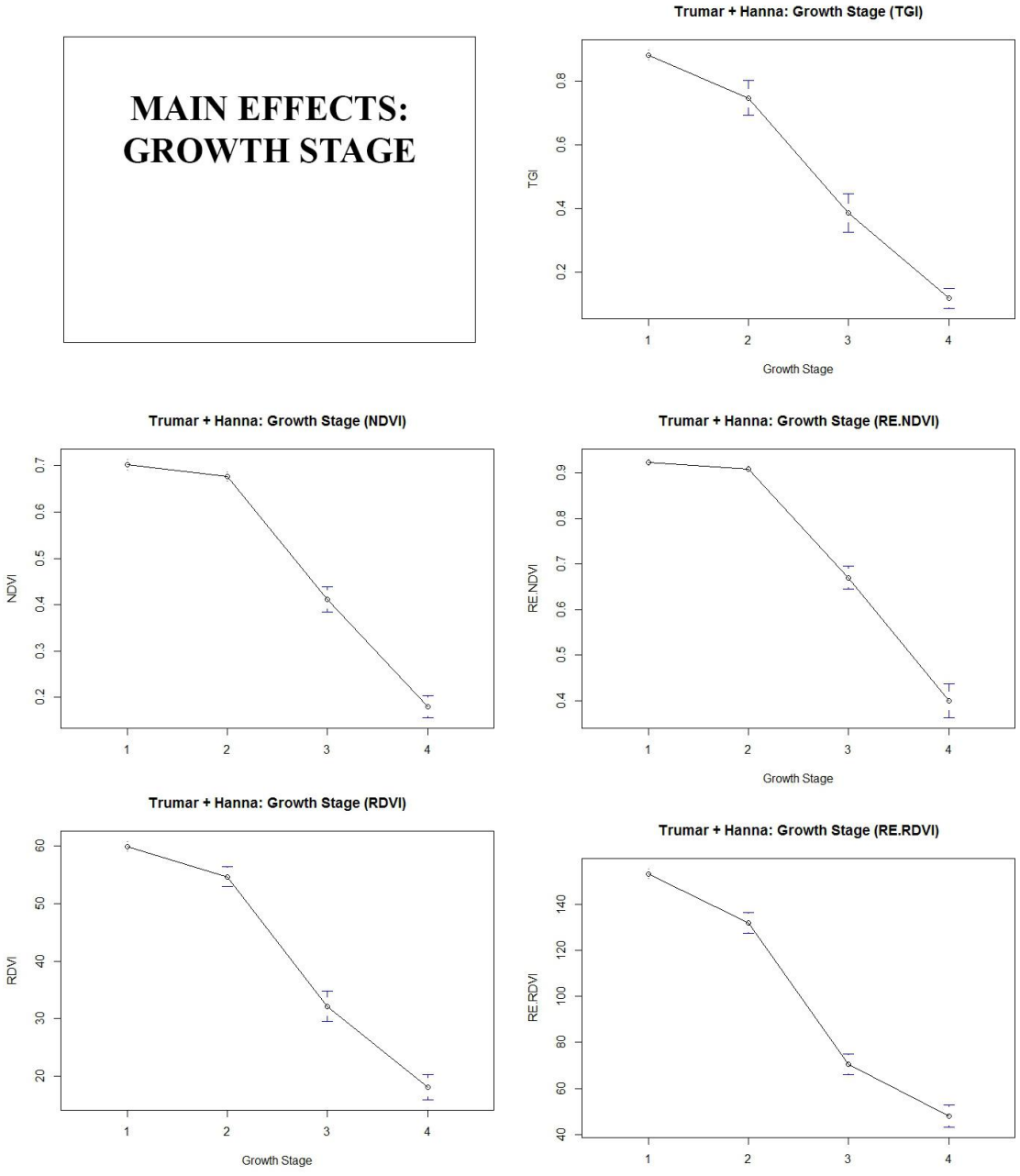

Figure 17. Main effect of growth stage on spectral response from all measured vegetation indices. Error bars represent one standard deviation.

INTERACTION EFFECTS ON VEGETATION INDICES

Figure 18 can be referenced while reading this section, showing plots of the interaction effect between treatments and fields. Most VIs yielded a

significant interaction between type of field and treatment. RE-RDVI and TGI had a non-significant interaction of p=0.289 and p=0.109, respectively. The Tukey HSD showed some indices had a significant difference between fields for control treatments (NDVI, RE-NDVI) while some showed a non-significant difference between field means combining all growth stages (RDVI, RE-RDVI, TGI). For the S treatment, with the exception of the TGI (p<0.001), all indices showed non-significant differences between field means, indicating a similar effect of Stratego on spectral response. The SP treatment had similar results to the S treatments, with only observed TGI being significantly different between fields (p<0.001).

Moving on, the interaction effects of field and treatment will be further analyzed from the Tukey HSD post hoc tests. The inter-field effect of treatment will be looked at here, irrespective of growth stage. Regarding all VIs, for Trumar Farm, there were significant observed differences between all combinations of treatments with the single exception of TGI (S-SP, p=0.346). Thus, the level of treatment for Trumar Farm generally had a unique effect on observed spectral response. For Hanna Farm, comparing the levels of treatments had a different result than that of Trumar Farm. VIs tended to perform very differently over Hanna field. First, there was a non-significant difference in means between C and S treatments for NDVI (p=0.225), RE-NDVI (p=0.581) and TGI (p=0.684). Measuring the difference between S and SP treatments, only RE-RDVI (p=0.137) and TGI (p=0.590) were non-significant. Lastly, the difference between C and SP treatments saw all VI means being

significantly different. The significant difference between C and SP treatments was expected for both fields, as the observed health between the lowest and highest treatment levels were highly evident in visual disease assessments as the season progressed.

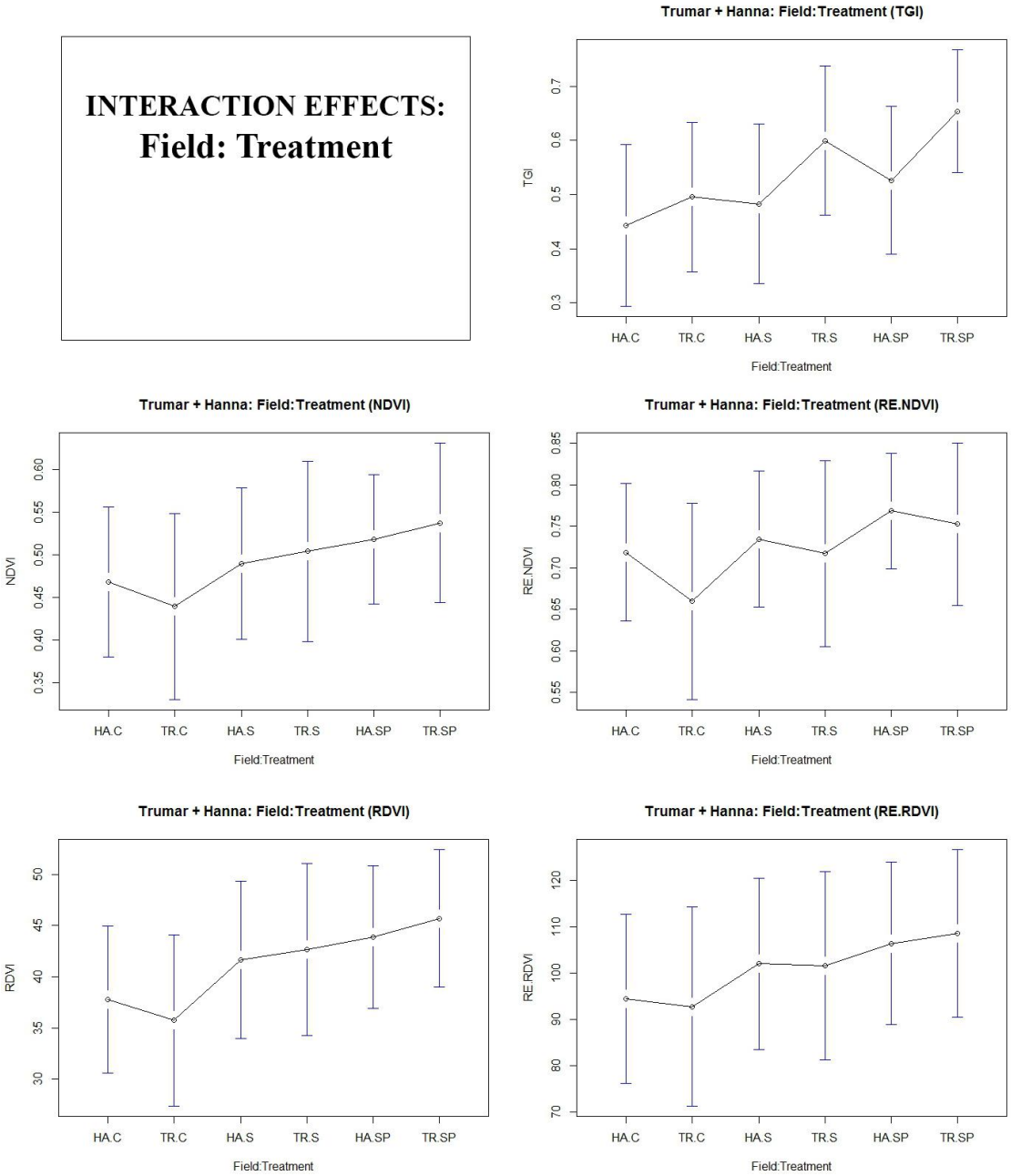

Figure 18. Plots for the interaction effect of Field and Treatments on spectral vegetation indices. Error bars show one standard deviation.

In general, it is important to note here the effect of consistently declining spectral response as the season progressed. This is clearly highlighted when looking at the plots for the interaction of Field and Growth Stage (Figure19).

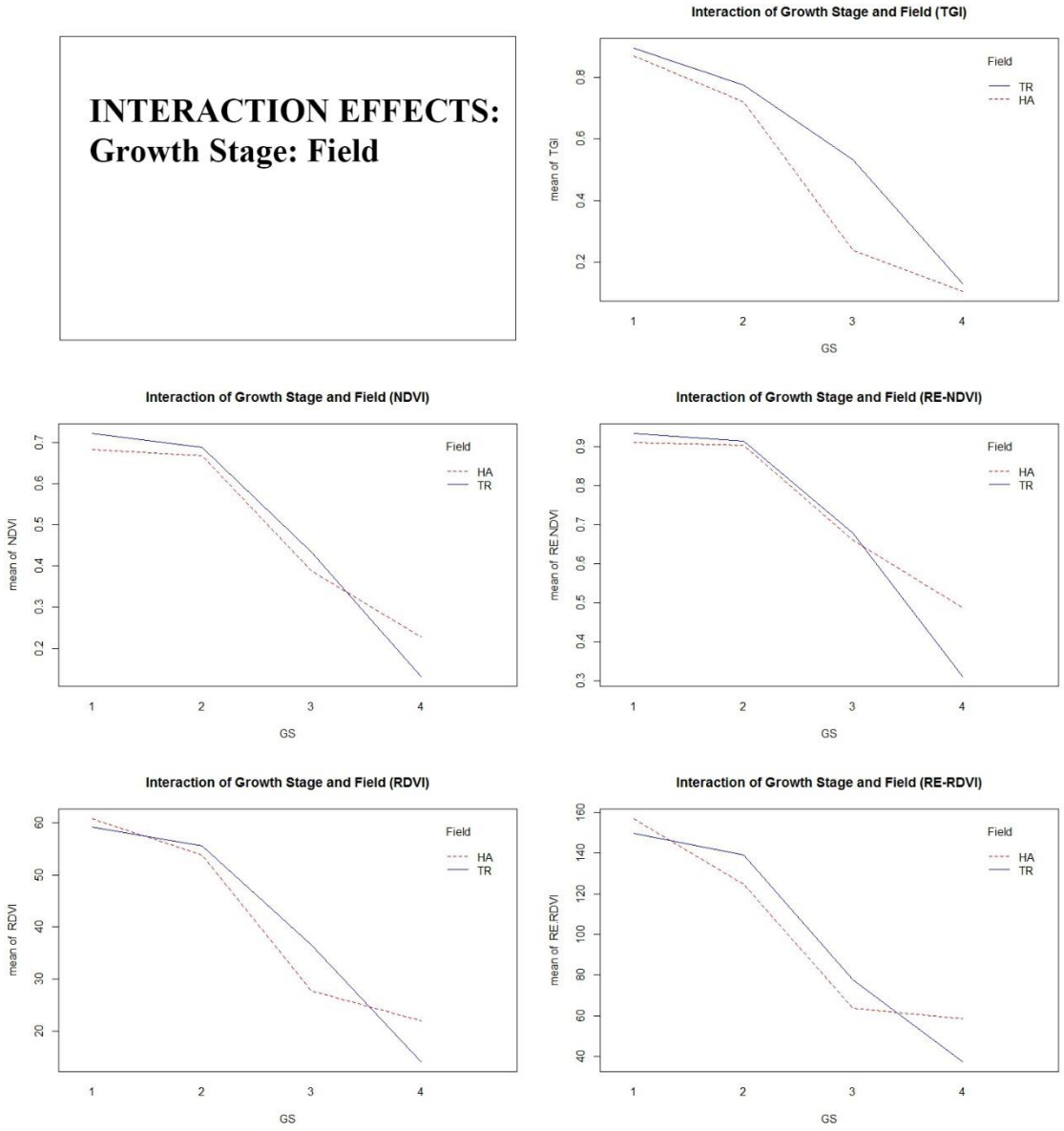

Figure 19. Plots for the interaction effect of Growth Stage and Field on spectral vegetation indices.

There was consistently a significant interaction effect between type of field and observed growth stage, on spectral response for all VIs, F (3, 120), p <

0.001. At times, the means between GS1 and GS2 were not significantly different, such as with NDVI for Hanna Farm (p=0.811) and RE-NDVI for Trumar Farm (p=0.639). Also, when comparing fields, the mean spectral response between growth stages are often statistically similar. This can be visualized when looking at both NDVI and RE-NDVI, in Figure 19. When the contrast of means between fields are significantly different for a respective growth stage, there is still a similar trend in the data. This trend is represented as declining spectral averages of the measured vegetation indices as the growth stages increase.

The interaction of treatment and growth stage was significant for all indices with the exception of TGI, which was marginally significant, F (6, 120)=2.103, p=0.058. Figure 20 shows the interaction plots for treatment and growth stage. It was important to show these interaction plots, as it was anticipated that the S and SP treatments would have statistically similar effects on mean VI values up until GS2. This similarity is verified when looking at the post-hoc tests, which showed non-significant differences for all VIs when comparing S and SP treatments for GS1 and GS2. Recall that the S treatment had been applied to 6 of 9 rows per field up until GS2; although Prosaro was applied on the date of GS2 flights, the fungicide effect had yet to take effect due to lag time. Thus, for GS2, S treatments are equivalent to SP. These plots verify the ability of the Micasense to detect crop areas by treatment type. In particular, the VIs were often able to determine significant dissimilarity between S and SP

treatments from GS3 onward, which was accurate to the fungicide application timing.

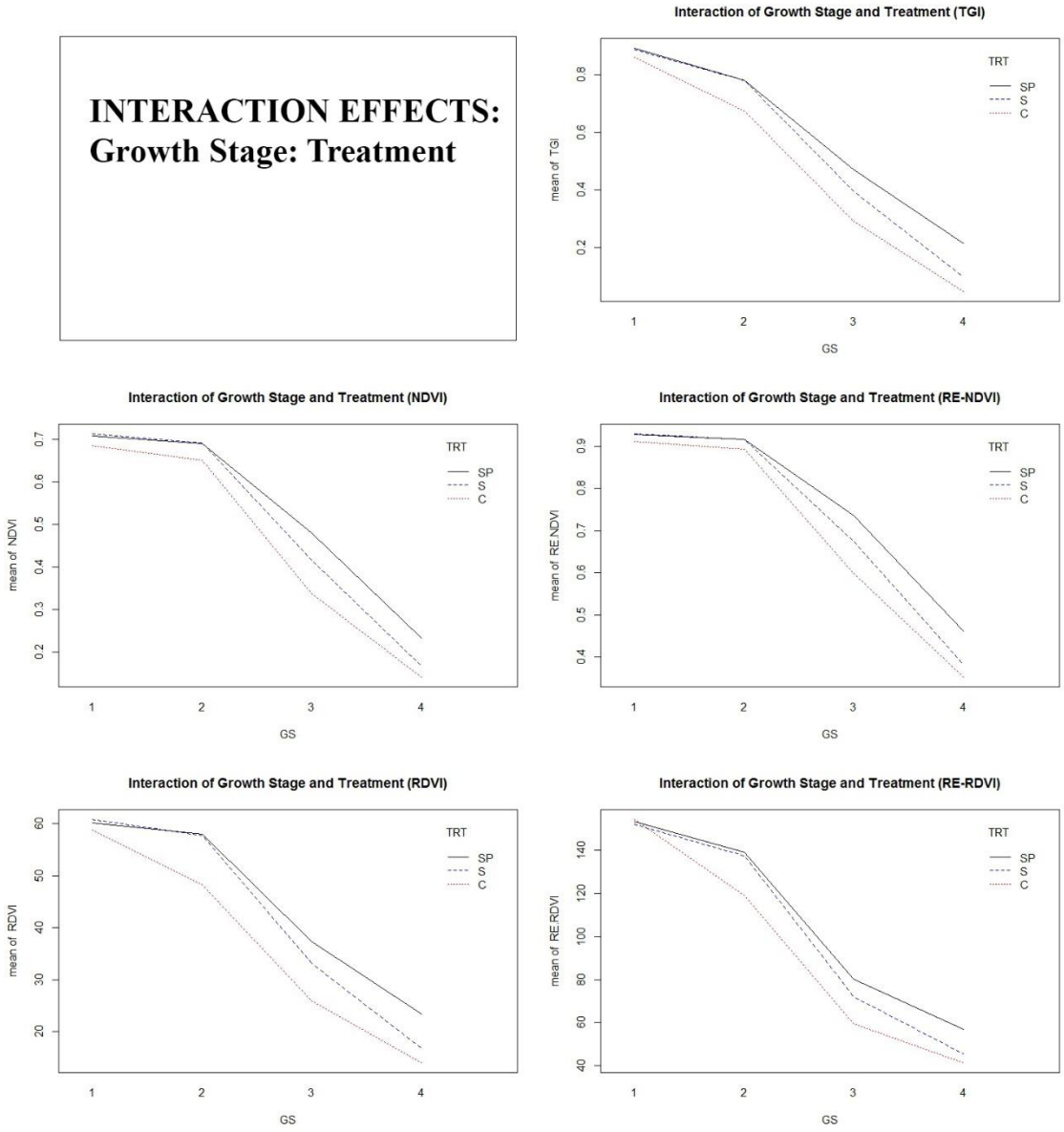

Figure 20. Interaction plots for the interaction effect of Growth Stage and Treatments on spectral vegetation indices.

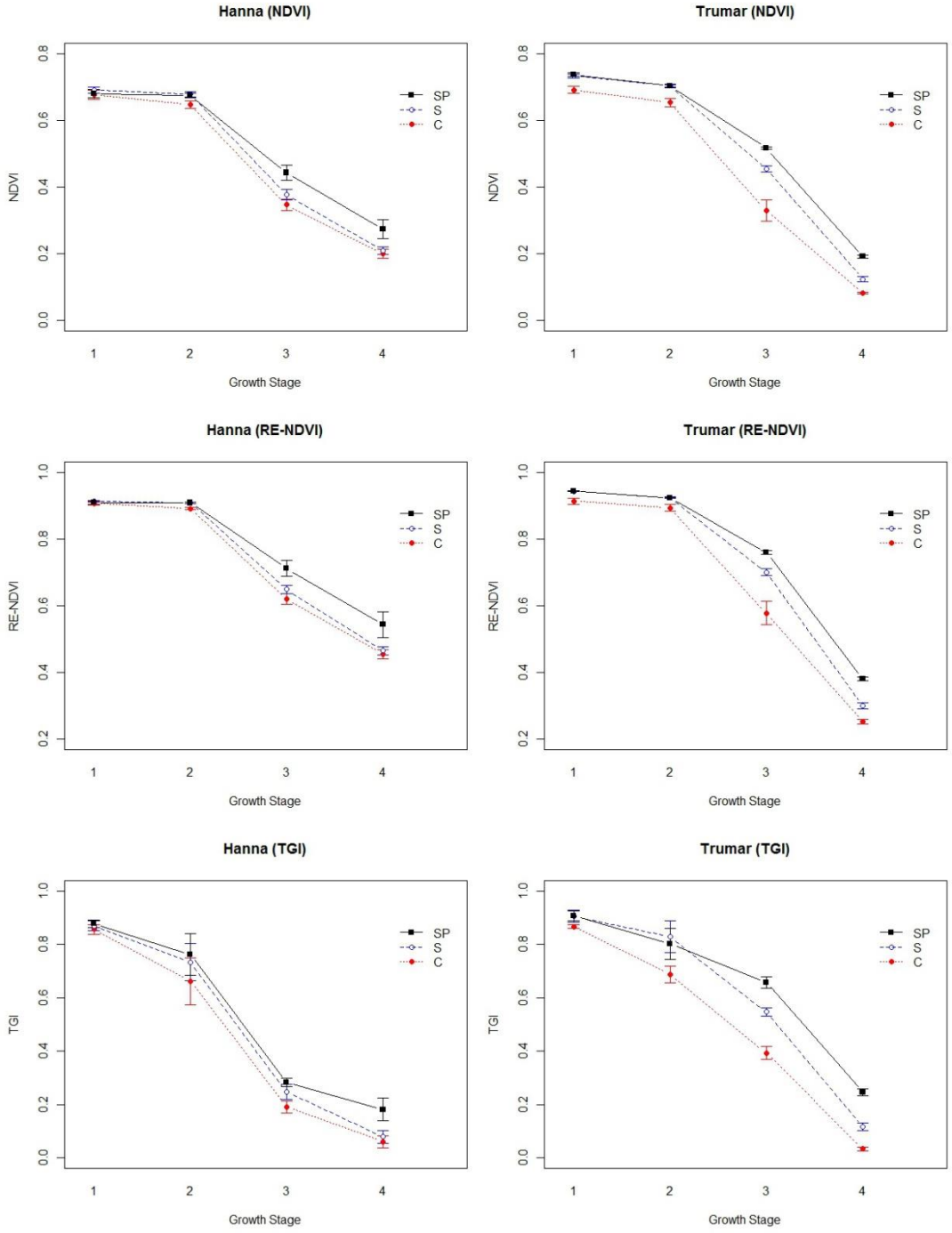

Figure 21. Non-significant 3-way interaction effects between Treatment x Growth Stage x Field. Error bars show one standard deviation.

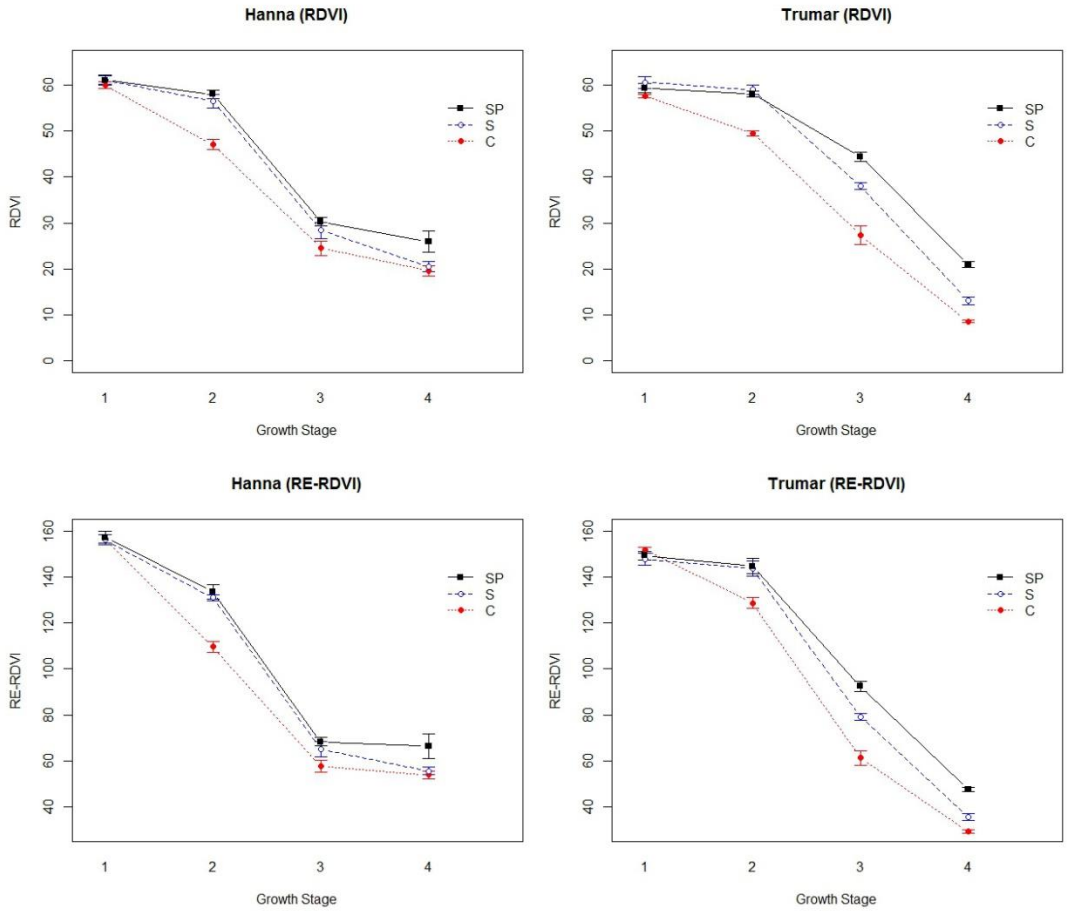

Figure 22. Significant 3-way interaction effects between Treatment x Growth Stage x Field. Error bars show one standard deviation.

Non-significant 3-way interactions were found in NDVI (p=0.415), RE-NDVI (p=0.383) and TGI (p=0.780). Figure 21 can be referenced showing how the interaction of growth stage and treatment performed on different levels of field. The non-significant interactions indicate that both fields responded similarly to treatments across all growth stages. RDVI (p=0.003) and RE-RDVI (p=0.005) had significant 3-way interactions indicating dissimilar spectral behaviour from treatment levels across all growth stages (Figure 22).

GRAIN YIELD RESULTS

The final results of the Two-Way ANOVA show a non-significant effect of the interaction of Treatment x Field on grain yield, F (2, 12)=1.575, p=0.247. Main effects were however significant for Treatment (p=0.018) and Field (p=0.045). For the interaction effect, the Tukey HSD post hoc test revealed that most comparisons of means were non-significant (p>0.05). Only the comparison of Trumar Farm C:Trumar Farm SP was considered significantly different. (p=0.046). A difference does clearly exist between treatments within respective fields. Inspecting Figure 23, yield has a pattern of consistently increasing with fungicide intensity. More replications would be desirable to obtain better results from this experiment.

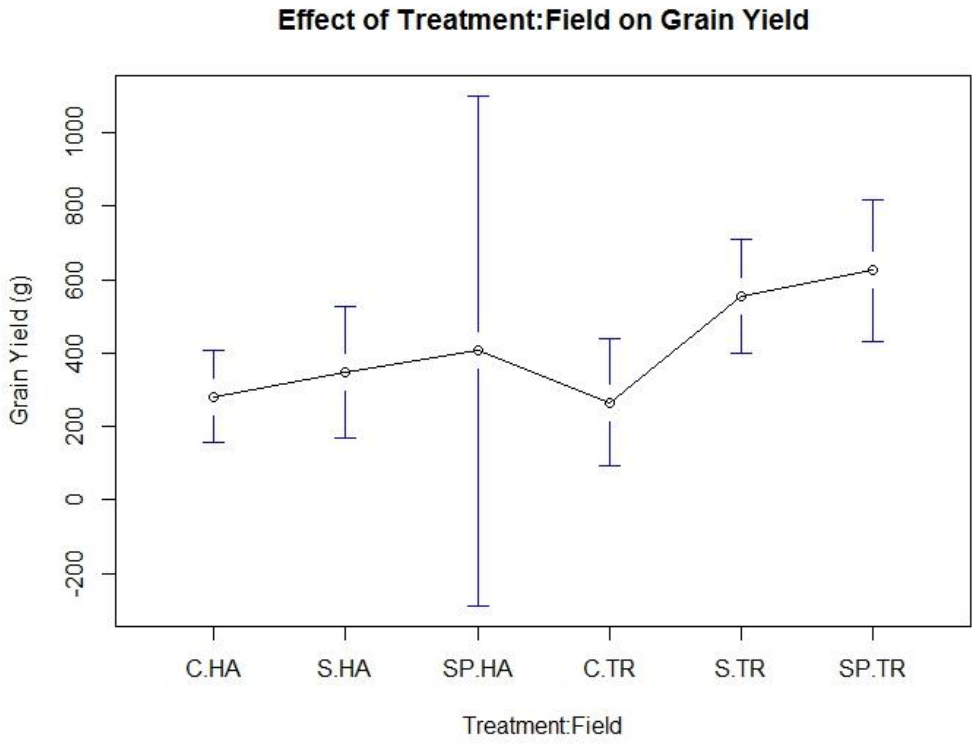

Figure 23. Mean grain yield values for each respective treatment type. Error bars show one standard deviation.

DISCUSSION

VISUAL ASSESSMENT ACCURACIES

EARLY DISEASE DETECTION

During all growth stages, the fungal pathogens observed were a combination of leaf rust (*Puccinia triticina*), net blotch (*Pyrenophora teres*) and spot blotch (*Cochliobolus sativuas*). Note that GS1 had only control treatments applied at the time of conducting the UAV flights. It was thus expected that visually assessed disease conditions on canopy-level foliage would remain homogeneous throughout both fields. It was hopeful that early fungal patches

would occur in the field; however, this was not verified in the visual assessment plots.

The homogeneity of crop health was further confirmed when reviewing both VA data and imagery from GS1. Particularly, the VA data showed little variation in rated disease, as well as consistently low disease presence for both Trumar Farm (M_{GS1}=1.643, SD_{GS1}=0.625) and Hanna Farm (M_{GS1}=1.753, SD_{GS1}=1.400). The removal of GS1 data from the regression pool consistently improved results for all vegetation indices. While these results were expected for GS1, it was hopeful that the sensor resolution would improve upon previously reported accuracies for early fungal detection. Franke and Menz (2007) noted the difficulty of early fungal disease detection in wheat, with coarser resolution data (2.4m/pixel QuickBird multispectral data) when observing the early leaf rust and powdery mildew development under different fungicide application intensities. It was highlighted by the authors that higher resolution data sets may improve fungal disease detection accuracy. Other researchers have reported that a lag time exists for fungal disease to impact spectral reflectance in the red and near-infrared regions. For example, Devadas et al. (2008) evaluated ten vegetation indices for identifying rust infection at different severity stages, and noted the difficulties in early detection could be attributed to the time lag in rust infection to break down the internal leaf structure. Building on this, the spatial resolution of the Micasense flown at 100 m (6.7 cm/pixel) was possibly not adequate for early disease detection of canopy leaves. Unfortunately, the Micasense parameters for exposure are

locked by the manufacturer which made flights at lower altitudes impossible for this experiment. Lower altitude flights would have been desired to increase the percentage of diseased flag leaf tissue contained within a pixel. During GS1, an average of less than 2 % of infected leaf area were recorded on leaves over each plot. The features contained in a pixel at this stage were likely to contain more non-infected green leaf tissue than that of chlorotic or necrotic lesions. In wheat (*Triticum* spp.), it has been shown that photosynthetic activity is negatively impacted only in infected lesions of leaf tissue, while healthy tissue on the same leaf will remain unchanged (Kuckenberg, 2009; Robert et al. 2005). Again, since most pixels contained a higher ratio of non-infected leaf tissue during GS1, the VI and VA data remained quite homogeneous until subsequent growth stages. As the season progressed, observed fungal severity increased, and an increased rate of senescence was observed on rows with control treatments. Increased contrast between disease ratings for respective treatments was observed from GS2 onward, which improved the regression results.

SOURCES OF ERROR

There are a few uncontrollable factors which could have impacted results regarding the regression analyses in this study. First, the possibility for disease rater bias exists when recording visual disease assessments in the field. Second, the amount of rated plants per plot could have impacted the accuracy of results. Third, the Micasense multispectral sensor and both its spectral and spatial resolution may have affected the observed accuracies. Fourth and lastly,

the robustness of radiometric corrections could have affected observed spectral plot averages.

It was discussed briefly in the methodology section how rater bias could potentially affect the ratings of disease. Two raters were working to assess disease from GS1-GS3. The same raters recorded and rated disease from the same plots from each field coinciding with each UAV flight. The SADs were designed to account for multiple types of rust and blotch disease common to barley in the region. Such reference diagrams proved to be useful in yielding consistent numerical results between both raters during this study. Other researchers have also found SADs to be useful; Nutter (1990) found that disease raters were more reliable when using a SAD than when without one; Godoy et al. (2006) developed a diagrammatic scale to assess soybean rust (*Phakospora pachyrhizi*), and Domiciano et al. (2014) for estimating spot blotch in wheat leaves, and both found that the use of SADs tended to reduce error and increase accuracy amongst raters. Other factors as well, not mentioned in previous studies, could have possibly affected the quality of VA data. These factors include high fatigue from extensive labour, and heat exhaustion on sunny days. It was documented by both raters how the excessive heat, or fatigue, would promote an urgency in recording a disease rating.

A second issue which could have impacted the regression results is related to the amount of plants rated per plot. Eighty plants (20 per corner) were rated per each 3 x 3 m plot, and compared against the clipped raster image covering the same area. The spectral plot average contains more plants than

were rated for disease, which could have potentially impacted the ability to establish solid relationships in the regression analyses. Rating more plants, or rating additional plants in the centre of each plot may have improved accuracy.

Third, the spatial resolution, and possibly the spectral resolution of the Micasense were not fine enough to distinguish low-to-medium disease levels with a high accuracy. The optimal spatial resolution with regards to predicting crop biophysical parameters has seldom been researched to date. One recent study by Hunt (2014) tested simulated UAV imagery by attaching a modified BGNIR and RGB camera to a pole pointed at nadir over cereal rye (*Secale cereale* L.) plots. The imagery were taken and analyzed at two resolutions: 0.5 mm and 1 mm. It was found that the 0.5 mm pixel data were better for establishing relationships with both above-ground biomass and chlorophyll content, when analyzing the plot VI spectral averages (gNDVI and Triangular Greenness Index (TGI)). For this study, perhaps a greater spatial resolution (<6.7 cm/pixel) could have yielded greater relationships in the regressions.

Another topic seldom explored in academic research is that of spectral resolution trade-off analysis. Evidently, hyperspectral sensors are well documented to perform better than most variations of multispectral counterparts for general crop analysis (Calderón, 2014; Calderón et al., 2013; Franke et al., 2005). This is due to the narrow and contiguous bands (~1 nm), which can discretely detect information in specific electromagnetic regions. However, much less focus is given towards bandwidth trade-off: how wide can a spectral band be until too much contamination impacts the data accuracy? Recall the

Micasense bandwidths (Blue- 475 nm +/- 20 nm, Green- 560 nm +/- 20 nm, Red- 668 nm +/- 10 nm, Red Edge- 717 nm +/- 10 nm, Near Infrared- 840 nm +/-40 nm), and note that it is possible electromagnetic contamination exists even within the 10 nm bands. Studies contrasting between narrow and broad bandwidths for the detection of vegetation generally show better performance with narrow bands. Thenkabail et al. (2002) evaluated between narrowband and broadband vegetation indices for determining LAI, wet biomass, dry biomass, plant height, and nitrogen. Six crops were evaluated, including wheat and barley. They concluded that in many cases the most important information was secluded to a few narrow bands (1.43 nm) within the VNIR range. This agrees with Zhao et al. (2007) who could better predict LAI and canopy chlorophyll density (CCD) with narrowband indices compared to broadband counterparts. However, most past studies in this specific area explore low spatial resolution datasets. More needs to be known regarding how spatial resolution affects bandwidths for crop parameter estimation.

Lastly, even with proper radiometric corrections to imagery, some variation can exist with pixels between scenes. Such change is likely to be from uncontrollable factors such as changing canopy architecture and bi-directional leaf scattering of light (Bravo et al., 2003). This can be simply understood when considering that a composition of canopy leaves may be distributed differently within a plot, when viewed between multiple dates.

ACCURACY RESULTS

Note that similar disease varieties were identified between fields: spot blotch, yellow leaf rust, and net blotch. GS2 and GS3 were pooled together and analyzed for each field, as highlighted earlier. For GS2, flag leaf area infection rates were slightly higher, up to 13.47 % for Hanna Farm and 34.37 % for Trumar Farm. GS3 had the highest disease severities, up to 92.7 % for Hanna Farm and 95 % for Trumar Farm. As the crop season progressed from GS1 to GS4, disease further developed and intensified, introducing higher levels of variation between disease ratings. This is attributed to the fact that some ratings occurred in severely infected plots (Control treatment) and some in low-infected plots (Stratego and Prosaro). The red-edge indices in general out-performed the near-infrared counterparts, showing a slightly stronger relationship with VA ratings (NDVI adjusted R^2 of 0.681 and 0.683, for Trumar and Hanna Farms, respectively; RE-NDVI adjusted R^2 of 0.737 and 0.703, for Trumar and Hanna Farms, respectively). Consistently, when inspecting spectral sample plots across all orthomosaic imagery, light in the RE region reflected much more strongly than within the NIR region (Figure 24). Greater spectral seperability existed between the RE and Red bands which likely influenced stronger relationships in the regressions.

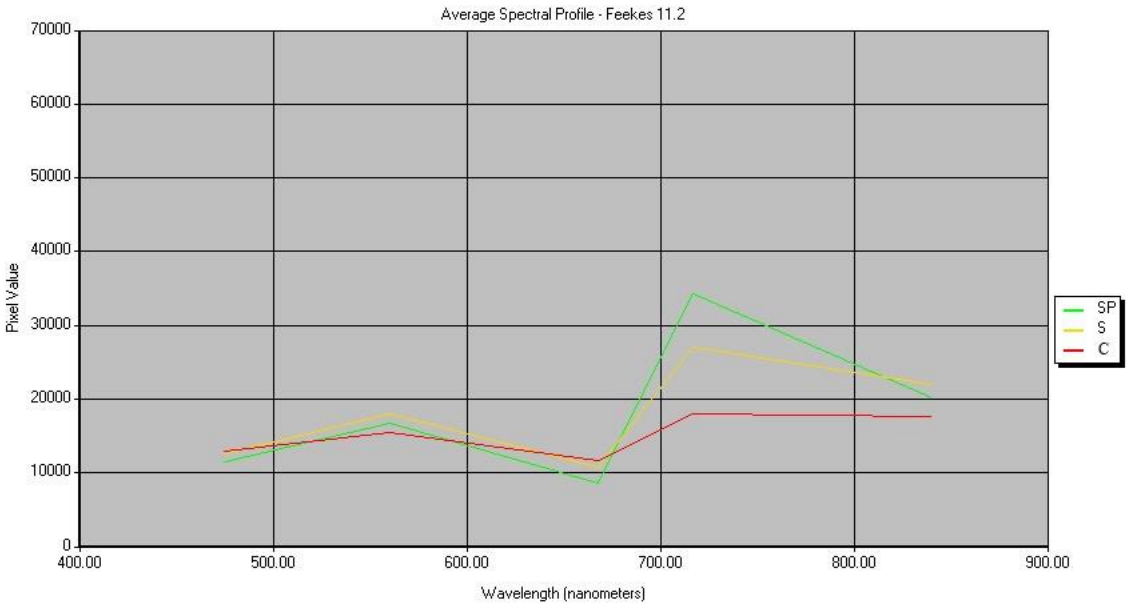

Figure 24. Spectral profile from equalized random point sampling regime. 100 points were collected and averaged within each respective treatment AOI. Feekes 11.2 (GS3), Trumar Farm.

The RDVI performed better for Trumar Farm (RDVI had an adjusted R^2 of 0.789 and 0.698, for Trumar and Hanna Farms, respectively; RE.RDVI had an adjusted R^2 of 0.734 and 0.633 for Trumar and Hanna Farms, respectively). Recall that the RDVI is an index specifically designed to work well for both dense and sparse vegetative canopies. Row spacings were slightly larger and vegetative cover was slightly less dense in Hanna Farm, which could have imposed differences between fields. Additionally, it should be mentioned that there are two different crop management regimes: till/dairy farm (Trumar Farm) and no-till/non-dairy farm (Hanna Farm). The main difference between the regimes was the amount of rogue weed species which appeared in Hanna Farm throughout the season, and retained moisture levels. While efforts were made to classify much of the weeds, the possibility remains that plot averages were impacted by weed presence during GS2 and GS3. Additional information

regarding the differences in farm management regimes are discussed further in the RCBD results section. In general, the results of the regression analysis have been satisfactory. There is an apparent relationship between the evaluated vegetation indices and visually rated disease within field plots.

RCBD RESULTS

The RCBD results demonstrate the capability of UAV multispectral imagery to distinguish fungal disease severity by three treatment intensities. This was achieved in each field regardless of management/field type, from GS2 to GS4. This allows the Null Hypothesis (H_0) to be rejected in favour of accepting the Alternative Hypothesis (H_a), indicating that treatment levels (C, S, SP) have a significant general effect on the spectral response of barley with UAV multispectral imagery in each field, and over growth stages (GS2 to GS4). This section will address the research questions proposed in the Introduction, as well as explore additional Tukey HSD post-hoc results.

THE IMPACT OF DIFFERENT CROP MANAGEMENT REGIMES ON REMOTELY SENSED DATA

The nature of experimenting on operational crop fields poses difficulty in maintaining a controlled experiment. While it was expected that spectral differences would be observed between fields due to different management regimes, quantitatively testing parameters such as soil moisture were beyond the scope and purpose of this study. This section will address the research question: *Did soil management regimes affect the 3 way interaction of Growth Stage and Treatment between different Fields?* Furthermore, possible reasoning

for why there were observed differences will be discussed by drawing inferences from relevant research.

Indeed, a difference occurred between fields when observing the 3-way interaction effects in the RCBD design. Even non-significant 3-way interactions, although statistically similar, exhibited differences when examining the post-hoc tests. Non-significant 3-way interactions were found in NDVI (p=0.415), RE-NDVI (p=0.383) and TGI (p=0.780) (Figure 21). The non-significant interactions indicate that both fields responded similarly to treatments across all growth stages. Significant 3-way interactions were found in RDVI (p=0.003) and RE-RDVI (p=0.005), indicating dissimilar spectral response of fields across growth stages and treatments. An anomaly can be observed when comparing the spectral response of GS3 between fields for respective treatments (Figure 21 & 22). The Tukey HSD revealed that the spectral mean of Control treatments were not significantly different between fields for four out of five indices; only TGI showed significant difference between the field means for Control (p=0.047). This was interesting as most VIs agree that fields responded similarly to the control treatment. For the Stratego, and Stratego + Prosaro treatments, four out of five indices had significantly different means between fields, with only RE-NDVI being similar for S (p=0.559) and SP (p=0.713). Evidently, most indices performed differently between fields during GS3, with the exception of similarity to the Control treatment, and RE-NDVI which exhibited different behaviour than other VIs. According to literature, the possibility of observed spectral differences

between fields could be attributed to soil moisture retention due to tillage practices, which are discussed here.

As indicated in the Methodology section, the two barley fields evaluated in this study were representative of different management practices. Trumar Farm is more intensively managed, including the input of variable rate fertilizers based on soil sampling data, and manure application. This also includes alternative soil tillage practice, which involves fall disking and spring cultivation. In comparison, Hanna Farm is a less intensively managed field. The soil is not managed for variations in nutrient deficiency, and conservation tillage (a form of zero tillage which also leaves left over crop residue from previous rotations) was performed. While it was assumed that moisture would be similar between both fields due to the presence of drainage tiles, differences in retained soil moisture may have existed. In the short-term, it is well-known that tilling practices affect evaporation (Schwartz et al., 2010), infiltration (Vervoort et al., 2001), run-off (Takken et al., 2001) and even crop yield (Alam et al., 2014). Conservation tillage often results in increased soil moisture due to reduced evaporation and runoff (Acharya et al., 1998; Baumhardt & Jones, 2002). Crop residue covering the soil, combined with little soil aeration restricts the rate of evaporation. The relative proximity of both fields is approximately 2.5 km, meaning that they were subject to similar climatic conditions and weather events throughout the season. It is possible that higher retained soil moisture in Hanna Farm impacted observed differences in crop health, when inspecting the significant 3-way interactions of all vegetation indices. Local research in the Thunder Bay region

indicates there is an effect of tillage practice on the productivity and health of barley plants. The Thunder Bay Agricultural Research Station (TBARS) performed experiments on a barley-soybean rotation from 2004 to 2007, evaluating 11 different tillage systems. In general, both alternative and conventional tillage systems out-performed zero-tillage, resulting in higher yields and crop vigour (Sahota, 2008).

It is known that soil moisture levels can impact vegetation indices such as NDVI (Huete et al., 1985), prompting the creation of alternative indices to adjust for the effects of soil background in crop canopies (Baret et al., 1989; Huete, 1988; Qi et al., 1994). Indices such as NDVI have been shown to be sensitive to changes in fractional vegetation cover when LAI is less than 100 % (Carlson & Ripley, 1997). The reason for this is due to soil background (Martin et al., 2012), which reflects differently than plant material and contaminates pixel values of vegetative targets. Once there is full canopy coverage, any additional increase in LAI has very minimal effect on NDVI readings, due to minimal to no soil presence (Huete et al. 1985). Fortunately, for both Hanna and Trumar Farms, minimal to no soil presence occurred in the imagery sets due to nearly consistent full canopy coverage. Bare patches of non-fertile soil were scarcely evident in both fields; however, corrections were made to eliminate soil noise as much as possible in the pre-processing methodology. The performance of the RDVI and RE-RDVI demonstrate a statistically significant difference between fields, which could be attributed to the indices' flexibility to work well between varying canopy densities and soil presence. In areas of 100 % canopy closure, it

is possible that differences in soil moisture existed which directly impacted observed canopy health. Unfortunately, little is known about the spectral response of crops with full canopy closure, when comparing different soil moisture conditions. What is known is that local data shows an impact of tillage practice on the progression of barley. Remote sensing observations made in this study may have been impacted due to the difference of tilling practices between fields. Regardless of this possible concept, and most importantly, fungal disease severity was able to be spectrally distinguished consistently in both fields.

DISTINGUISHING FUNGAL DISEASE SEVERITY

Certainly, as a result of monitoring barley after initial disease breakout from GS1 (Feekes 8-9) to GS4 (Feekes 11.2), disease intensity and resiliency has been observed by comparison of the spectral response of VIs to fungicide treatment types. This is verified from the general main effect of treatment on VIs, and evident when viewing the 3-way interaction plots in Figure 21 & 22. Of course, it is of interest to farmers to apply fungicide spatially before the occurrence, development and spread of fungal disease in crops. In wheat, early detection of fungal disease has been shown to be difficult. For example. a similar study by Franke & Menz (2007) explored the impact of different fungicide intensities on disease severity in wheat, using moderate resolution (2.4 m/pixel) multispectral QuickBird satellite imagery. Multi-temporal data were collected over the season (Feekes 6, Feekes 10, Feekes 10.7) and visual assessments were conducted to rate disease severity on flag leaves. The authors expressed

difficulty in detecting of powdery mildew at Feekes 6, noting a high misclassification accuracy at this early growth stage. As the season progressed they were able to distinguish between four defined regions of fungal disease (powdery mildew and leaf rust) severity using a decision-tree classification methodology. While their methodology was robust, they were bound by the defined thresholds of their classes in the decision-tree algorithm. Taking on crop health variability into defined classes introduced a higher chance for error. Additionally, they only explored one index (NDVI) when developing their supervised classification maps. The authors were still nonetheless capable of localizing fungal disease presence earlier than this study; however, note that fungal infections were verified to be low for Trumar Farm (infection rates up to 12.35 %) and Hanna Farm (infection rates up to 7.53 %) during GS1 (Feekes 8-9). The findings in this work show that fungal disease severity could be distinguished as early as GS2 (Feekes 10.51, booting complete and onset of flowering), when only the Prosaro treatment was applied. Recall that Prosaro was applied on the same date as the GS2 flights; thus, there is no measurable effect of SP due to the lag time required for fungicide (for GS2: S=SP). In some cases, there was no significant statistical difference between C-S, and C-SP treatments during GS2. The 3-way interaction post-hoc test for NDVI showed non-significant differences between C-S (p=0.555) and C-SP (p=0.549) for Trumar Farm (GS2), and C-S (p=0.992), C-SP (p=0.998) for Hanna Farm (GS2). Regardless, there are still notable patterns, being consistently lower mean C treatment values for all measured VIs during GS2. This is a consistent

trend apparent in all vegetation indices for both fields, and such differences are more prominent in the TGI, RDVI and RE-RDVI, which all had statistically significant differences between C-S and C-SP (p<0.05) for GS2.

The most important trend to bring to light is the reliable separation of mean VI treatment values from GS3 to GS4. Consistently, control treatments had the lowest means, with the mean VIs increasingly positively with fungicide intensity. This trend was similar for each field and vegetation index from GS3 to GS4, and demonstrates how fungicide treatment intensity/fungal severity can be reliably distinguished. Furthermore, Trumar Farm exhibited a more pronounced separation of treatment intensity mean VI values when compared to Hanna Farm. Figures 21 & 22 to prove that this is particularly the case for GS3, where large differences in mean VI values exist between treatment types for Trumar Farm. This agrees with the visual inspection of the imagery (Figure 14 and Appendix I) where treatments strips are easily distinguishable by GS3; in Hanna Farm, treatment strips are often hard to distinguish and identify by visual inspection of the imagery (Figure 14 and Appendix I). The TGI displayed comparable performance to other indices for the detection and separation of fungal disease severity. This index only uses RGB bands and does not rely upon the near-infrared or red-edge regions of the electromagnetic spectrum. The performance of this index further verifies findings by Hunt (2013), where they concluded that there is a close relationship with TGI to canopy chlorophyll content. The utilization of RGB sensors over multispectral counterparts is

drastically cheaper, and in this study, the TGI was just as reliable in the RCBD design as other indices.

FUNGICIDE TIMING AND IMPACT ON YIELD AND SENESCENCE

Often a fungicide's effectiveness relies upon precise application timing related to growth stage, infection severity, and even meteorological parameters such as rainfall and temperature (Moschini & Pérez, 1999).This is the case with both Stratego, which is applied shortly after herbicide application when infection severity is low (Feekes 4), and Prosaro, which is applied at the onset of flowering (Feekes 10.51). Stratego is the more versatile of the two fungicides used in this study, as it allows for up to two applications during a season, occurring between the four-leaf stage to the early heading stage of barley, and other cereals. On the other hand, Prosaro requires critical application timing towards the end of the barley heading stage. While both fungicides are broad spectrum, Prosaro specifically works well for the suppression of fusarium head blight (FHB) in cereals; this disease seldom occurs in barley crops within the Thunder Bay region.

As already observed, the effects of SP treatments in this study improved upon the health of S treatments consistently. However, obviously there are high costs associated with the utilization of two fungicides. Considering this, the benefits of spot treating with Prosaro may only be realized when met with heavy FHB infestation. The performance of Stratego in this study improved the health of crops drastically over the control treatments, with Prosaro often offering only little improvements over Stratego. Additionally, only control treatment rows

experienced early senescence before August 31st, 2015 in Trumar Farm. The Trumar Farm operator noted that both Prosaro and Stratego rows could have had prolonged harvest times as the crops had yet to complete senescence (M. Bolt, personal communication, February 1, 2016). Imagery for Trumar Farm on GS4 could also clearly detect which rows were still green, hinting at an ability to monitor for optimal harvest times with UAV multispectral imagery. An additional blanket application of glyphosate was applied in Trumar Farm on August 29th to increase the senescence rate for rapid harvest. In the cases where non-senesced areas can be easily detected, the spatial application of herbicides can be applied to speed up harvest time. Or, harvest time can be prolonged in specific areas to increase grain development.

Grain yield was also analyzed in this experiment. It is already known that fungicides can have a positive effect on the amount of grain yield in cereals, prolonging the greenness of flag leaves throughout the season (Gooding et al., 2000; Pepler et al., 2005). Since this was a small experiment with few replications, yield appeared to have a weak relationship with the intensity of fungicide application. In many cases the differences between mean yields of treatment types are non-significant; however, a consistent pattern is seen where grain yield increases with fungicide intensity (Figure 23). Visual inspection of grain heads before hand-harvesting also showed huge differences in size and girth (Figure 13). More replications and observations would be desirable to verify a significant effect of fungicides/fungal presence on yield.

Findings in this study aided local farmers in the optimal selection of fungicides for their barley crops for subsequent seasons. Drastic improvements in overall crop health was observed in rows with Stratego and Prosaro, indicating a utility to assess fungicide effectiveness with the data.

SEPARATING FUNGAL DISEASE FROM OTHER STRESSES

This section will address the research question: *If alternative stress sources appear during the season in ground-truthing plots, can the multispectral sensor distinguish between types of stresses in those respective plots?* Other than fungal disease presence in both Hanna and Trumar Farms, very few other stress types were verified from the visual assessment plots. For the purposes of this thesis this is unfortunate, as the ability to spectrally separate fungal infections from different stress types could not be properly evaluated. Hanna Farm had a few distinct patches of barley yellow dwarf virus (BYDV) that broke out from GS2. BYDV typically shows up as yellowed tissue in the upper canopy leaves of barley or wheat, and characteristically forms as patches in crops. The presence of such patches in Hanna Farm were scarce and there was no distinct spectral signature within the imagery which allowed for delineation of verified areas. Other authors have verified the ability to detect BYDV in crop canopies (Gaborjanyi et al., 2003; Riedell et al., 2003); however it is likely that viral severity and the impact on leaf colour were too low for detection in Hanna Farm. Another source of stress was weed presence. The results of conventional tillage on Trumar Farm have reportedly produced consistently less weeds in the past (M. Bolt, personal communication, February 1, 2016). The low presence of

weeds in Trumar Farm was also verified when conducting visual assessments during the season. This was not the case for Hanna Farm. A mix of perennial and annual weeds emerged early in the season, and unlike Trumar, were irresponsive to herbicide application after June 26th, 2015 (Feekes 4). Most weed suppression in Hanna Farm occurred once there was full canopy closure of barley. However, clover patches remained and continued to overtake barley in the north portion of the field. Additional outbreak patches occurred along tram lines, and secluded sections of Hanna. The robustness of the presented methodology for clover pixel classification was satisfactory for this study. However, other weeds which often appeared in small isolated patches were difficult to classify and could not be separated from asymptomatic or symptomatic barley. Also, note that weed infected areas of barley will often display higher reflectance intensity values, which can impact a pixel's value when the ratio of observed weeds is higher than that of the target (Peña et al., 2013; Rasmussen et al., 2013).

For this study, since little other stress types were apparent in the fields, it cannot be determined if the Micasense can distinguish fungal disease from other stressors. However, it is unlikely that this is possible without the aid of hyperspectral data. In barley fields where fungal disease is known to be a primary stressor, developing fungal infection maps with UAV multispectral data may still be practical. However, ground-truthing will remain a requirement to verify the accuracy of such maps; this will slow the response process of immediate spraying post-UAV flights.

ROBUSTNESS OF RCBD MODEL USED IN THIS RESEARCH

As a final note regarding the RCBD design in this research, fields (Trumar, Hanna) were chosen as blocks due to the inherent differences between farm management practices. Blocking was indeed the appropriate approach for this experiment. In contemplation about the fixed variables chosen for this model (Field, Growth Stage, Treatment), it may have been desirable to refrain from modifying a temporal continuous variable (Growth Stage) into a categorical variable. Since temporal variables are often continuous in such experiments, an additional option could be to analyze the growth stages independently (each in a separate One-way ANOVA) maintaining the field blocks and having one independent variable (3 levels of fungicide treatment). This would have eliminated any observed differences in temporal variation between treatment lag time and vegetation health. However, the field-to-field response to fungal infections and treatments were obvious in all image sets, and similar results would likely have been observed. Ii is important to mention though, that in considering any future approaches for either replicating or building upon this work, this is a possible approach which should be considered.

CONCLUSION

This was the first study to evaluate UAV multispectral imagery for the spatio-temporal detection of fungal disease in barley. The effects of fungal disease and fungicide treatment intensity were monitored over four general growth stages, spanning from Feekes 8-9 (onset of flag-leaf development) until Feekes 11.4 (hardened kernels and senesced straw). Regardless of field or management type, the ability to spectrally separate crops by fungicide intensity/fungal severity was confirmed. As fungicide intensity increased, less fungal disease was evident in the fields, which was consistently detected in the imagery from GS2 (Feekes 10.51) to GS4 (Feekes 11.4). A limitation in this work was the inability to assess minimal fungal disease presence at GS1 (Feekes 8-9). Infected leaf areas were too low for the detection of heterogeneity in barley during GS1. More success may be seen when more severe fungal outbreaks occur earlier, when other crop types are monitored, or when other sensor types are utilized.

To integrate real-time remote sensing data to on-ground solutions requires more background research towards the reliable detection and spectral separation of crop stress types. In this study, ground truth data was necessary in order to prove the presence of fungal disease in remotely sensed imagery. Without ground truth data, depending purely on the spectral response of barley for fungal disease detection is unreliable. This highlights the current drawback of

most commercial or industrial multispectral sensors designed for agriculture. However, when soil and other stressors are well managed for, the spatial mapping of fungal disease can be achieved with UAV multispectral data. It is also important to note that the performance of RGB bands in the TGI index was comparable to other indices which utilize the NIR and RE bands, showing how the Micasense multispectral sensor may not be necessary to achieve similar results to this study.

In summary, the findings here give light to potential applications in monitoring for the implementation and success of new seed varieties, new chemical sprays in a given field or region, spatial herbicide or fungicide application, and even to the optimization of crop harvest times. The traditional method of physical disease assessment may yet be replaced by UAV technology, but current limitations in multispectral sensor precision push the focus towards hyperspectral technologies. To build upon this study, more work needs to be done in delaying fungicide application until foliar disease is further developed and detectable, to evaluate if spatial applications can be feasible after Feekes 8-9 in barley.

LITERATURE CITED

Acharya, C. L., Kapur, O. C., & Dixit, S. P. (1998). Moisture conservation for rainfed wheat production with alternative mulches and conservation tillage in the hills of north-west India. Soil and Tillage Research, 46(3–4), 153–163. https://doi.org/10.1016/S0167-1987(98)00030-0

Alam, M. K., Islam, M. M., Salahin, N., Hasanuzzaman, M. (2014). Effect of Tillage Practices on Soil Properties and Crop Productivity in Wheat-Mungbean-Rice Cropping System under Subtropical Climatic Conditions. The Scientific World Journal, 2014, e437283. https://doi.org/10.1155/2014/437283

Al-amri, S. S., Kalyankar, N. V., & Khamitkar, S. D. (2010). A Comparative Study of Removal Noise from Remote Sensing Image.

Anderson, K., & Croft, H. (2009). Remote sensing of soil surface properties. Progress in Physical Geography, 33(4), 457–473. https://doi.org/10.1177/0309133309346644

Armstrong, J. (2007). The Use of Early Season Multispectral Images for Weed Detection in Corn. Weed Technology, 21(4), 857. https://doi.org/10.1614/WT-06-074.1

Arshad, M. A., Gill, K. S., & Coy, G. R. (1995). Barley, Canola, and Weed Growth with Decreasing Tillage in a Cold, Semiarid Climate. Agronomy Journal, 87(1), 49. https://doi.org/10.2134/agronj1995.00021962008700010009x

Ashourloo, D., Mobasheri, M. R., & Huete, A. (2014). Developing Two Spectral Disease Indices for Detection of Wheat Leaf Rust (Pucciniatriticina). Remote Sensing, 6(6), 4723–4740. https://doi.org/10.3390/rs6064723

Asner, G. P., & Heidebrecht, K. B. (2002). Spectral unmixing of vegetation, soil and dry carbon cover in arid regions: Comparing multispectral and hyperspectral observations. International Journal of Remote Sensing, 23(19), 3939–3958. https://doi.org/10.1080/01431160110115960

Aubert, M., Baghdadi, N. N., Zribi, M., Ose, K., El Hajj, M., Vaudour, E., & Gonzalez-Sosa, E. (2013). Toward an Operational Bare Soil Moisture Mapping Using TerraSAR-X Data Acquired Over Agricultural Areas. IEEE Journal of Selected Topics in Applied Earth Observations and Remote Sensing, 6(2, 3), 900–916. https://doi.org/10.1109/JSTARS.2012.2220124

Avena, G. C., Ricotta, C., & Volpe, F. (1999). The influence of principal component analysis on the spatial structure of a multispectral dataset. International Journal of Remote Sensing, 20(17), 3367–3376. https://doi.org/10.1080/014311699211381

Baranoski, G. V. G., & Rokne, J. G. (2005). A practical approach for estimating the red edge position of plant leaf reflectance. International Journal of Remote Sensing, 26(3), 503–521. https://doi.org/10.1080/01431160512331314029

Baret, F., Champion, I., Guyot, G., & Podaire, A. (1987). Monitoring wheat canopies with a high spectral resolution radiometer. Remote Sensing of Environment, 22(3), 367–378. https://doi.org/10.1016/0034-4257(87)90089-7

Baret, F., Guyot, G., & Major, D. J. (1989). TSAVI: A Vegetation Index Which Minimizes Soil Brightness Effects On LAI And APAR Estimation. In Geoscience and Remote Sensing Symposium, 1989. IGARSS'89. 12th Canadian Symposium on Remote Sensing., 1989 International (Vol. 3, pp. 1355–1358). https://doi.org/10.1109/IGARSS.1989.576128

Baumhardt, R. L., & Jones, O. R. (2002). Residue management and tillage effects on soil-water storage and grain yield of dryland wheat and sorghum for a clay loam in Texas. Soil and Tillage Research, 68(2), 71–82. https://doi.org/10.1016/S0167-1987(02)00097-1

Bauriegel, E. (2011). Early detection of Fusarium infection in wheat using hyper-spectral imaging. Computers and Electronics in Agriculture, 75(2), 304–312.

Bellvert, J., Zarco-Tejada, P., Girona, J., & Fereres, E. (2014). Mapping crop water stress index in a "Pinot-noir" vineyard: comparing ground

measurements with thermal remote sensing imagery from an unmanned aerial vehicle. Precision Agriculture, 15(4), 361.

Berni, J. A. J., Zarco-Tejada, P., Suarez, L., & Fereres, E. (2009). Thermal and narrowband multispectral remote sensing for vegetation monitoring from an unmanned aerial vehicle. IEEE Transactions on Geoscience and Remote Sensing, (3), 722.

Blazquez, C. H., & Edwards, G. J. (1986). Spectral reflectance of healthy and diseased watermelon leaves. Annals of Applied Biology, 108(2), 243–249. https://doi.org/10.1111/j.1744-7348.1986.tb07646.x

Bojović, B., & Marković, A. (2009). Correlation between nitrogen and chlorophyll content in wheat (Triticum aestivum L.). ResearchGate, 31. https://www.researchgate.net/publication/266609505_Correlation_between_nitrogen_and_chlorophyll_content_in_wheat_Triticum_aestivum_L

Bolt, M. (2016, February 1). Personal communication.

Bongiovanni, R., & Lowenberg-Deboer, J. (2004). Precision Agriculture and Sustainability. Precision Agriculture, 5(4), 359–387. https://doi.org/10.1023/B:PRAG.0000040806.39604.aa

Broscious, S. C. (1985). Influence of Winter Wheat Management Practices on the Severity of Powdery Mildew and Septoria Blotch in Pennsylvania. Phytopathology, 75(5), 538. https://doi.org/10.1094/Phyto-75-538

Buttafuoco, G., Annamaria Castrignanò, Antonio, S. C., & Ricca, N. (2010). Delineation of Management Zones Using Soil Properties and a Multivariate Geostatistical Approach. Italian Journal of Agronomy, (Journal Article). https://doi.org/10.4081/ija.2010.323

Bock, C. H. (2010). Plant Disease Severity Estimated Visually, by Digital Photography and Image Analysis, and by Hyperspectral Imaging. Critical Reviews in Plant Sciences, 29(2). https://doi.org/10.1080/07352681003617285

Calderón, R. (2014). Detection of downy mildew of opium poppy using high-resolution multi-spectral and thermal imagery acquired with an unmanned aerial vehicle. Precision Agriculture, 15(6), 639–661.

Calderón, R., Navas-Cortés, J. A., Lucena, C., & Zarco-Tejada, P. J. (2013). High-resolution airborne hyperspectral and thermal imagery for early detection of Verticillium wilt of olive using fluorescence, temperature and narrow-band spectral indices. Remote Sensing of Environment, 139, 231–245. https://doi.org/10.1016/j.rse.2013.07.031

Cao, X., Luo, Y., Zhou, Y., Fan, J., Xu, X., West, J. S., & Cheng, D. (2015). Detection of Powdery Mildew in Two Winter Wheat Plant Densities and Prediction of Grain Yield Using Canopy Hyperspectral Reflectance. PLoS ONE, 10(3), 1–14. https://doi.org/10.1371/journal.pone.0121462

Carlson, T. N., & Ripley, D. A. (1997). On the relation between NDVI, fractional vegetation cover, and leaf area index. Remote Sensing of Environment, 62(3), 241–252. https://doi.org/10.1016/S0034-4257(97)00104-1

Chavez, P. S., & Mackinnon, D. J. (1994). Automatic detection of vegetation changes in the southwestern United States using remotely sensed images. Photogramm Eng Remote Sens. Photogrammetric Engineering and Remote Sensing, 60(5), 571–582.

Chenghai, Y., Everitt, J. H., Qian Du, Bin Luo, & Chanussot, J. (2013). Using High-Resolution Airborne and Satellite Imagery to Assess Crop Growth and Yield Variability for Precision Agriculture. Proceedings of the IEEE, 101(3), 582–592. https://doi.org/10.1109/JPROC.2012.2196249

Collins, W. (1978). Remote sensing of crop type and maturity. *Photogrammetric Engineering and Remote Sensing*. 44, 43-55.

Colwell, R. N. (1956). Determining the prevalence of certain cereal crop diseases by means of aerial photography. Hilgardia, 26(5), 223–286. https://doi.org/10.3733/hilg.v26n05p223

Dammer, K. H., & Ehlert, D. (2006). Variable-rate fungicide spraying in cereals using a plant cover sensor. Precision Agriculture, 7(2), 137–148. https://doi.org/10.1007/s11119-006-9005-x

Daughtry, C., Walthall, C. L., Kim, M. S., de Colstoun, E. B., & McMurtrey III, J. E. (2000). Estimating Corn Leaf Chlorophyll Concentration from Leaf and

Canopy Reflectance. Remote Sensing of Environment, 74(2), 229–239. https://doi.org/10.1016/S0034-4257(00)00113-9

Demetriades-Shah, T. H., Steven, M. D., & Clark, J. A. (1990). High resolution derivative spectra in remote sensing. Remote Sensing of Environment, 33(1), 55–64. https://doi.org/10.1016/0034-4257(90)90055-Q

Demšar, U., Harris, P., Brunsdon, C., Fotheringham, A. S., & McLoone, S. (2013). Principal Component Analysis on Spatial Data: An Overview. Annals of the Association of American Geographers, 103(1), 106–128. https://doi.org/10.1080/00045608.2012.689236

Derpsch, R., Friedrich, T., Kassam, A., & Li, H. (2010). Current Status of Adoption of No-till Farming in the World and Some of its Main Benefits. International Journal of Agricultural and Biological Engineering, 3(1), 1–25. https://doi.org/10.3965/ijabe.v3i1.223

Devadas, R., Lamb, D. W., Backhouse, D., & Simpfendorfer, S. (2015). Sequential application of hyperspectral indices for delineation of stripe rust infection and nitrogen deficiency in wheat. Precision Agriculture, 1–15. https://doi.org/10.1007/s11119-015-9390-0

Devadas, R., Lamb, D. W., Simpfendorfer, S., & Backhouse, D. (2008). Evaluating ten spectral vegetation indices for identifying rust infection in individual wheat leaves. Precision Agriculture, 10(6), 459–470. https://doi.org/10.1007/s11119-008-9100-2

Dewitte, O., Jones, A., Elbelrhiti, H., Horion, S., & Montanarella, L. (2012). Satellite remote sensing for soil mapping in Africa: An overview. Progress in Physical Geography, 36(4), 514–538. https://doi.org/10.1177/0309133312446981

Domiciano, G. P., Duarte, H. S. S., Moreira, E. N., & Rodrigues, F. A. (2014). Development and validation of a set of standard area diagrams to aid in estimation of spot blotch severity on wheat leaves. Plant Pathology, 63(4), 922–928. https://doi.org/10.1111/ppa.12150

Eddy, P. R., Smith, A. M., Hill, B. D., Peddle, D. R., Coburn, C. A., & Blackshaw, R. E. (2014). Weed and crop discrimination using hyperspectral image data and reduced bandsets. Canadian Journal of Remote Sensing, 39(6), 481–490. https://doi.org/10.5589/m14-001

Filella, I., Serrano, L., Serra, J., & Peñuelas, J. (1995). Evaluating Wheat Nitrogen Status with Canopy Reflectance Indices and Discriminant Analysis. Crop Science, 35(5), 1400. https://doi.org/10.2135/cropsci1995.0011183X003500050023x

Fitzgerald, G. (2010). Measuring and predicting canopy nitrogen nutrition in wheat using a spectral index—The canopy chlorophyll content index (CCCI). Field Crops Research, 116(3), 318–324.

Franke, J., & Menz, G. (2007). Multi-temporal wheat disease detection by multi-spectral remote sensing. Precision Agriculture.

Franke, J., Menz, G., Oerke, E. C., & Rascher, U. (2005). Comparison of multi- and hyperspectral imaging data of leaf rust infected wheat plants (Vol. 5976, p. 59761D–59761D–11). https://doi.org/10.1117/12.626531

Gaborjanyi, R., Pasztor, L., Papp, M., Szabo, A., Mesterhazy, A., Nemeth, T., & Komives, T. (2003). Use of remote sensing to detect virus infected wheat plants in the field. Cereal Research Communications Hungary. http://agris.fao.org/agris-search/search.do?recordID=HU2003000373

Gevaert, C. M., Tang, J., García-Haro, F. J., Suomalainen, J., & Kooistra, L. (2014). Combining Hyperspectral UAV and Multispectral Formosat-2 Imagery for Precision Agriculture Applications. In ResearchGate. https://www.researchgate.net/publication/270897304_Combining_Hyperspectral_UAV_and_Multispectral_Formosat-2_Imagery_for_Precision_Agriculture_Applications

Gitelson, A., Gritz, Y., & Merzlyak, M. N. (2003). Relationships between leaf chlorophyll content and spectral reflectance and algorithms for non-destructive chlorophyll assessment in higher plant leaves. Journal of Plant Physiology, 160(3), 271–282. https://doi.org/10.1078/0176-1617-00887

Gitelson, A. A., & Merzlyak, M. N. (1996). Signature Analysis of Leaf Reflectance Spectra: Algorithm Development for Remote Sensing of Chlorophyll. Journal of Plant Physiology, 148(3–4), 494–500. https://doi.org/10.1016/S0176-1617(96)80284-7

Gitelson, A. A., Viña, A., Arkebauer, T. J., Rundquist, D. C., Keydan, G., & Leavitt, B. (2003). Remote estimation of leaf area index and green leaf biomass in maize canopies. Geophysical Research Letters, 30(5), 1248. https://doi.org/10.1029/2002GL016450

Gitelson, A. A., Viña, A., Ciganda, V., Rundquist, D. C., & Arkebauer, T. J. (2005). Remote estimation of canopy chlorophyll content in crops. Geophysical Research Letters, 32(8), L08403. https://doi.org/10.1029/2005GL022688

Godoy, C. V., Koga, L. J., & Canteri, M. G. (2006). Diagrammatic scale for assessment of soybean rust severity. Fitopatologia Brasileira, 31(1), 63–68. https://doi.org/10.1590/S0100-41582006000100011

Goldman, D. B. (2010). Vignette and Exposure Calibration and Compensation. IEEE Transactions on Pattern Analysis and Machine Intelligence, 32(12), 2276–2288. https://doi.org/10.1109/TPAMI.2010.55

Gooding, M. J., Dimmock, J. P. R. E., France, J., & Jones, S. A. (2000). Green leaf area decline of wheat flag leaves: the influence of fungicides and relationships with mean grain weight and grain yield. Annals of Applied Biology, 136(1), 77–84. https://doi.org/10.1111/j.1744-7348.2000.tb00011.x

Goodman, M. (1959). A technique for the identification of farm crops on aerial photographs. Photogrammetric Engineering, 25, 131-137.

Green, A. A., Berman, M., Switzer, P., & Craig, M. D. (1988). A transformation for ordering multispectral data in terms of image quality with implications for noise removal. IEEE Transactions on Geoscience and Remote Sensing, 26(1), 65–74. https://doi.org/10.1109/36.3001

Hakala, T., Suomalainen, J., & Peltoniemi, J. I. (2010). Acquisition of Bidirectional Reflectance Factor Dataset Using a Micro Unmanned Aerial Vehicle and a Consumer Camera. Remote Sensing, 2(3), 819–832. https://doi.org/10.3390/rs2030819

Hall, A., & Wilson, M. A. (2013). Object-based analysis of grapevine canopy relationships with winegrape composition and yield in two contrasting vineyards using multitemporal high spatial resolution optical remote sensing. International Journal of Remote Sensing, 34(5), 1772–1797. https://doi.org/10.1080/01431161.2012.726753

Hall, F. G., Strebel, D. E., Nickeson, J. E., & Goetz, S. J. (1991). Radiometric rectification: Toward a common radiometric response among multidate, multisensor images. Remote Sensing of Environment, 35(1), 11–27. https://doi.org/10.1016/0034-4257(91)90062-B

Hansen, J. G., Secher, B. J. M., Jørgensen, L. N., & Welling, B. (1994). Thresholds for control of Septoria spp. in winter wheat based on precipitation and growth stage. Plant Pathology, 43(1), 183–189. https://doi.org/10.1111/j.1365-3059.1994.tb00569.x

Hedley, C. (2014). The role of precision agriculture for improved nutrient management on farms. Journal of the Science of Food and Agriculture, 95(1).http://ezproxy.lakeheadu.ca/login?url=http://search.ebscohost.com/login.aspx?direct=true&db=cmedm&AN=24816925&site=eds-live&scope=site

Heege, H. J. (2013). Precision in Crop Farming: Site Specific Concepts and Sensing Methods: Applications and Results. Springer Science & Business Media.

Herrero-Huerta, M., Hernandez-Lopez, D., Rodriguez-Gonzalvez, P., Gonzalez-Aguilera, D., & Gonzalez-Piqueras, J. (2014). Vicarious radiometric calibration of a multispectral sensor from an aerial trike applied to precision agriculture. Computers and Electronics in Agriculture, 28. https://doi.org/10.1016/j.compag.2014.07.001

Hong, G., & Zhang, Y. (2008). A comparative study on radiometric normalization using high resolution satellite images. International Journal of Remote Sensing, 29(2), 425–438. https://doi.org/10.1080/01431160601086019

Horler, D. N. H., Dockray, M., & Barber, J. (1983). The red edge of plant leaf reflectance. International Journal of Remote Sensing, 4(2), 273–288. https://doi.org/10.1080/01431168308948546

Huete, A. R. (1988). A soil-adjusted vegetation index (SAVI). Remote Sensing of Environment, 25(3), 295–309. https://doi.org/10.1016/0034-4257(88)90106-X

Huete, A. R., Jackson, R. D., & Post, D. F. (1985). Spectral response of a plant canopy with different soil backgrounds. Remote Sensing of Environment, 17(1), 37–53. https://doi.org/10.1016/0034-4257(85)90111-7

Hunt, E. R., Cavigelli, M., Daughtry, C. S. T., Iii, J. E. M., & Walthall, C. L. (2005). Evaluation of Digital Photography from Model Aircraft for Remote Sensing of Crop Biomass and Nitrogen Status. Precision Agriculture, 6(4), 359–378. https://doi.org/10.1007/s11119-005-2324-5

Hunt, E. R. (2013). A visible band index for remote sensing leaf chlorophyll content at the canopy scale. International Journal of Applied Earth Observations and Geoinformation, 21, 103–112.

Hunt, E. R. (2014). Remote Sensing With Simulated Unmanned Aircraft Imagery for Precision Agriculture Applications. IEEE Journal of Selected Topics in Applied Earth Observations and Remote Sensing, 7(11), 4566–4571.

Hunt, E. R., Long, D. S., Eitel, J. U. H., & Daughtry, C. S. T. (2010). Remote sensing of leaf chlorophyll content at multiple scales using red, green, and blue bands (Vol. 7809, pp. 780902-780902–6). https://doi.org/10.1117/12.859142

Ingenhousz, J. (1779). Experiments upon vegetables: discovering their great power of purifying the common air in the sun-shine, and of injuring it in the shade and at night. To which is joined, a new method of examining the accurate degree of salubrity of the atmosphere. Printed for P. Elmsly and H. Payne.

Jones, H. G., & Vaughan, R. A. (2010). Remote sensing of vegetation : principles, techniques, and applications / Hamlyn G. Jones, Robin A. Vaughan. Oxford ; New York : Oxford University Press, 2010.

Kelcey, J., & Lucieer, A. (2012). Sensor Correction of a 6-Band Multispectral Imaging Sensor for UAV Remote Sensing. Remote Sensing, 4(5), 1462–1493. https://doi.org/10.3390/rs4051462

Klemas, V., Finkl, C. W., & Kabbara, N. (2014). Remote Sensing of Soil Moisture: An Overview in Relation to Coastal Soils. Journal of Coastal Research, 30(4), 685–696. https://doi.org/10.2112/JCOASTRES-D-13-00072.1

Knipling, E. B. (1970). Physical and physiological basis for the reflectance of visible and near-infrared radiation from vegetation. Remote Sensing of Environment, 1(3), 155–159. https://doi.org/10.1016/S0034-4257(70)80021-9

Kuckenberg, J. (2009). Temporal and spatial changes of chlorophyll fluorescence as a basis for early and precise detection of leaf rust and powdery mildew infections in wheat leaves. Precision Agriculture, 10(1), 34–44.

Lafond, G. P., Loeppky, H., & Derksen, D. A. (1992). The effects of tillage systems and crop rotations on soil water conservation, seedling establishment and crop yield. Canadian Journal of Plant Science, 72(1), 103–115. https://doi.org/10.4141/cjps92-011

Laliberte, A. S., Goforth, M. A., Steele, C. M., & Rango, A. (2011). Multispectral remote sensing from unmanned aircraft: image processing workflows and applications for rangeland environments. ARS USDA Submissions, (11).

Large, E. C. (1954). Growth Stages in Cereals Illustration of the Feekes Scale. Plant Pathology, 3(4), 128–129. https://doi.org/10.1111/j.1365-3059.1954.tb00716.x

Larsolle, A., & Muhammed, H. H. (2007). Measuring crop status using multivariate analysis of hyperspectral field reflectance with application to disease severity and plant density. Precision Agriculture, 8(1–2), 37–47. https://doi.org/10.1007/s11119-006-9027-4

Lelong, C. C. D., Burger, P., Jubelin, G., Roux, B., Labbé, S., & Baret, F. (2008). Assessment of Unmanned Aerial Vehicles Imagery for Quantitative Monitoring of Wheat Crop in Small Plots. Sensors, 8(5), 3557–3585. https://doi.org/10.3390/s8053557

Lopez Granados, F. (2011). Weed detection for site-specific weed management: mapping and real-time approaches. Weed Research, 51(1), 1–11.

López-López, M., Calderón, R., González-Dugo, V., Zarco-Tejada, P. J., & Fereres, E. (2016). Early Detection and Quantification of Almond Red Leaf Blotch Using High-Resolution Hyperspectral and Thermal Imagery. Remote Sensing, 8(4), 276. https://doi.org/10.3390/rs8040276

Ma, Y., Qin, H., Yin, C., Gao, W., Zhang, H., Sui, P., Li, X. (2008). Dynamics of soil water content under different tillage systems in agro-pastural eco-zone. Frontiers of Agriculture in China, 2(2), 208–215. https://doi.org/10.1007/s11703-008-0034-2

Mahlein, A. K., Oerke, E. C., Steiner, U., & Dehne, H. W. (2012). Recent advances in sensing plant diseases for precision crop protection. European Journal of Plant Pathology, 133(1), 197–209. https://doi.org/10.1007/s10658-011-9878-z

Mahlein, A. K., Rumpf, T., Welke, P., Dehne, H. W., Plümer, L., Steiner, U., & Oerke, E. C. (2013). Development of spectral indices for detecting and identifying plant diseases. Remote Sensing of Environment, 128, 21–30. https://doi.org/10.1016/j.rse.2012.09.019

Martin, D. E., Lopez Jr., & Lan, Y. (2012). Laboratory evaluation of the GreenSeeker handheld optical sensor to variations in orientation and height above canopy. International Journal of Agricultural and Biological Engineering, 5(1), 43–47. https://doi.org/10.3965/ijabe.v5i1.572

Mitchell, J. J., Glenn, N. F., Anderson, M. O., Hruska, R. C., Halford, A., Baun, C., & Nydegger, N. (2012). Unmanned aerial vehicle (UAV) hyperspectral remote sensing for dryland vegetation monitoring. In 2012 4th Workshop on Hyperspectral Image and Signal Processing: Evolution in Remote Sensing (WHISPERS), 1–10. https://doi.org/10.1109/WHISPERS.2012.6874315

Moges, S. M., Raun, W. R., Mullen, R. W., Freeman, K. W., Johnson, G. V., & Solie, J. B. (2004). Evaluation of Green, Red, and Near Infrared Bands for Predicting Winter Wheat Biomass, Nitrogen Uptake, and Final Grain Yield#. Journal of Plant Nutrition, 27(8), 1431–1441. https://doi.org/10.1081/PLN-200025858

Moran, M. S., Bryant, R., Thome, K., Ni, W., Nouvellon, Y., Gonzalez-Dugo, M. P., Clarke, T. R. (2001). A refined empirical line approach for reflectance factor retrieval from Landsat-5 TM and Landsat-7 ETM+. Remote Sensing of Environment, 78(1–2), 71–82. https://doi.org/10.1016/S0034-4257(01)00250-4

Moschini, R. C., & Pérez, B. A. (1999). Predicting Wheat Leaf Rust Severity Using Planting Date, Genetic Resistance, and Weather Variables. Plant Disease, 83(4), 381–384. https://doi.org/10.1094/PDIS.1999.83.4.381

Mulla, D. (2013). Special Issue: Sensing in Agriculture: Twenty five years of remote sensing in precision agriculture: Key advances and remaining knowledge gaps. Biosystems Engineering, 114(4), 358–371. https://doi.org/10.1016/j.biosystemseng.2012.08.009

Mullikin, J. C., van Vliet, L. J., Netten, H., Boddeke, F. R., van der Feltz, G., & Young, I. T. (1994). Methods for CCD camera characterization (Vol. 2173, pp. 73–84). https://doi.org/10.1117/12.175165

Murray, G. M., Ellison, P. J., Watson, A., & Cullis, B. R. (1994). The relationship between wheat yield and stripe rust as affected by length of epidemic and

temperature at the grain development stage of crop growth. Plant Pathology, 43(2), 397–405. https://doi.org/10.1111/j.1365-3059.1994.tb02701.x

Myers, V. I., & Allen, W. A. (1968). Electrooptical Remote Sensing Methods as Nondestructive Testing and Measuring Techniques in Agriculture. Applied Optics, 7(9), 1819. https://doi.org/10.1364/AO.7.001819

Nellis, M., Price, K., & Rundquist, D. (2009). Remote sensing of cropland agriculture. Papers in Natural Resources. 217. http://digitalcommons.unl.edu/natrespapers/217

Nutter, F. W. J. (1990). Remote sensing and image analysis for crop loss assessment. Presented at the International Workshop on Crop Loss Assessment to Improve Pest Management in Rice and Rice-based Cropping Systems In South and Southeast Asia, Los Banos, Laguna (Philippines), 11-17 Oct 1987, IRRI. Retrieved from http://agris.fao.org/agris-search/search.do?recordID=PH9011119

Oerke, E. C., Lindenthal, M., Fröhling, P., & Steiner, U. (2005). Digital infrared thermography for the assessment of leaf pathogens. (pp. 91–98). Wageningen Academic Publishers.

Oerke, E. C. (1999). Chapter 3 - Estimated crop losses due to pathogens, animal pests and weeds. Crop Production and Crop Protection, 72–741. http://www.sciencedirect.com/science/article/pii/B9780444820952500099

Park, R. F., Ash, G. J., & Rees, R. G. (1992). Effects of temperature on the response of some Australian wheat cultivars to Puccinia striiformis f. sp. tritici. Mycological Research, 96(3), 166–170. https://doi.org/10.1016/S0953-7562(09)80961-1

Peña, J. M., Torres-Sánchez, J., de Castro, A., Ana, I., Kelly, M., & López-Granados, F. (2013). Weed Mapping in Early-Season Maize Fields Using Object-Based Analysis of Unmanned Aerial Vehicle (UAV) Images. PLoS ONE, 8(10), e77151.

Peña-Barragán, J. M., Ngugi, M. K., Plant, R. E., & Six, J. (2011). Object-based crop identification using multiple vegetation indices, textural features and crop phenology. Remote Sensing of Environment, 115, 1301–1316. https://doi.org/10.1016/j.rse.2011.01.009

Pepler, S., Gooding, M. J., Ford, K. E., & Ellis, R. H. (2005). A temporal limit to the association between flag leaf life extension by fungicides and wheat yields. European Journal of Agronomy, 22(4), 363–373. https://doi.org/10.1016/j.eja.2004.06.002

Pereira, J. M. C., & Carreiras, J. M. B. (2005). SPOT‐4 VEGETATION multi‐temporal compositing for land cover change studies over tropical regions. International Journal of Remote Sensing, 26(7), 1323–1346. https://doi.org/10.1080/01431160512331338005

Piwowar, J. M., & Millward, A. A. (2002). Multitemporal change analysis of multispectral imagery using principal components analysis. In Geoscience and Remote Sensing Symposium, 2002. IGARSS ’02. 2002 IEEE International (Vol. 3, pp. 1851–1853 vol.3). https://doi.org/10.1109/IGARSS.2002.1026276

Qi, J., Chehbouni, A., Huete, A. R., Kerr, Y. H., & Sorooshian, S. (1994). A modified soil adjusted vegetation index. Remote Sensing of Environment, 48(2), 119–126. https://doi.org/10.1016/0034-4257(94)90134-1

Qin, Z., & Zhang, M. (2005). Detection of rice sheath blight for in-season disease management using multispectral remote sensing. International Journal of Applied Earth Observation and Geoinformation, 7(2), 115–128. https://doi.org/10.1016/j.jag.2005.03.004

Rasmussen, J., Nielsen, J., Garcia-Ruiz, F., Christensen, S., Streibig, J. C., & Lotz, B. (2013). Potential uses of small unmanned aircraft systems (UAS) in weed research. Weed Research, 53(4), 242–248. https://doi.org/10.1111/wre.12026

Riedell, W. E., Osborne, S. L., Hesler, L. S., Langham, M. A. C., & Robert, P. C. (2003). Remote sensing of barley yellow dwarf and wheat streak mosaic disease in winter wheat canopies. (pp. 1696–1701). Presented at the Proceedings of the 6th International Conference on Precision Agriculture and Other Precision Resources Management, Minneapolis, MN, USA, 14-17 July, 2002., American Society of Agronomy. http://isplb03-

aux3.semantico.net/abstracts/20043029911.html;jsessionid=39B4FA483F751B412F1F6D5352696E68

Robert, C., Bancal, M. O., Ney, B., & Lannou, C. (2005). Wheat leaf photosynthesis loss due to leaf rust, with respect to lesion development and leaf nitrogen status. New Phytologist, 165(1), 227–241. https://doi.org/10.1111/j.1469-8137.2004.01237.x

Robert, C., Bancal, M.-O., Nicolas, P., Lannou, C., & Ney, B. (2004). Analysis and modelling of effects of leaf rust and Septoria tritici blotch on wheat growth. Journal of Experimental Botany, 55(399), 1079–1094. https://doi.org/10.1093/jxb/erh108

Roermund, H. J. W. V., & Spitters, C. J. T. (1990). Simulation of yield reduction by leaf rust in winter wheat, applied to the analysis of genetic variation in partial resistance. Netherlands Journal of Plant Pathology, 96(1), 17–28. https://doi.org/10.1007/BF01976603

Roujean, J.-L., & Breon, F.-M. (1995). Estimating PAR absorbed by vegetation from bidirectional reflectance measurements. Remote Sensing of Environment, 51(3), 375–384. https://doi.org/10.1016/0034-4257(94)00114-3

Rouse, J. W., Jr., Haas, R. H., Schell, J. A., & Deering, D. W. (1974). Monitoring Vegetation Systems in the Great Plains with Erts. NASA Special Publication, 351, 309.

Sahota, T. (2008). Alternative tillage systems to save time and fuel. http://tbars.net/alternativetil.pdf

Schlemmer, M., Gitelson, A., Schepers, J., Ferguson, R., Peng, Y., Shanahan, J., & Rundquist, D. (2013). Remote estimation of nitrogen and chlorophyll contents in maize at leaf and canopy levels. International Journal of Applied Earth Observation and Geoinformation, 25, 47–54. https://doi.org/10.1016/j.jag.2013.04.003

Schnug, E., Panten, K., & Haneklaus, S. (1998). Sampling and nutrient recommendations - the future. Communications in Soil Science and Plant Analysis, 29(11–14), 1455–1462. https://doi.org/10.1080/00103629809370042

Schwartz, R. C., Baumhardt, R. L., & Evett, S. R. (2010). Tillage effects on soil water redistribution and bare soil evaporation throughout a season. Soil and Tillage Research, 110(2), 221–229. https://doi.org/10.1016/j.still.2010.07.015

Shaw, D. R., & Kelley, F. S. (2005). Evaluating Remote Sensing for Determining and Classifying Soybean Anomalies. Precision Agriculture, 6(5), 421–429. https://doi.org/10.1007/s11119-005-3681-9

Simpson, A., Stombaugh, T., Wells, L., & Jacob, J. (2003). Imaging Techniques and Applications for UAV's in Agriculture. American Society of

Agricultural and Biological Engineers. https://doi.org/10.13031/2013.14929

Smith, G. M., & Milton, E. J. (1999). The use of the empirical line method to calibrate remotely sensed data to reflectance. International Journal of Remote Sensing, 20(13), 2653–2662. https://doi.org/10.1080/014311699211994

Spitters, C. J. T., Roermund, H. J. V., Nassau, H. G., Schepers, J., & Mesdag, J. (1990). Genetic variation in partial resistance to leaf rust in winter wheat: disease progress, foliage senescence and yield reduction. Netherlands Journal of Plant Pathology, 96(1), 3–15. https://doi.org/10.1007/BF01976602

Statistics Canada. (2011). Climate trends in Thunder Bay. http://www.farmnorth.com/websites/farmnorth.com/districts/11/files/Climate-Trends-Thunder-Bay.pdf

Takken, I., Govers, G., Jetten, V., Nachtergaele, J., Steegen, A., & Poesen, J. (2001). Effects of tillage on runoff and erosion patterns. Soil and Tillage Research, 61(1–2), 55–60. https://doi.org/10.1016/S0167-1987(01)00178-7

Thenkabail, P. S., Smith, R. B., & Pauw, E. D. (2002). Evaluation of Narrowband and Broadband Vegetation Indeces for Determining Optimal Hyperspectral Wavebands for Agricultural Crop Characterization. ResearchGate, 68(6), 607–621.

Thomasson, J. A., Sui, R., Cox, M. S., & Al-Rajehy, A. (2001). Soil Reflectance Sensing for Determining Soil Properties in Precision Agriculture. Transactions of the ASAE. Retrieved from http://agris.fao.org/agris-search/search.do?recordID=US201600033021

Torres Sanchez, J., Pena-Barragan, J. M., Gomez Candon, D., De-Castro, A. I., & Lopez Granados, F. (2013). Imagery from unmanned aerial vehicles for early site specific weed management, (Generic), 193–199.

Tucker, C. J. (1979). Red and Photographic Infrared Linear Combinations for Monitoring Vegetation. Remote Sensing of Environment, 8(2). https://doi.org/10.1016/0034-4257(79)90013-0

United States, Dept. of Agriculture., Statistical Reporting Service., United States., Huddleston, H. F., Roberts, E. H., & 1930-. (1968). Use of remote sensing for livestock inventories.

Urbahs, A., & Jonaite, I. (2013). Features of the use of unmanned aerial vehicles for agriculture applications. Aviation (1648-7788), 17(4), 170.

Vaudour, E., Moeys, J., Gilliot, J. M., & Coquet, Y. (2008). Spatial retrieval of soil reflectance from SPOT multispectral data using the empirical line method. International Journal of Remote Sensing, 29(19), 5571–5584. https://doi.org/10.1080/01431160802060920

Velandia, M., Rejesus, R. M., Bronson, K., & Segarra, E. (2008). Economics of Management Zone Delineation in Cotton Precision Agriculture. Journal of Cotton Science, 12(3), 210.

Vervoort, R. W., Dabney, S. M., & Römkens, M. J. M. (2001). Tillage and Row Position Effects on Water and Solute Infiltration Characteristics. Soil Science Society of America Journal, 65(4), 1227. https://doi.org/10.2136/sssaj2001.6541227x

Viscarra Rossel, R. A., Walvoort, D. J. J., McBratney, A. B., Janik, L. J., & Skjemstad, J. O. (2006). Visible, near infrared, mid infrared or combined diffuse reflectance spectroscopy for simultaneous assessment of various soil properties. Geoderma, 131(1–2), 59–75. https://doi.org/10.1016/j.geoderma.2005.03.007

Von Steen, D. H. (1969). Remote sensing relationship of aerial photography reflectance to crop yields. https://www.nass.usda.gov/Education_and_Outreach/Reports,_Presentations_and_Conferences/GIS_Reports/Remote%20Sensing%20Relationship%20of%20Aerial%20Photography%20Reflectance%20to%20Crop%20Yields.pdf

Wang, A., Qiu, T., & Shao, L. (2009). A Simple Method of Radial Distortion Correction with Centre of Distortion Estimation. Journal of Mathematical Imaging and Vision, 35(3), 165–172. https://doi.org/10.1007/s10851-009-0162-1

West, J. S., Bravo, C., Oberti, R., Lemaire, D., Moshou, D., & McCartney, H. A. (2003). The Potential of Optical Canopy Measurement for Targeted Control of Field Crop Diseases. Annual Review of Phytopathology, 41(1), 593–614.

Willis, W. O., & Bond, J. J. (1971). Soil Water Evaporation: Reduction by Simulated Tillage1. Soil Science Society of America Journal, 35(4), 526. https://doi.org/10.2136/sssaj1971.03615995003500040016x

Wilson, J. (2014). Separating Crop Species in Northeastern Ontario Using Hyperspectral Data. Remote Sensing, 6(2), 925–945. https://doi.org/10.3390/rs6020925

Yang, C., & Everitt, J. H. (2010). Mapping three invasive weeds using airborne hyperspectral imagery. Ecological Informatics, 5(5), 429–439. https://doi.org/10.1016/j.ecoinf.2010.03.002

Yu, W. (2004). Practical anti-vignetting methods for digital cameras. IEEE Transactions on Consumer Electronics, 50(4), 975–983. https://doi.org/10.1109/TCE.2004.1362487

Yue, J., Lei, T., Li, C., & Zhu, J. (2012). The application of unmanned aerial vehicle remote sensing in quickly monitoring crop pests. Intelligent Automation and Soft Computing, 18(8), 1043–1052. https://doi.org/10.1080/10798587.2008.10643309

Zhang, J., Pu, R., Huang, W., Yuan, L., Luo, J., & Wang, J. (2012). Using in-situ hyperspectral data for detecting and discriminating yellow rust disease from nutrient stresses. Field Crops Research, 134, 165–174. https://doi.org/10.1016/j.fcr.2012.05.011

Zhang, J., Pu, R., Yuan, L., Wang, J., Huang, W., & Yang, G. (2014). Monitoring Powdery Mildew of Winter Wheat by Using Moderate Resolution Multi-Temporal Satellite Imagery. PLoS ONE, 9(4), 1–16. https://doi.org/10.1371/journal.pone.0093107

Zhao, D., Huang, L., Li, J., & Qi, J. (2007). A comparative analysis of broadband and narrowband derived vegetation indices in predicting LAI and CCD of a cotton canopy. ISPRS Journal of Photogrammetry and Remote Sensing, 62(1), 25–33. https://doi.org/10.1016/j.isprsjprs.2007.01.003

APPENDICES

APPENDIX I: ADDITIONAL INDEX FIGURES

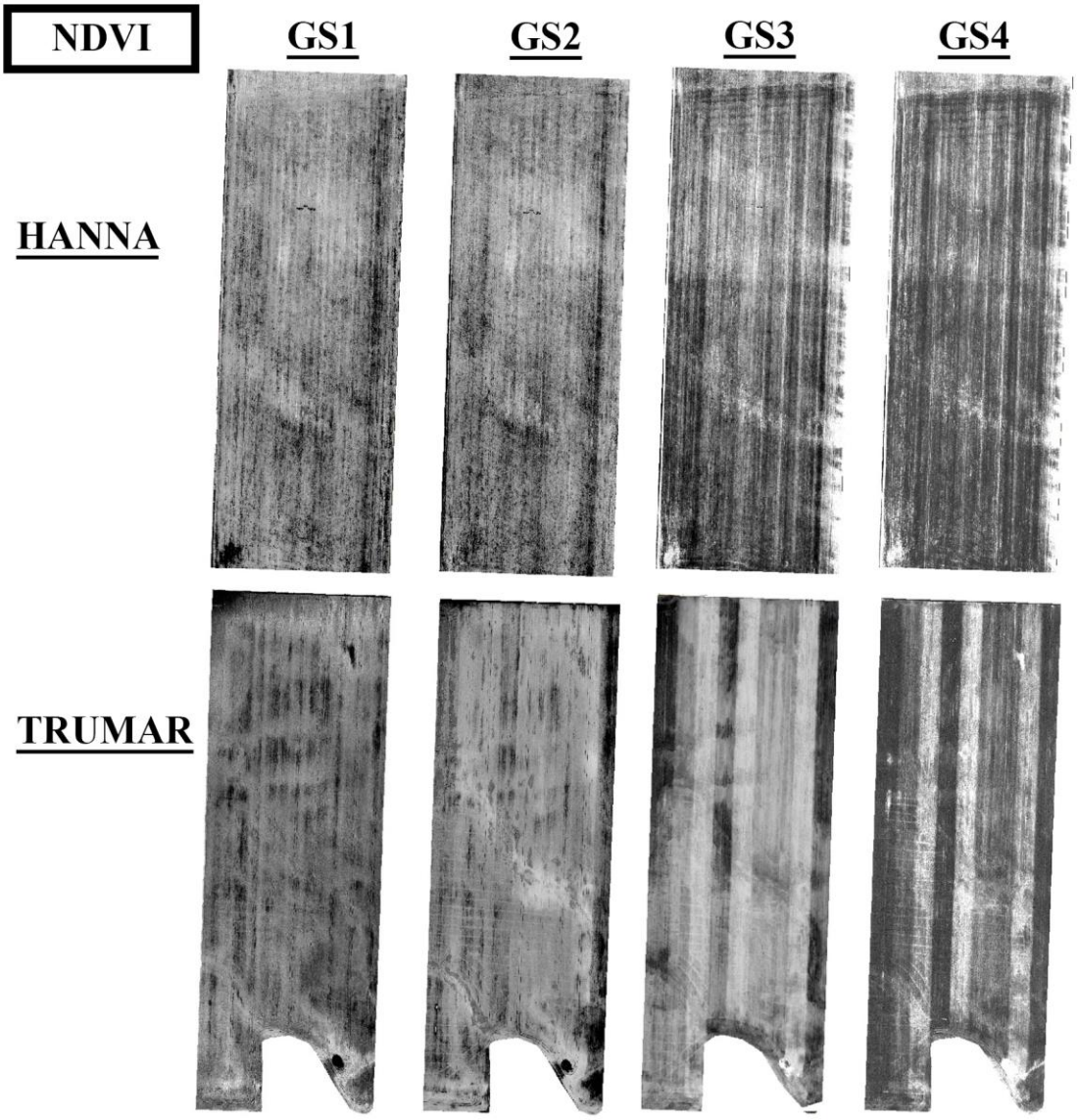

A. NDVI imagery before inter-scene histogram matching and clipping. Not to scale.

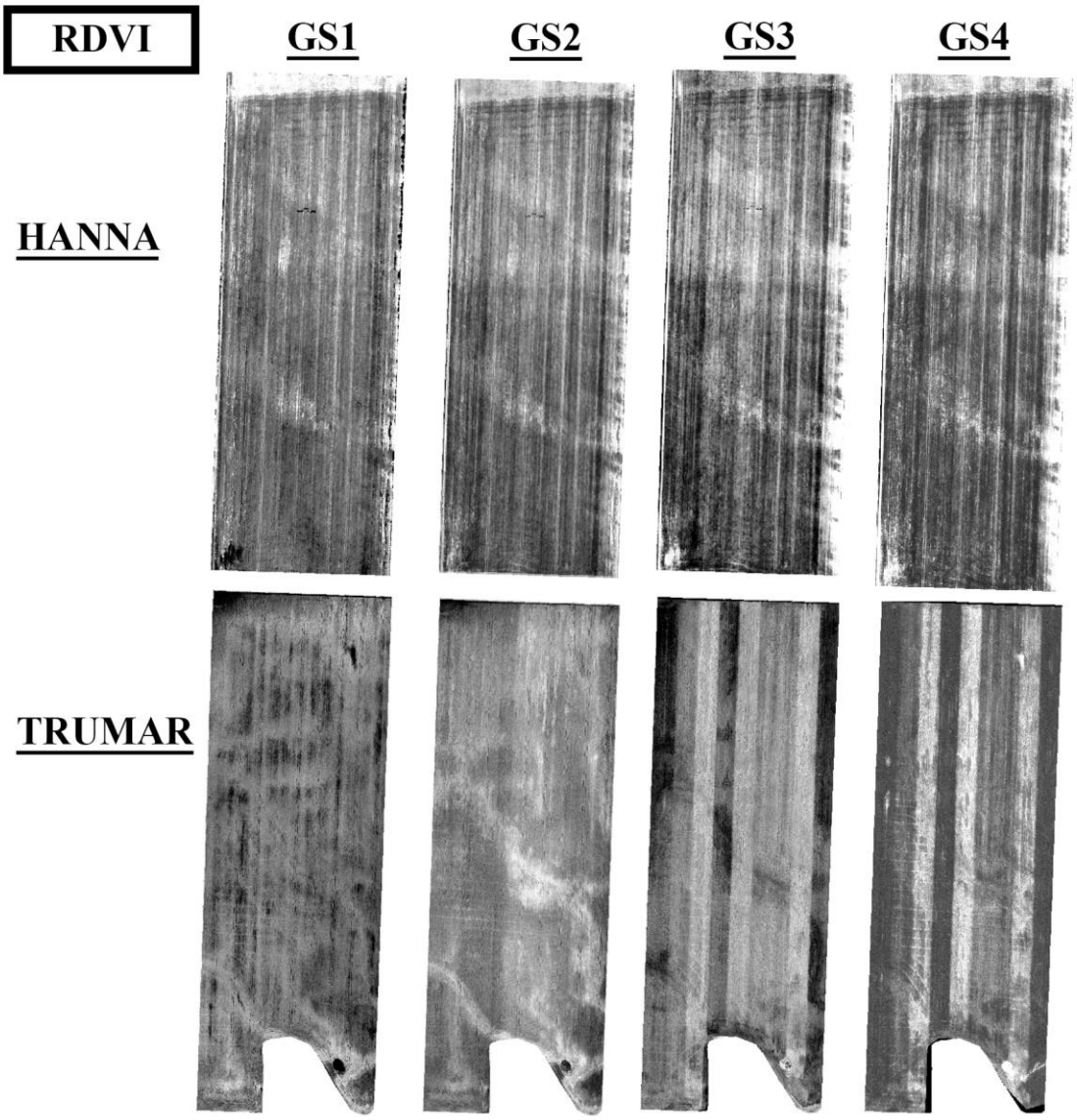

B. RDVI imagery before inter-scene histogram matching and clipping. Not to scale.

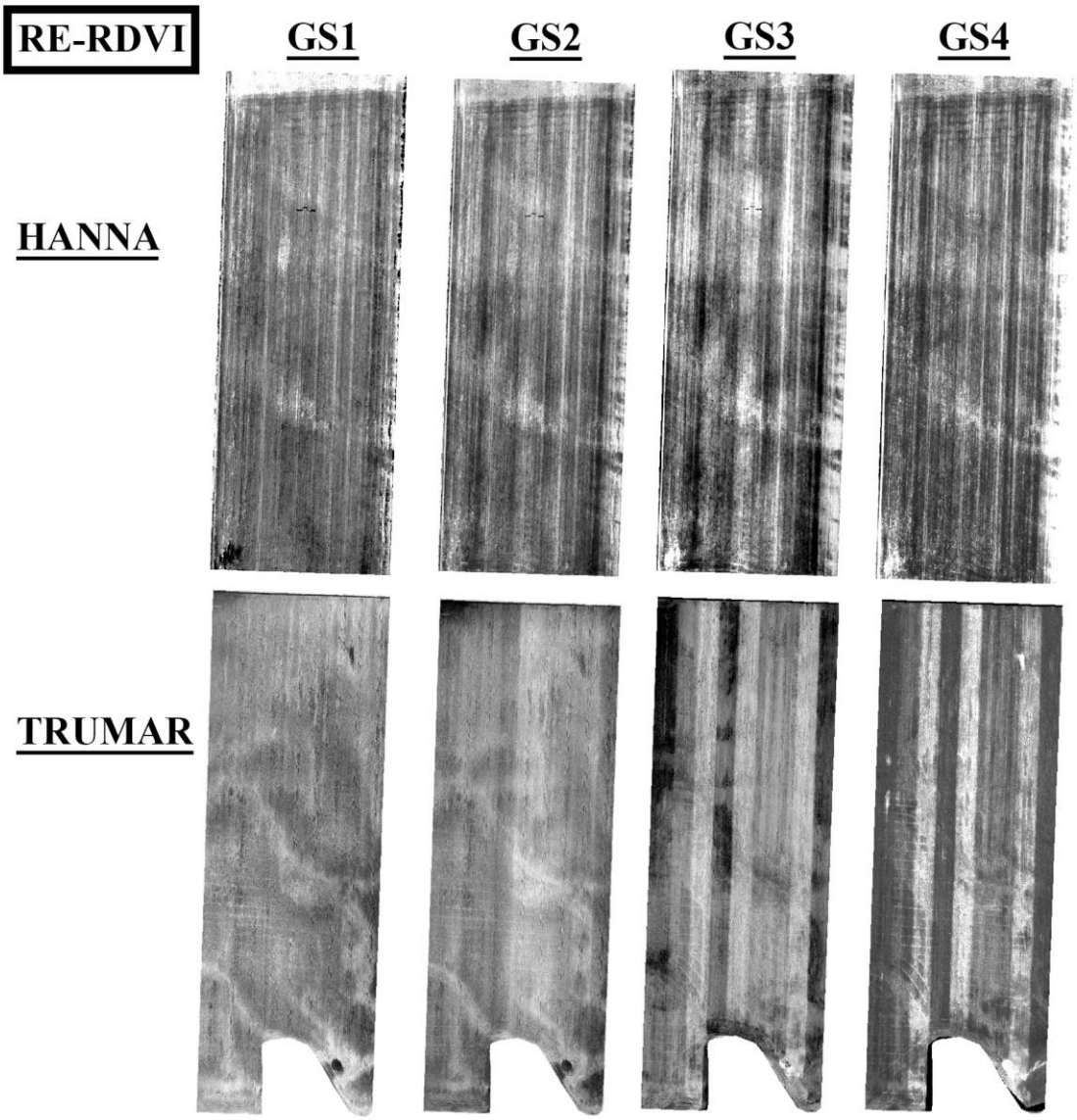

C. RE-RDVI imagery before inter-scene histogram matching and clipping. Not to scale.

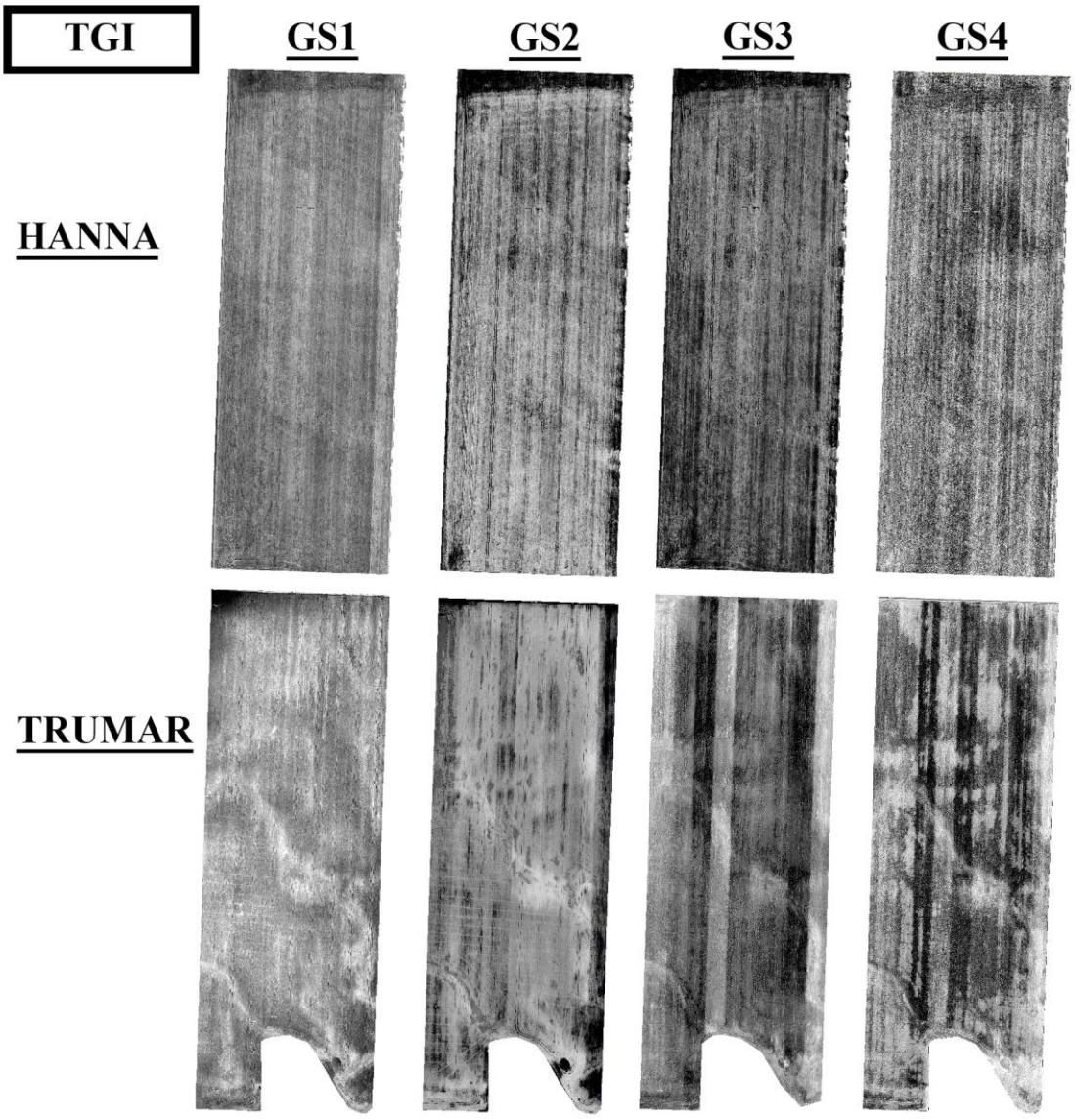

D. TGI imagery before inter-scene histogram matching and clipping. Not to scale.

APPENDIX II: F-TESTS FOR RCBD

The following F-Tests were derived from the Expected Mean Squares (EMS) table: $MS_T/MS_E=F(2, 120)$, $MS_{BT}/MS_E=F(2, 120)$, $MS_G/MS_E=F(3, 120)$, $MS_{BG}/MS_E=F(3, 120)$, $MS_{TG}/MS_E=F(6, 120)$, $MS_{BTG}/MS_E=F(6, 120)$. Due to the high number of numerical results, Table A was created for ease of viewing.

Table A. F-Tests and results from Randomized Complete Block Design for all Vegetation Indices.

EFFECTS	F-TEST
Normalized Difference Vegetation Index (NDVI)	
MS_T/MS_E	F (2, 120)=62.298, p<0.001
MS_G/MS_E	F (3, 120)=2051.694, p<0.001
MS_{BT}/MS_E	F (2, 120)=8.000, p<0.001
MS_{BG}/MS_E	F (3, 120)=36.676, p <0.001
MS_{TG}/MS_E	F (6, 120)=9.467, p< 0.001
MS_{BTG}/MS_E	F (6, 120)=1.020, p=0.415
Red-Edge Normalized Difference Vegetation Index (RE-NDVI)	
MS_T/MS_E	F (2, 120)=53.355, p<0.001
MS_G/MS_E	F (3, 120)=1903.653, p<0.001
MS_{BT}/MS_E	F (2, 120)=6.250, p=0.002
MS_{BG}/MS_E	F (3, 120)=74.310, p<0.001
MS_{TG}/MS_E	F (6, 120)=10.710, p<0.001
MS_{BTG}/MS_E	F (6, 120)=1.071, p=0.383
Renormalized Difference Vegetation Index (RDVI)	
MS_T/MS_E	F (2, 120)=97.189, p<0.001
MS_G/MS_E	F (3, 120)=1678.518, p<0.001
MS_{BT}/MS_E	F (2, 120)=6.028, p=0.003
MS_{BG}/MS_E	F (3, 120)=52.940, p<0.001
MS_{TG}/MS_E	F (6, 120)=10.813, p<0.001
MS_{BTG}/MS_E	F (6, 120)=3.403, p=0.003
Red-Edge Renormalized Difference Vegetation Index (RE-RDVI)	
MS_T/MS_E	F (2, 120)=63.243, p<0.001
MS_G/MS_E	F (3, 120)=2403.927, p<0.001
MS_{BT}/MS_E	F (2, 120)=1.254, p=0.289
MS_{BG}/MS_E	F (3, 120)=72.870, p<0.001
MS_{TG}/MS_E	F (6, 120)=11.312, p<0.001
MS_{BTG}/MS_E	F (6, 120)=3.267, p=0.005
Triangular Greenness Index (TGI)	
MS_T/MS_E	F (2, 120)=20.244, p<0.001
MS_G/MS_E	F (3, 120)=491.117, p<0.001
MS_{BT}/MS_E	F (2, 120)=2.258 , p=0.109
MS_{BG}/MS_E	F (3, 120)=17.312, p<0.001
MS_{TG}/MS_E	F (6, 120)=2.103, p=0.058
MS_{BTG}/MS_E	F (6, 120)=0.537, p=0.780